

WP3 - Activity 3.1

Geophysical surveys

Deliverable 3.1.1. *Conceptual model of the morphostratigraphic framework of the port area in project test sites through the very shallow water VHRS surveys in order to reconstruct changes triggered by human-induced modifications.*

Deliverable 3.1.2. *Characterization of the seawater morphology, identification of geological geometries in relation to the dynamics of exchange between sweet and salty waters*

Deliverable 3.1.3. *High-resolution bathymetry features.*

Deliverable 3.1.4. *Evolutionary scenarios at short, medium and long-term of the morphological features.*

Project Acronym	ECOMAP
Project ID Number	10047543
Project Title	Ecosustainable management of marine and tourist ports
Priority Axis	3
Specific objective	3.3
Work Package Number	3
Work Package Title	Monitoring / research of sea environment in marinas / ports ecosystems
Activity Number	1
Activity Title	High-resolution bathymetry (Multibeam and boomer) of the nearshore areas to characterize the morphology of the seafloor. Remote sensing (from drone robot / thermo frames from satellite images or analysis of density variations in the water column from multibeam and boomer data) for the identification of the freshwater outputs at the seafloor and for mapping their distribution
Partner in Charge	PP8 – University of Ferrara
Partners involved	PP7 - OGS
Status	Final
Distribution	Public

AUTHORS OF THIS REPORT

F. Accaino, F. Da Col, M. De Ponte, D. Cotterle, F. Zgur, G. Böhm, F. Meneghini, A. Schleifer, S. Picotti, M. Giorgi, L. Facchin, L. Baradello, E. Gordini and C. Vaccaro.

Index

1. Introduction	4
2. Split – Croatia	4
2.1 Land data	4
2.2 Marine data	17
3. Ancona - Italy	25
3.1 Land data	25
3.2 Marine Data	31
4. Bibione – Italy	66
4.1 Land data	66
4.1 Marine data	85
5. Evolutionary scenarios	124

1. Introduction

As part of the Interreg Italy-Croatia ECOMAP project, the OGS carried out geophysical surveys in the three test sites of Ancona, Bibione, Split both on land and at Sea. This report is divided in three sections, one per each test site. Each section is then divided in two sub-sections relative to the data acquired on land and sea respectively.

2. Split – Croatia

In Croatia geophysical surveys are located in the area of Split, specifically close to the Marina Špinut and in the town of Podstrana.

2.1 Land data

In Croatia both electrical resistivity and seismic data were acquired. Electrical resistivity data was acquired both in Podstrana and in Spinut, while seismic data were acquired in the Podstrana site.

2.1.1 *Electrical resistivity data*

This subsection contains a summary description of the processing activities of two-dimensional electrical resistivity tomography (ERT) measurements acquired during the spring 2019 exploration campaign at Podstrana and Spinut sites (Croatia – Figure 1).

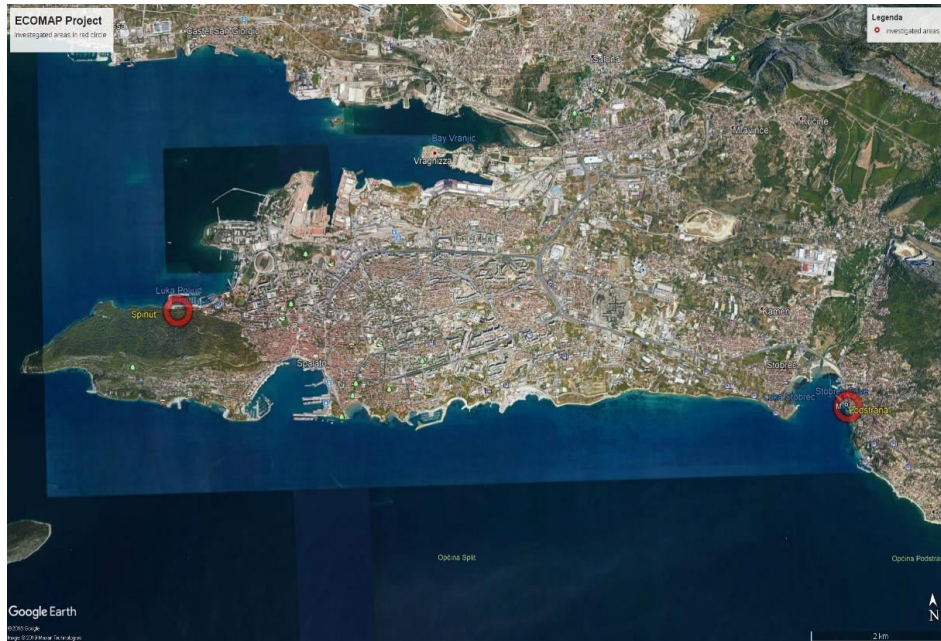


Figure 1. Map of the investigated areas: Podstrana site and Spinut site (Export from G.E. Pro)

The data processing activity described below involved a total of four data sets acquired with different electrode configurations:

1. Wenner measurements acquired on a surface 2D profile of 48 electrodes spaced 2 meters in Podstrana, along the beach (ERT1 - Figure 2a).
2. Wenner measurements acquired on a marine 2D profile of 48 electrodes spaced 2.5 meters in Podstrana (ERT2 - Figure 2a).
3. Wenner measurements acquired on a surface 2D profile of 48 electrodes spaced 2 meters in Spinut (ERT3 - Figure 2b).
4. Wenner measurements acquired on a surface 2D profile of 48 electrodes spaced 2 meters in Spinut (ERT4 - Figure 2b).

a)



b)

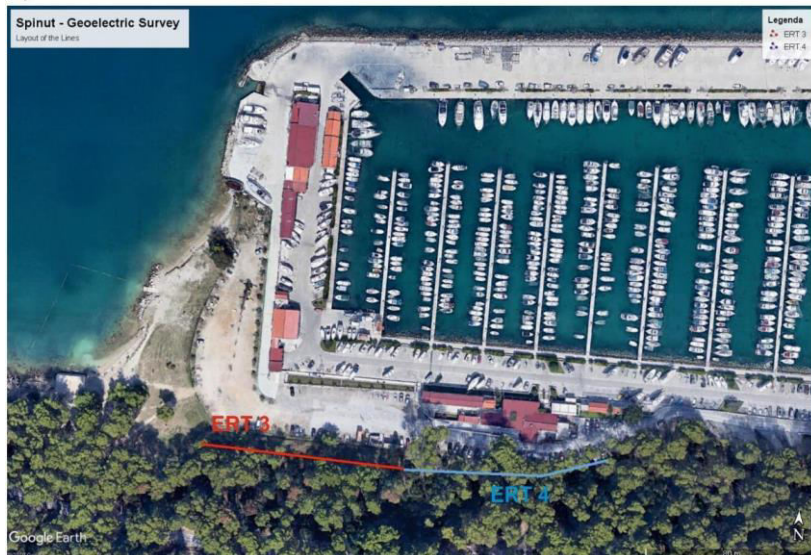


Figure 2. Map of the ERT surveys in Podstrana (a) and Spinut (b).

The combination of the acquisitions described above consists of a total of approximately 1440 measures.

The geoelectric datasets show good values of the measured electric potentials. The average value is around 115 mV at Podstrana and 2600 mV at Spinut. This difference is mainly due to the different settings of the two surveys, the former very close to the sea and the latter deployed among carbonate outcrops, especially in correspondence of the ERT4 profile.

Figure 3 shows the point cloud 2D distribution of the apparent resistivities acquired along the ERT3 profile; Figure 4 shows the histogram of the statistical distribution of potentials, currents and the same apparent resistivities after filtering the noisy measurements. The negative apparent resistivities, admitted only in 3D surveys, were filtered.

Preliminarily to the inversion procedure for the production of the resistivity model (imaging), the dataset must be subjected to a quality control. We removed approximately 30 noisy measurements at Spinut, equal to approximately 4% of the total quadrupoles. The removed measurements were approximately 11 at Podstrana, equal to approximately 1.5% of the total quadrupoles.

Removal criteria included:

- Elimination of measurements with instrumental standard deviation (obtained through multiple measurement stacks) larger than 10%.
- Removal of the receiver potentials V lower (in absolute value) than 0.01 mV. - Filtering of negative apparent resistivity values.

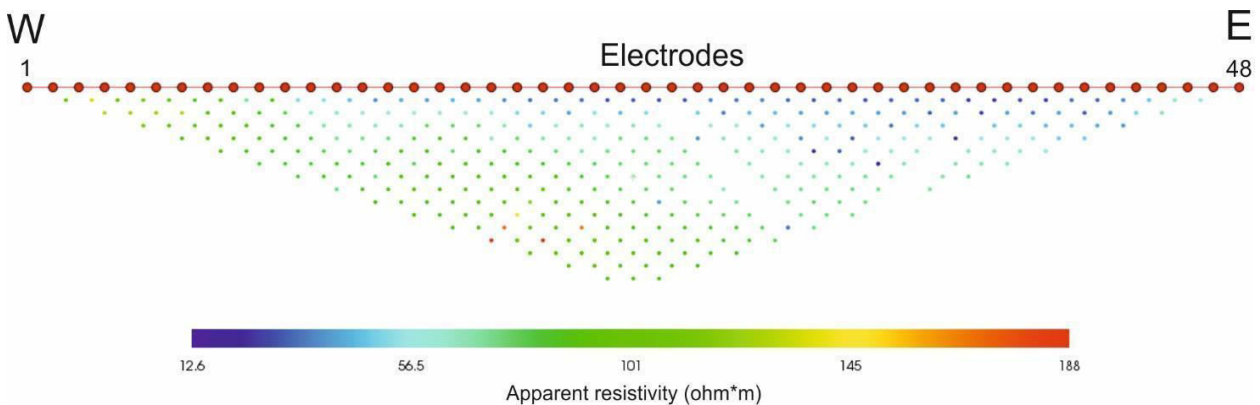


Figure 3. Pseudo-plot of the apparent resistivity measurements after the quality control, corresponding to ERT 3 profile.

The apparent resistivity values at Podstrana, after filtering the noisy measurements, are characterized by the following statistical behavior:

- minimum value around 0.17 Ohm*m; - maximum value around 23.3 Ohm*m; - average value of 3.7 Ohm*m;
- median value of 2.6 Ohm*m;

- average standard deviation equal to 3.2 Ohm*m.

The currents injected at the transmission electrodes have an average value of about 573 mA.

The statistical behavior of the apparent resistivity values at Spinut is the following:

- minimum value around 6.26 Ohm*m; - maximum value around 484 Ohm*m; - average value of 108 Ohm*m;

- median value of 103 Ohm*m;

- average standard deviation equal to 43 Ohm*m.

The currents injected at the transmission electrodes have an average value of about 841 mA.

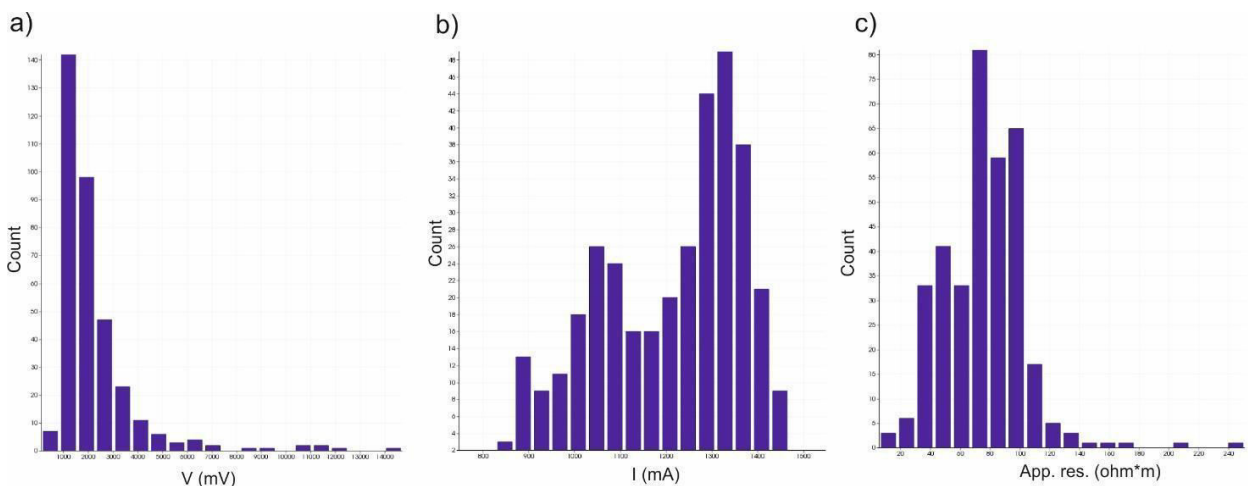


Figure 4. Histograms of potentials (a), currents (b) and apparent resistivities (c), corresponding to ERT 3 profile.

Note the difference in resistivity between the two sites: Podstrana shows resistivities lower than Spinut, because of the proximity of the sea in Podstrana, and the presence of outcropping limestones in Spinut

Electrical resistivity tomography (ERT) was performed using the VIEWLab Studio software, after removing inaccurate measurements. The entire set of measures was inverted in order to perform the imaging and characterize the correct resistive behavior of the subsol.

The three-dimensional inversion of the measures is based to the following configuration:

- - *mesh* size 1 m * 1 m * 1 m in the x, y, and z directions of space.

- - Starting resistivity close to the average of the apparent resistivities.
- - Estimated noise on the data equal to 3%.

The tomographic inversion converged after a maximum of 6 iterations, for all the considered datasets. The inversion of the marine profile ERT 2 at Podstrana required also the modelling of the sea water column at surface, because the electrodes were placed at the sea bottom and sea water is very conductive. The concordance of the modeled measures with respect to the measured values is very good, as evidenced by the example of Figure 5, which shows the progress details at the final iteration for the profile ERT 3.

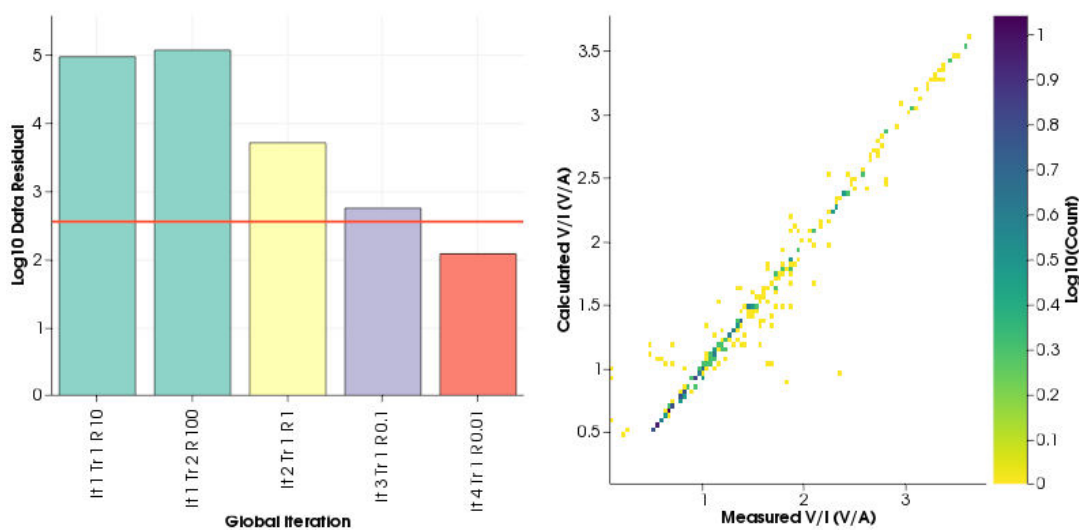


Figure 5. Progress details at the final iteration for the profile ERT 3. Trend of the misfit measures-modeled data, as the iterations proceed (left). *cross-plot* of the modelled data vs measured data (right), at the end of the tomographic inversion.

The results of the inversions are displayed in Figures 6-8. As expected, Podstrana (Figures 6 and 7) shows resistivities lower than Spinut (Figures 8 and 9), because ERT1 is very close to the sea and ERT2 is at the sea (see Figure 2a), while the surveys at Spinut are more distant from the sea (see Figure 2b). Some features of ERT1 and ERT2 sections, characterized by resistivity higher than the background, probably indicate plumes of fresh water (eventually mixed with sea water). On the other hand, ERT3 and ERT4 sections show areas characterized by resistivity quite lower than the background, probably indicating plumes of fresh water mixed with sea water.

ERT 1 - Podstrana

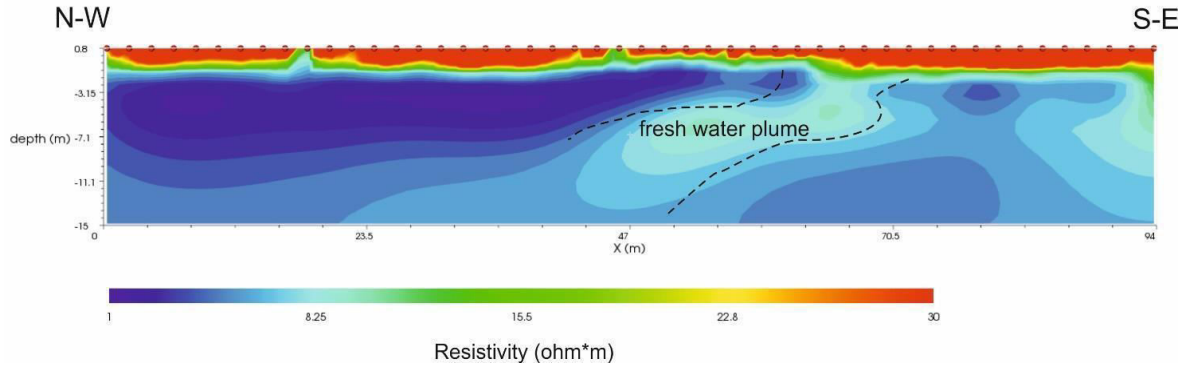


Figure 6. Tomography resistivity imaging corresponding to ERT 1 profile.

ERT 2 - Podstrana

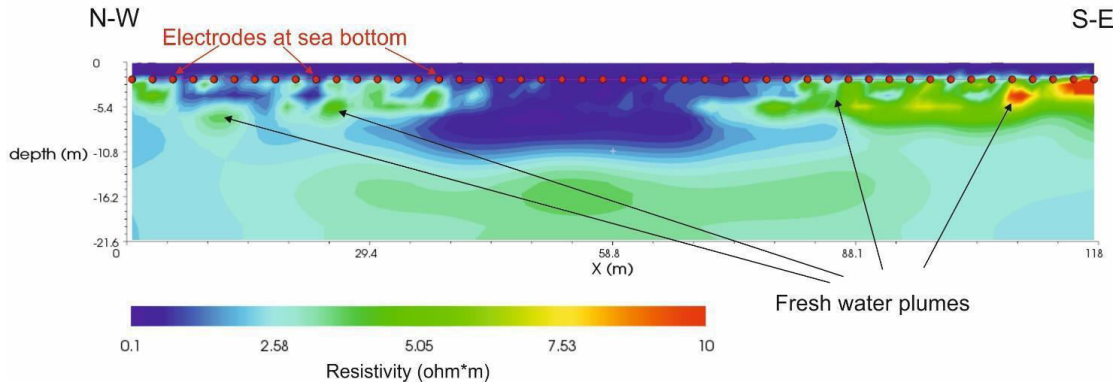


Figure 7. Tomography resistivity imaging corresponding to ERT 2 profile.

ERT 3 - Spinut

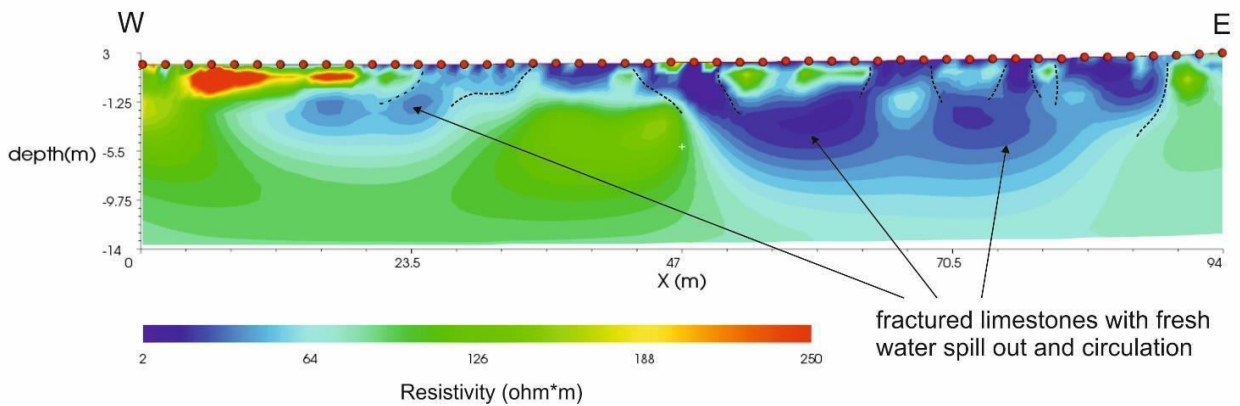


Figure 8. Tomography resistivity imaging corresponding to ERT 3 profile.

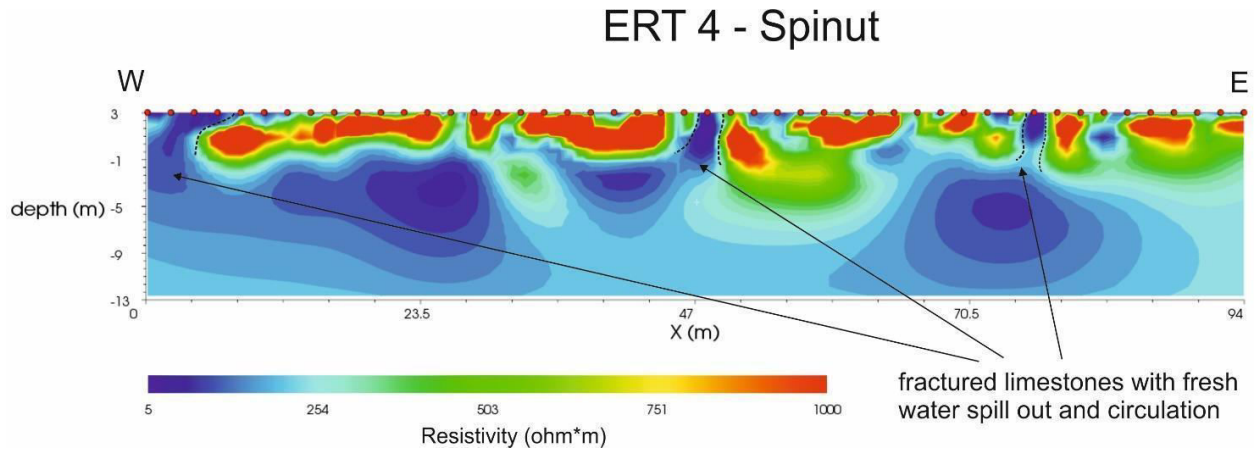


Figure 9. Tomography resistivity imaging corresponding to ERT 4 profile

2.1.2 Seismic data

A shallow-depth seismic survey took place in Podstrana, close to Split (HR) from June 9th to 12th, 2021, following a geoelectric survey that took place in May 2019 in the same location.

The area interested in this study covers a seashore, as shown in Figure 10. As in most of the seismic surveys that took place in the context of ECOMAP project, the source employed is one small handy- operated vibrator, producing P-waves.

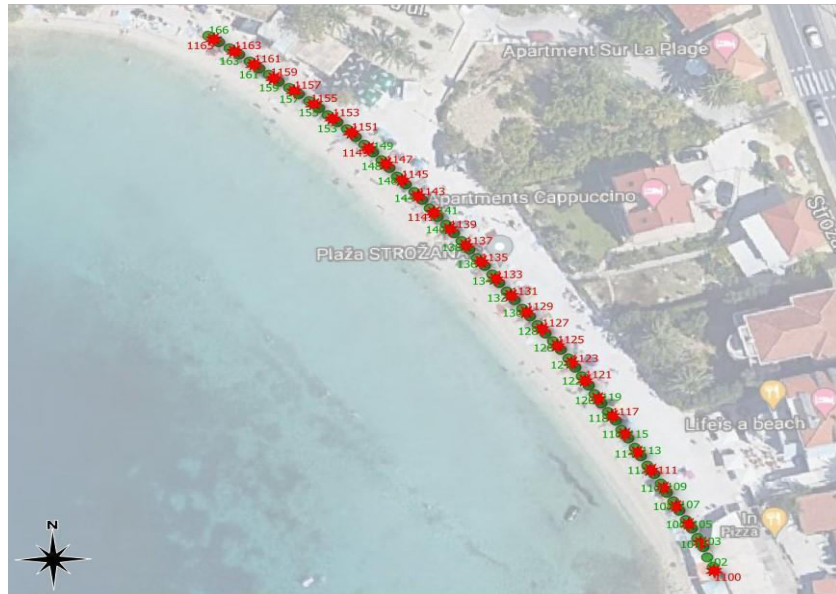


Figure 10. overview of the extent of the survey area

Based on the project's targets requirements, the main acquisition aspects taken into consideration are:

1. Instrumentation
2. Acquisition parameters
3. Source points
4. Data management

These are described in this chapter.

The instrumentation required for the survey can be divided in two groups:

1. Sensors
2. Acquisition system
3. Seismic source

Sensors

Vertical mount 10 Hz geophones were used as seismic receivers.

Acquisition system

The whole acquisition equipment includes one laptop PC that runs the acquisition control interface, as well as the digitizer's interface, and has QC capabilities (data visualization and inspection). The digitizer employed is the Summit from DMT, driven by its proprietary software, which handles the acquisition settings, records and exports the SEG2 data.



Figure 11. Vibroseis source Elvis VII from Geosym

The vibrating source for this survey is a P-wave Elvis VII from Geosym GmbH. The vibrating mass is entirely mounted, together with its battery and the electronic power amplifier, on a light and robust wheelbarrow so that can be handled easily. The controller offers manual triggering capability, providing a timebreak signal to the acquisition system.

The following parameters have been set as a result of the tuning phase:

- Sweep type: linear
- Peak Force: 1100 N
- Frequency range (Hz): 20 - 160 Taper type: cosine
- Start taper (s): .100
- Load force (Kg): 112

- Sweep length (s): 10

In order to maximize the information content of the data to match the investigation purposes, at first the following survey parameters have to be tuned:

- record parameters
- acquisition channels
- vibration points
- source parameters

Record parameters

- record length (s): 12.8
- sampling interval (ms): 1
- cross-correlation listening time window: from -0.8 to 2.0 s.

The spacing between the sensors is always fixed to 2 m. For vibroseis operations, the reference (pilot) signal trace is always identified by track number 90, which has been previously recorded by a high resolution, low-noise A/D converter in OGS laboratory. The seismic receivers are placed along paths mostly parallel to the sea shore. The receiver stations numbering starts with 101, and proceeds in ascending order from South to North. See the next chapter for a detailed description of each receiver station.

Typically the source points have been designed to fall in the middle point of two subsequent receivers, every two receivers couples thus resulting in 4 m. source spacing. The rule for the numbering is that each VP is numbered as the stake of the previous receiver (in numeric terms), incremented by 1000. So, for instance, VP 1143 is placed 1 m. ahead stake/receiver 143 (taking into account the direction of the increment is from North to South), which is 1 m. before stake 144 as well.

The records files produced by the Summit are automatically gathered, managed and preprocessed by OGS custom-made acquisition software 'PyACQ'. This application software interfaces the user to the records database and computes the first quality control on the acquired data, by means of checking the incoming data consistency, includes information in each trace header, then cross-correlates each trace with the pilot. The system also allows the user to insert comments about each individual record, enabling the software to automatically discard bad or noisy records from later re-processing. Finally, both correlated and uncorrelated raw data are secured in a safe storage.

The records set produced has been organized as follows. The main data folder contains the correlated data (RAW uncorrelated will always be available in the OGS data storage system). This contains several sub-folders, named after the source type. Each record is related to a specific position (numbered as described in the previous section) of the Vibroseis along the line.

The correlated file name is formatted as in the following example: "F005 S1101.corr" means the record has been acquired on VP 1101, corresponding to Field Record number 5. The file format is Seismic Unix SU, with inner standard SEG-Y trace headers, explained in detail in the following paragraph.

Most of the acquisition information are recorded in the header of the SEG-Y files, such as source and receiver position, start time, trace identification codes, etc. The meaning and the position of the header fields follows the SEG-Y standard definition. The most relevant subset of the header parameters is reported in detail in table 1.

SEG-Y header parms		
Na m e	Description	byte
fld r	field record number	9-12
ns	number of samples	115- 116
dt	sample interval in microseconds	117- 118
tr ac f	field trace number	13- 16
off se t	distance between source and receiver	37- 40
sx	X coordinate of the source position	73- 76
sy	Y coordinate of the source position	77- 80
gx	X coordinate of the receiver position	81- 84
gy	Y coordinate of the receiver	85-

	position	88
--	----------	----

Table 1. SEGY header Parameters

In this chapter we report a brief summary of the operations related to each activity.

Refer to the following table as the description of OGS crew attending the whole surveys:

OGS Crew			
Name	Title	Activity	Initials
Flavio Accaino	Senior Geophysicist	Survey Scientific Leader	FA
Federico Da Col	Geophysicist	Quality Control	FC
Fabio Meneghini	Field Engineer	Data Acquisition	FM
Stefano Picotti	Geophysicist	Quality Control	SP
Massimo Giorgi	Geologist	Quality Control	MG

Table 2. OGS crew attending the surveys

The table 3 shows a synthetic overview of the attendance of OGS crew in the period from June 9th to 12th.

Activities calendar						
date	Activity	FA	FC	FM	SP	MG
9/6	move-in	x	x	x	x	x
10/6	acquisition	x	x	x	x	x
11/6	move-out	x	x	x	x	x
12/6	move-out	x	x	x		

Table 3. OGS crew and activities

After moving the register van onto a suitable position along the survey line, while preparing and connecting all the instruments and equipment, the operators coupled the geophones to ground, then deployed the line cable and the data collector units. Figures 12 below show details of these different steps. After a few tests, the optimal number of records per shot point has been set to two.

It took the first few records to tune some of the acquisition and sweep parameters. The number of records for each EP has been set to two. See below for some relevant notes about the records:

Start time: 10-06-21 08:13:28 with VP 1100. The following VP is the 1103, then the 1105 and so on.

Stop time: 10-06-21 10:42:02 Field records range: 6 - 70

on field record numbers 20, 25 and 43 there was a worker operating a chainsaw nearby the shore.



Figure 12. line set-up steps (a) deploy sensors and digitizers (b) coupling geophones to ground (c) detail of the map with stake numbers. The red symbols indicate the VP, the green dots the receiver's stakes

2.2 Marine data

In September 2019 boomer and sparker data were acquired in order to obtain information about the thickness of the sediments and to investigate the presence of fresh water outflows at sea.

The two investigated areas are located offshore the town of Podstrana and the touristic marina “Spinut”, as defined in the project. In the Podstrana area 25 boomer profiles were acquired, while in Spinut area 12 boomer profiles and 7 sparker profiles. Sparker profiles were acquired to investigate the geological structures of the basement, as the sparker source has a greater penetration depth than the boomer one. In Figure 13 and 14 the position maps of the profiles acquired in the two investigated areas are shown.

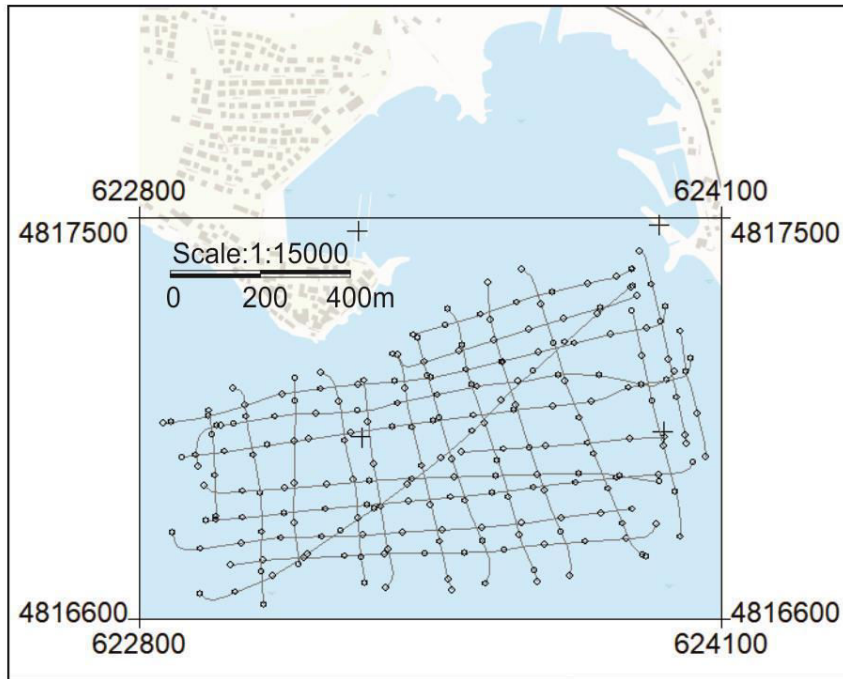


Figure 13. Position map of the boomer lines acquired in the Podstrana area



Figure 14. Position map of the boomer and sparker lines acquired in the Spinut area.

The aim of the data analysis was to define the thickness of the sediments and to investigate the presence of freshwater outflows at sea. In order to obtain these information, the data were processed with the aim to obtain the best image of the subsoil structures. In Figure 15 a final result of boomer line after the processing is shown. The layers in the sediments are well imaged and the top of the basement is easily interpretable. In this line a freshwater outflow is also visible, so we can state that boomer data is a good choice to define and map this feature.

After the processing and the application of the geometries to the data, the seismic lines were imported in the Kingdom software in order pick the top of the basement in all the lines, obtaining a 3D map of the top of the basement (see Figure 16). One of the aims of the work was to define the thickness of the sediments, so the picking of the seabed was performed (see figure 17). Then, calculating the difference between the seabed time and the top of the basement, and multiplying the difference by 1600 m/s, which is a reasonable estimate of the velocities in the sediments, and finally dividing by 2, we obtained the thickness of the sediments. In figure 18 the 3D map of the thickness of the sediments is shown.

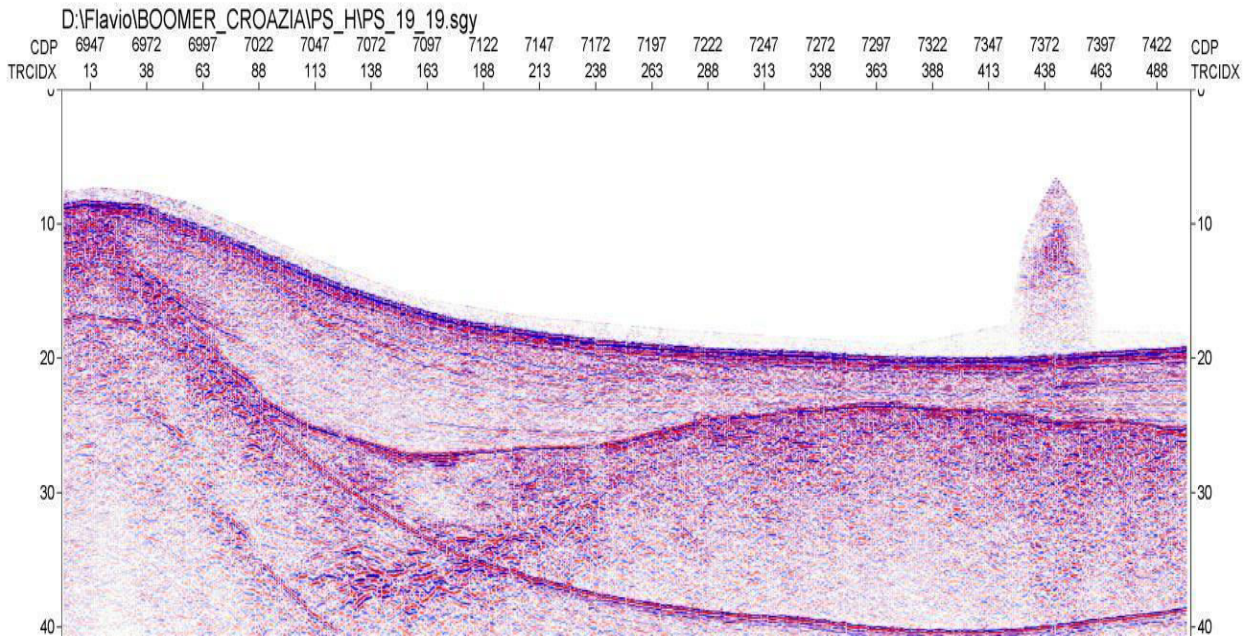


Figure 15. Example of boomer data acquired in Podstrana area. A freshwater outflow is clearly visible.

Analyzing the data, also the presence of freshwater outflows in the sea water is evident, as can be clearly seen in Figure 15. The presence of these plumes was investigated on the whole area and a map of the location of the detected plumes is shown in Figure 19.

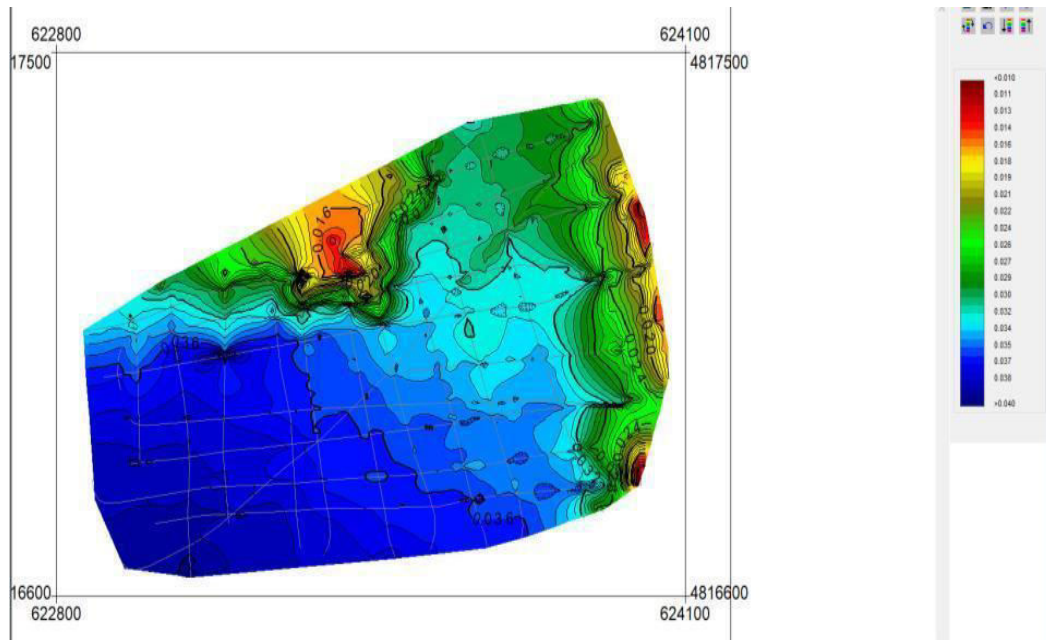


Figure 16. Map of the top of the basement obtained by the picking of the boomer lines

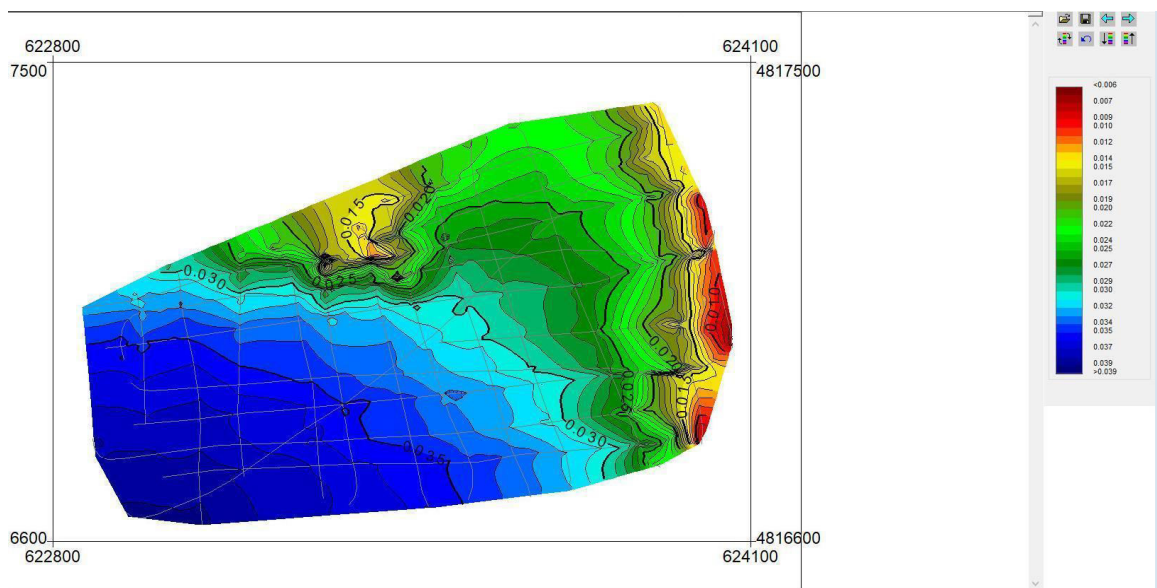


Figure 17. Map of the seabed obtained by the picking of the boomer line

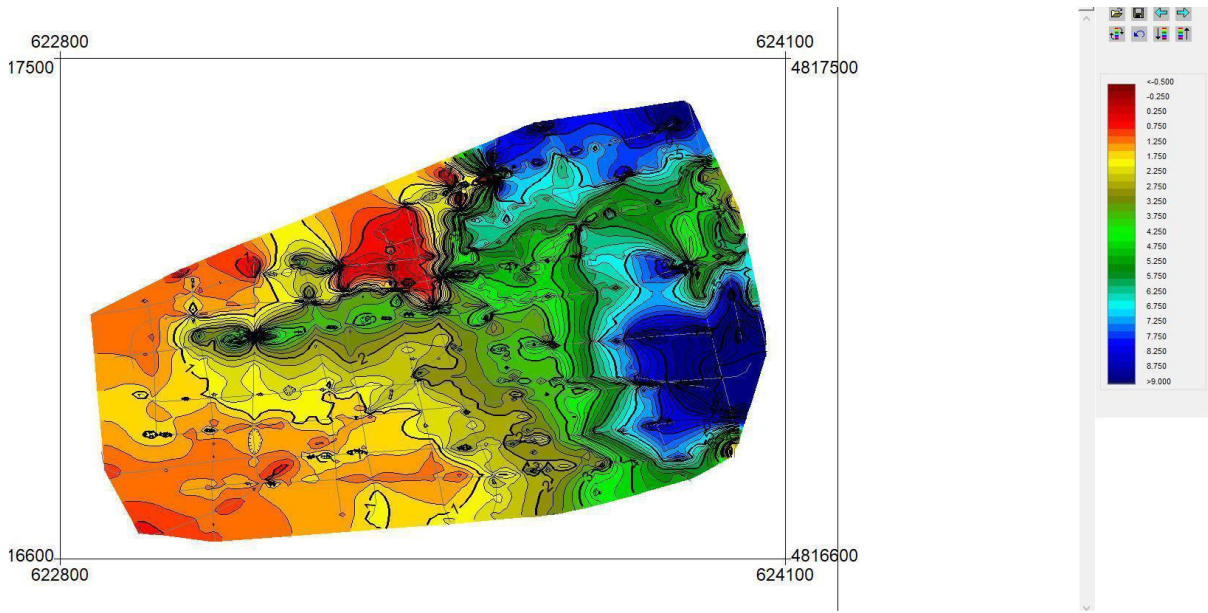


Figure 18. Thickness of the sediments obtained considering a velocity in the sediments of 1600 m/s.

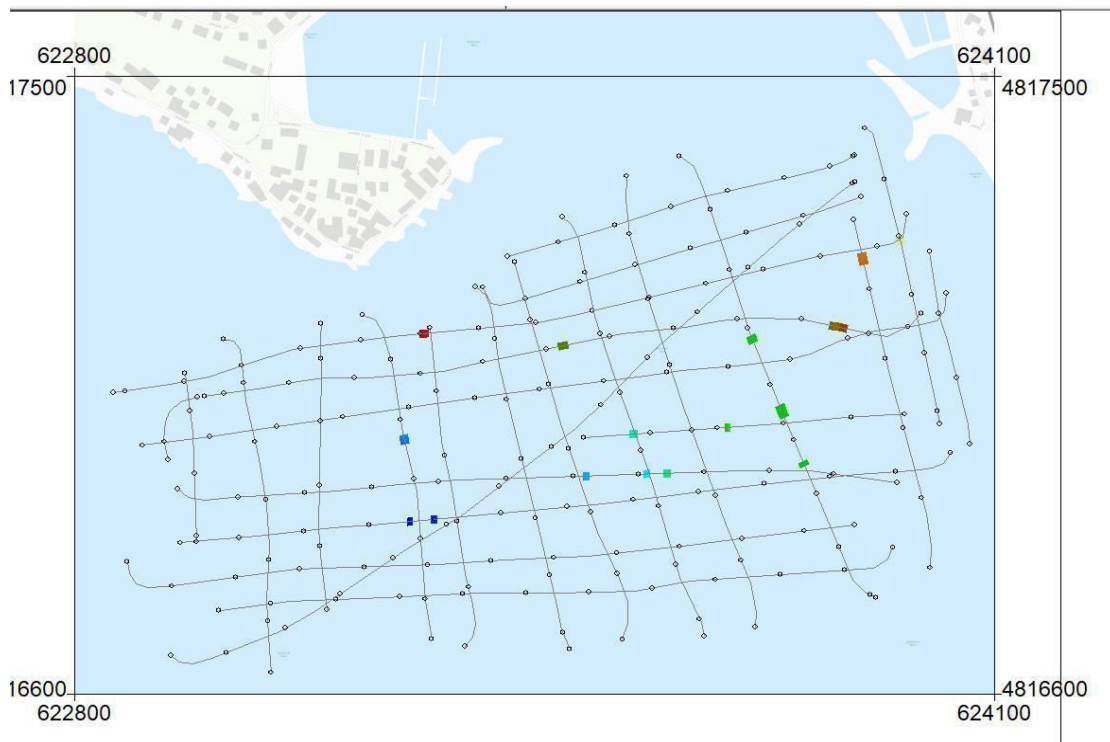


Figure 19. Map of the outflows identified in the 2D boomer lines.

The same procedure described for Podstrana data was applied to the data acquired in the Spinut area. In this location also sparker data were acquired in order to investigate the possibility to define the structures of the basement. Same small reflections characterizing the data are visible in the basement, which furnish the information that the basement is composed by alternance of very dipping layers with different seismic velocities. This is in agreement with what is described in the literature, which identified the basement of the area to be composed of flysch, highly deformed by tectonic activity.

As for the results of the boomer data, similarly to the Podstrana data, we computed the top of the basement, the seabed level and the thickness of the shallow sediments. The resulting maps are shown in Figures 20, 21 and 22.

Finally, in Figure 23, the location of the detected freshwater outflows is shown.

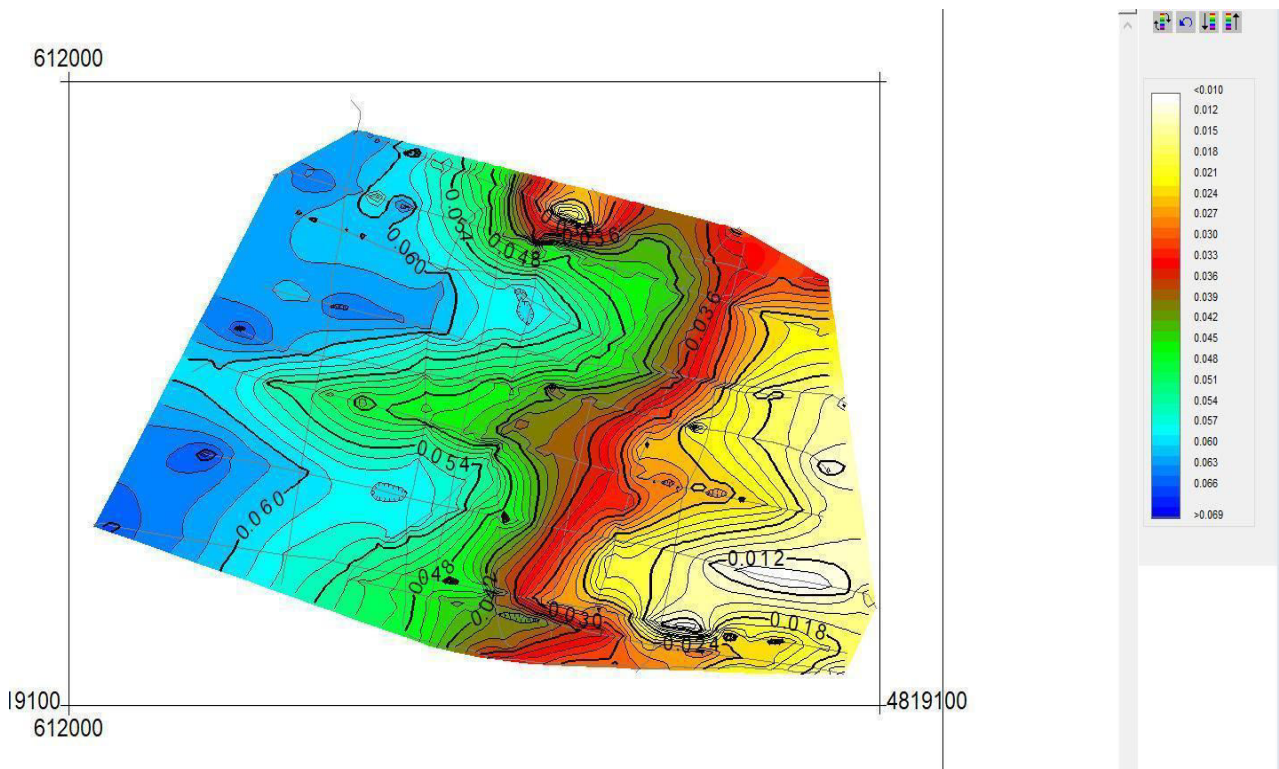


Figure 20. Map of the basement obtained by the picking in the boomer and sparker data

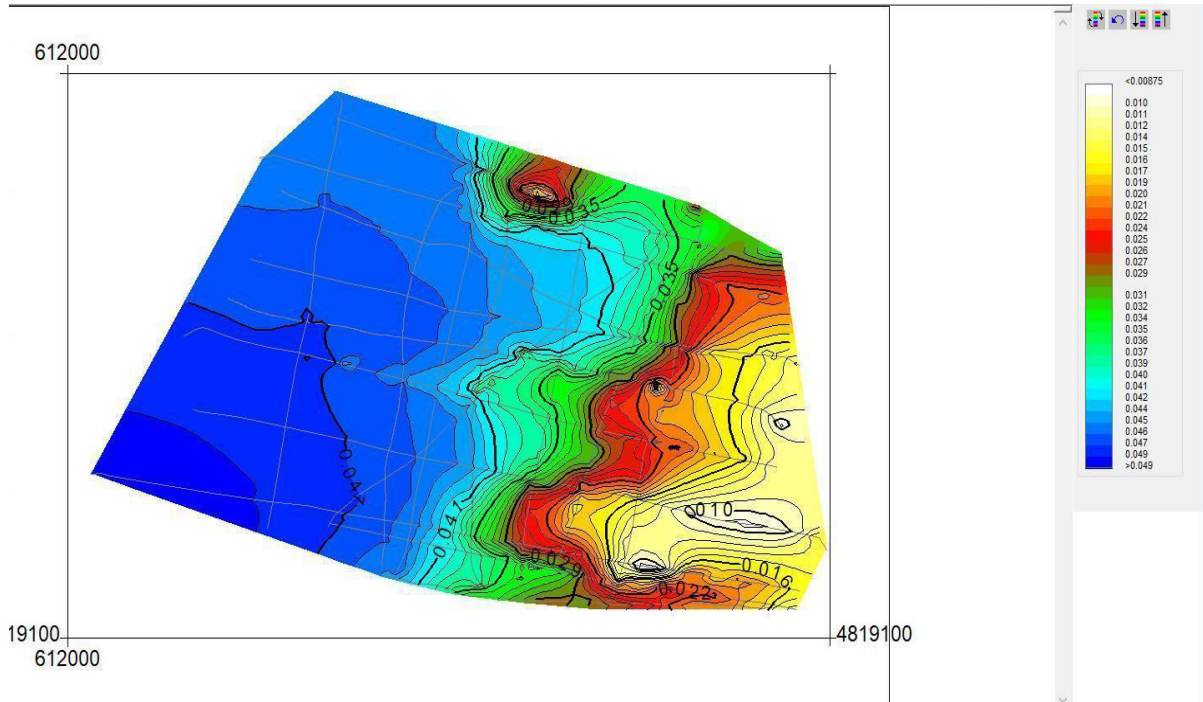


Figure 21. Map of the seabed obtained by the picking of the boomer and sparker data.

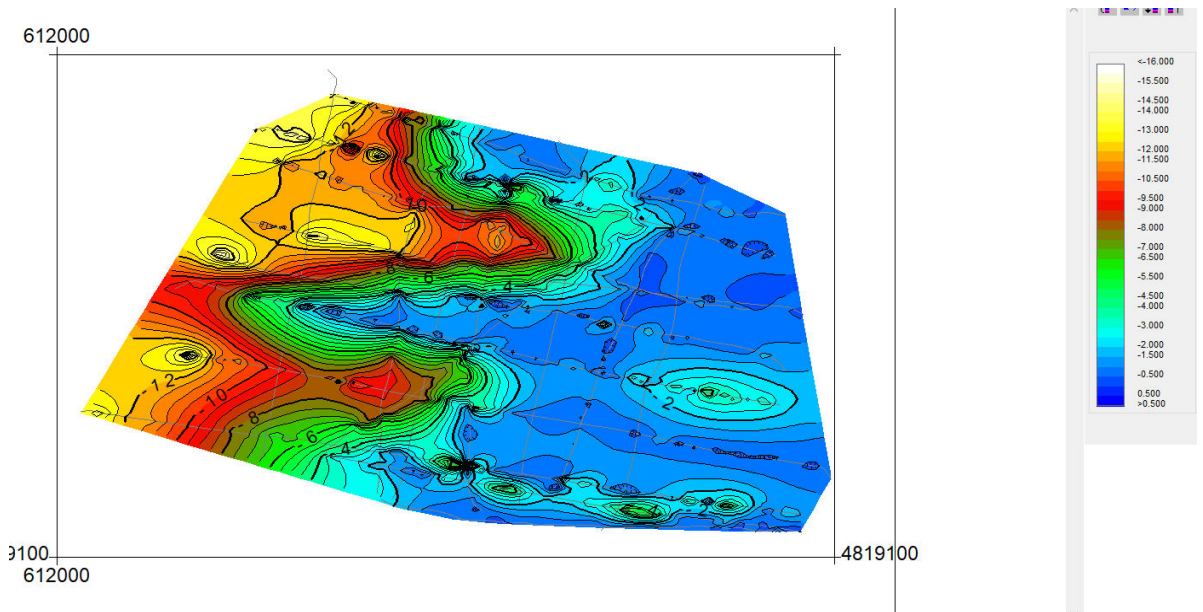


Figure 22. Map of the thickness of the shallow sediments

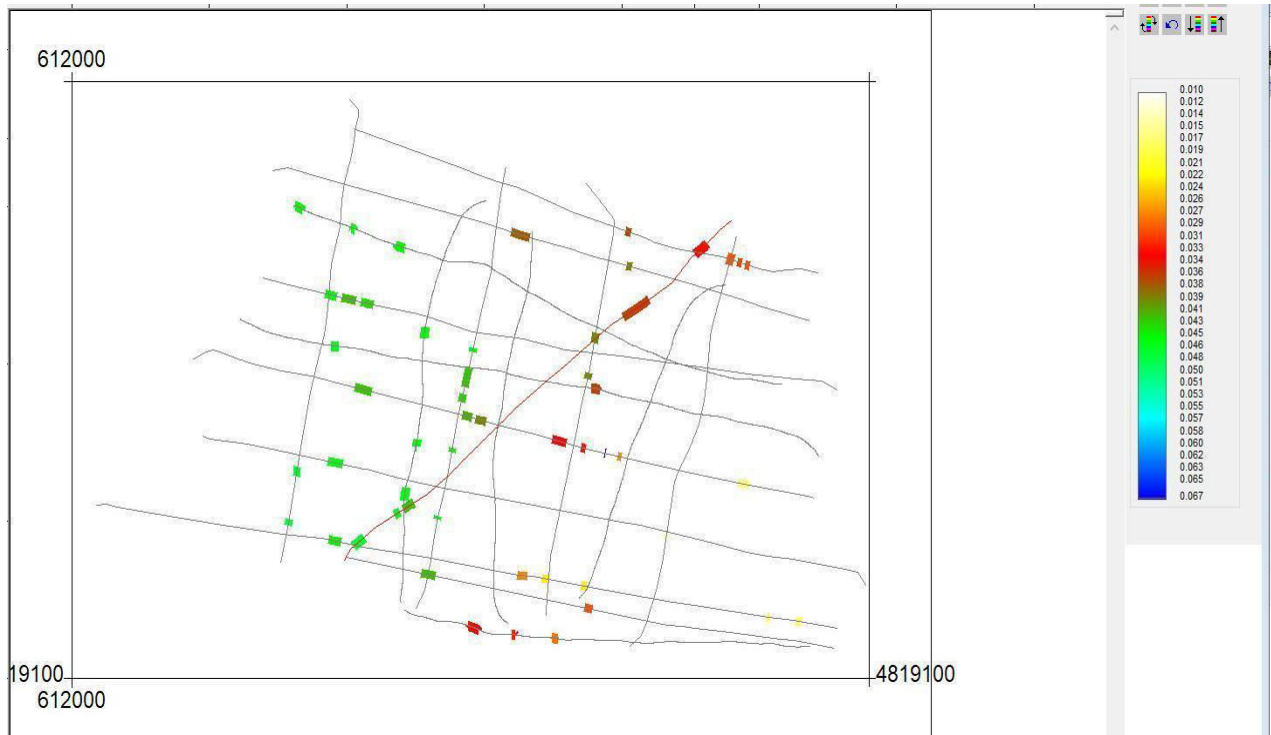


Figure 23. Outflows in the Spinut area.

Very high resolution seismic allowed us to define the thickness of the sediments and to map the fresh water outflows. This was the aim of the work, so we can affirm that the adopted method is adequate.

Regarding the outflows in the two investigation areas, it appears that in the Spinut area the outflows are greater in number than in the Podstrana area.

Another interesting point is that the outflows don't appear constant in time. In fact, at a cross point of two lines, in one line the outflow is present, while in the other one, acquired one hour later, it is not present.

3. Ancona - Italy

3.1 Land data

3.1.1 Legacy seismic data

Since in Ancona several seismic profiles had already been acquired, we based our analyses on those. To further investigate the area, we acquired and processed electrical resistivity data

We used a previous seismic survey as a reference to plan the geophysical acquisitions within the ECOMAP project. The survey was carried out in 2011 to characterize the Great Ancona Landslide which occurred in 1982 and it consisted of three lines covering both land and sea. The location of the lines can be seen in Figure 1 while a migrated section, where the position of the landslide is highlighted with a red rectangle can be seen in Figure 2.

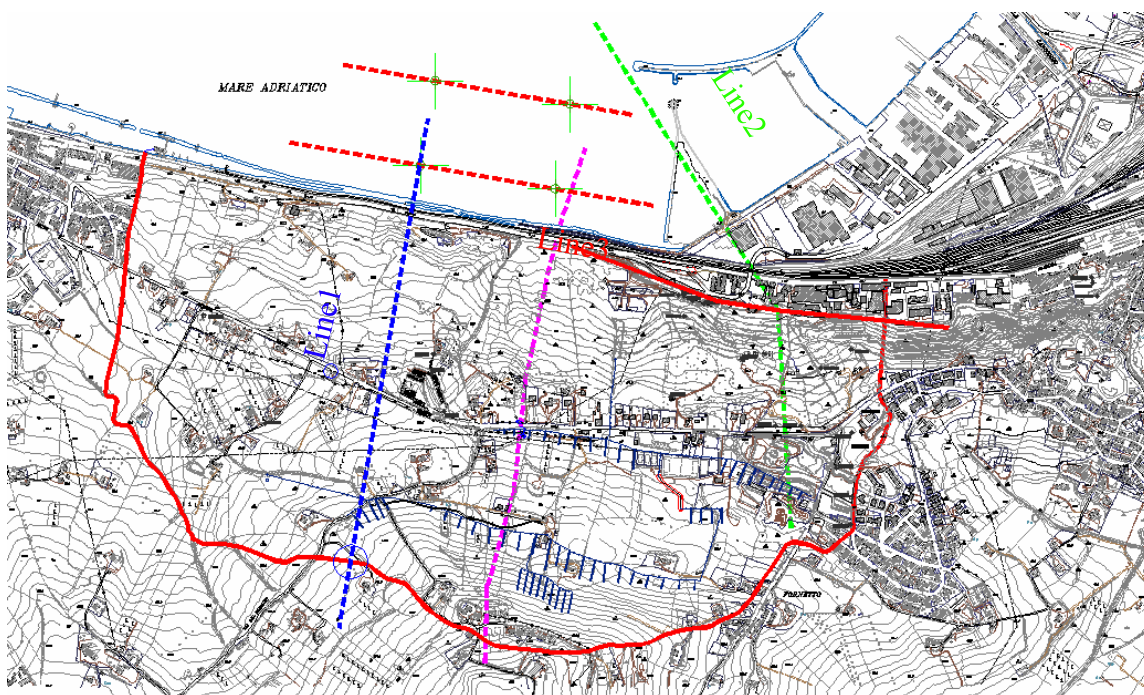


Figure 1. Map of the three land-sea seismic lines acquired in 2011.

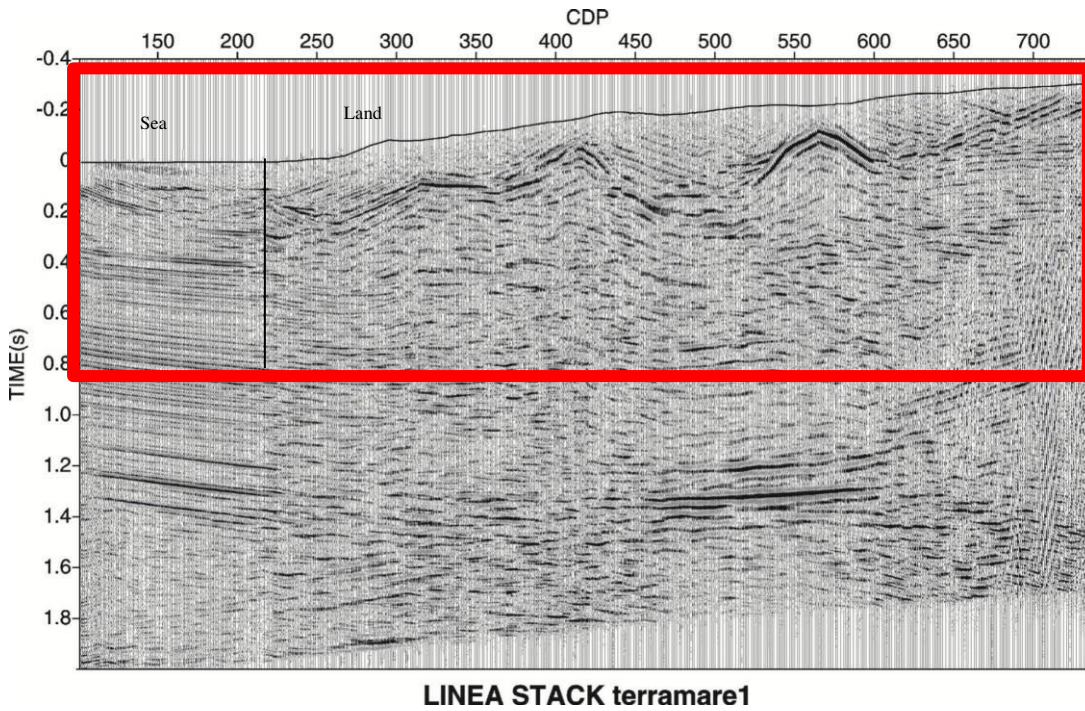


Figure 2. Migrated section of Line 1 from the 2011 seismic survey. The position of the landslide is highlighted with the red box.

3.1.2 Electrical resistivity data

Along the same Line as seismic Line 3 shown above, a geoelectrical survey was carried out. In this subsection, we summarize the acquisition and processing activities of two-dimensional electrical resistivity tomography (ERT) measurements acquired during March 2022 exploration campaign in the Ancona site (Italy – Figure 3).



Figure 3. Map of the investigated area close to Ancona (Export from G.E. Pro)

The 2D geoelectric data set has been acquired adopting the Dipole-Dipole electrode configuration. A total of 42 electrodes, spaced 5 m, were deployed. The Line is approximately WNW-ESE oriented and 210 m long (Figure 4). The surveys were designed to image the shallow structure of the subsol, providing a maximum theoretical depth of investigation of about 40 m. The data consists of a total of approximately 2240 measures. Resistivity data were collected using a new-concept georesistivimeter Multi-Source System (MSS) (<http://www.mpt3d.com> – Multy-Phase Technology). The MSS System comprises several stand-alone transceivers synchronized via GPS timing and controlled via a 900 MHz radio signal (Wireless Protocol). Each transceiver (indicated as Multisource Unit in Figure 4) is capable of handling a maximum of three electrodes. Therefore, a total of 14 MS units were deployed. It is worth to notice that with this peculiar design transmitting and receiving dipoles must belong to different units. The peculiar and innovative feature of this system, beyond the wireless communication between units, is its capability of transmitting the current simultaneously with multiple dipoles, each one connected to a different transceiver.

The dataset consists in approximately 2240 measurements.

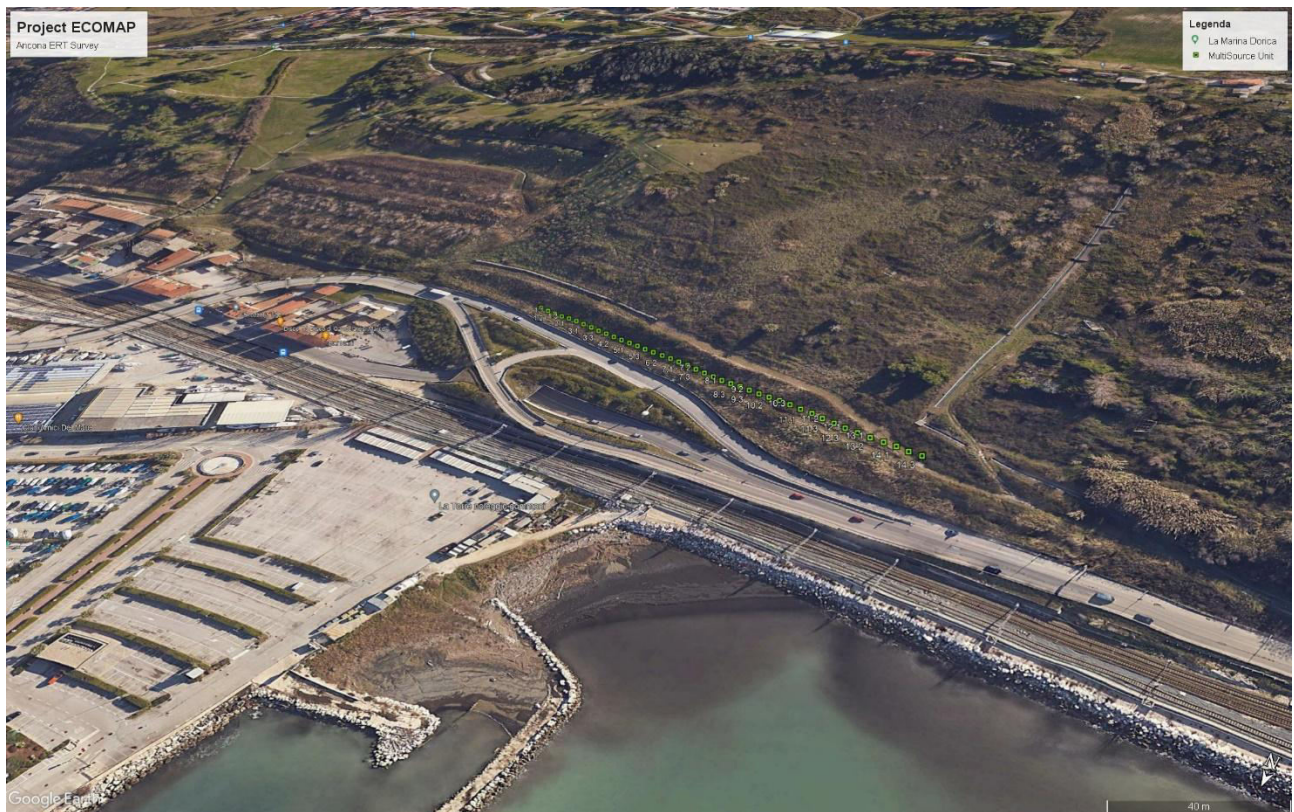


Figure 4. Map of the ERT survey close to Ancona.

The geoelectric dataset show good values of the measured electric potentials. The average apparent resistivity value is around $17.0 \text{ Ohm}\cdot\text{m}$. This low resistivity value is probably due to the very high clay content of the soil in this area.

Preliminarily to the inversion procedure for the production of the resistivity model (imaging), the dataset must be subjected to a quality control. We removed approximately 30% of the total quadrupoles of Line (about 700 measures).

Removal criteria included:

- Removal of the reciprocal measurements. We removed approximately 20.3% of the total number of quadrupoles.
- Elimination of measurements with instrumental standard deviation (obtained through multiple measurement stacks) larger than 30%.
- Removal of the receiver potentials V lower (in absolute value) than 0.01 mV.
- Filtering of negative apparent resistivity values.

Figure 5 shows the histogram of the statistical distribution of potentials, currents and the same apparent resistivities after filtering the noisy and the reciprocal measurements. The negative apparent resistivities, admitted only in 3D surveys, were filtered.

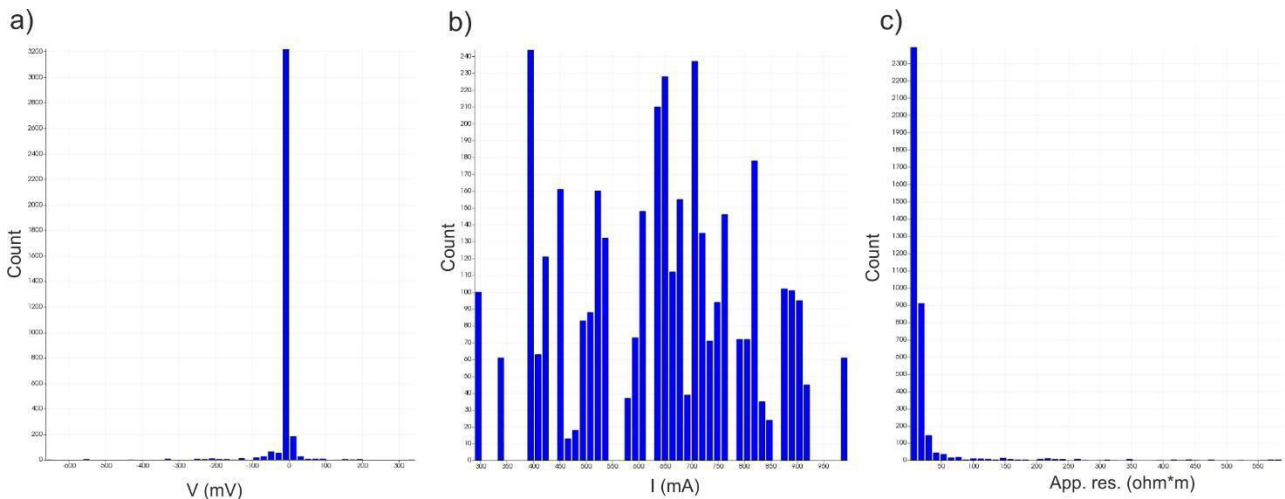


Figure 5. Histograms of potentials (a), currents (b) and apparent resistivities.

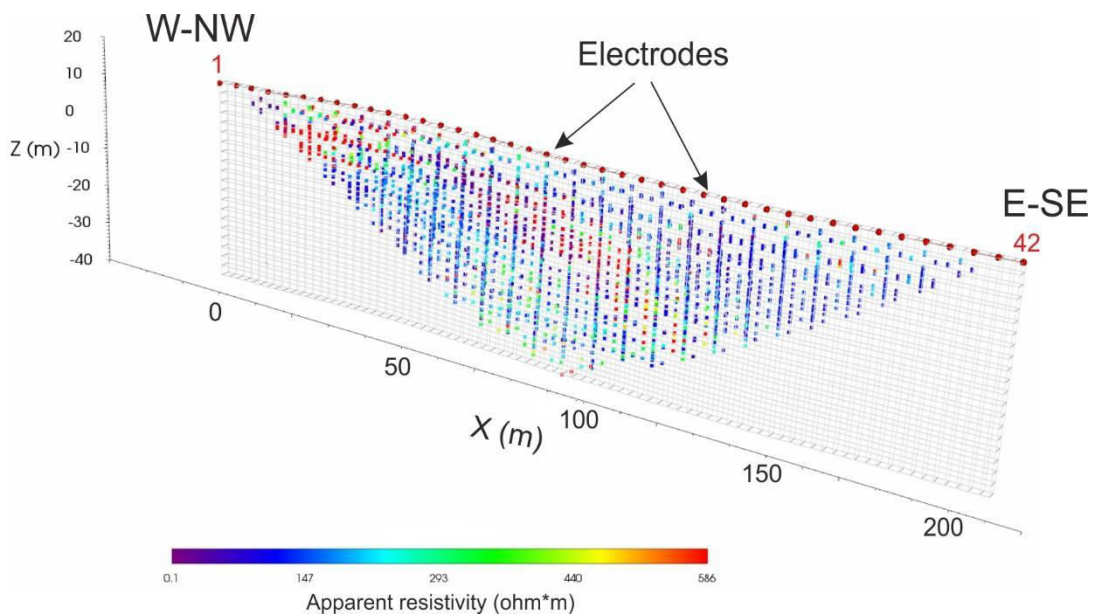


Figure 6. Pseudo-plot of the apparent resistivity measurements after the quality control. The mesh used for the inversion procedure and the electrodes are also represented.

The apparent resistivity values of the profile after filtering the noisy measurements, are characterized by the following statistical behavior:

- minimum value around 0.1 Ohm*m;
- maximum value around 586 Ohm*m;
- average value of 17 Ohm*m;
- median value of 4.6 Ohm*m;
- average standard deviation equal to 56 Ohm*m.

The currents injected at the transmission electrodes have a range between 300 mA and 1 A, with an average value of about 637 mA.

Figure 6 shows the point cloud 2D distribution of the apparent resistivities.

Electrical resistivity tomography (ERT) was performed using the VIEWLab Studio software, after removing inaccurate measurements. The entire set of measures was inverted in order to perform the imaging and characterize the correct resistive behavior of the subsoil.

The three-dimensional inversion of the measures is based to the following configuration:

- *mesh* size in the x, y, and z directions of space: 2.5 m, equal to half electrode spacing.
- Starting resistivity close to the average of the apparent resistivities.
- Estimated noise on the data equal to 3%.

The tomographic inversion converged after a maximum of 3 iterations, for all the considered datasets. The concordance of the modeled measures with respect to the measured values is very good, as evidenced by Figure 7, which shows the progress details at the final iteration.

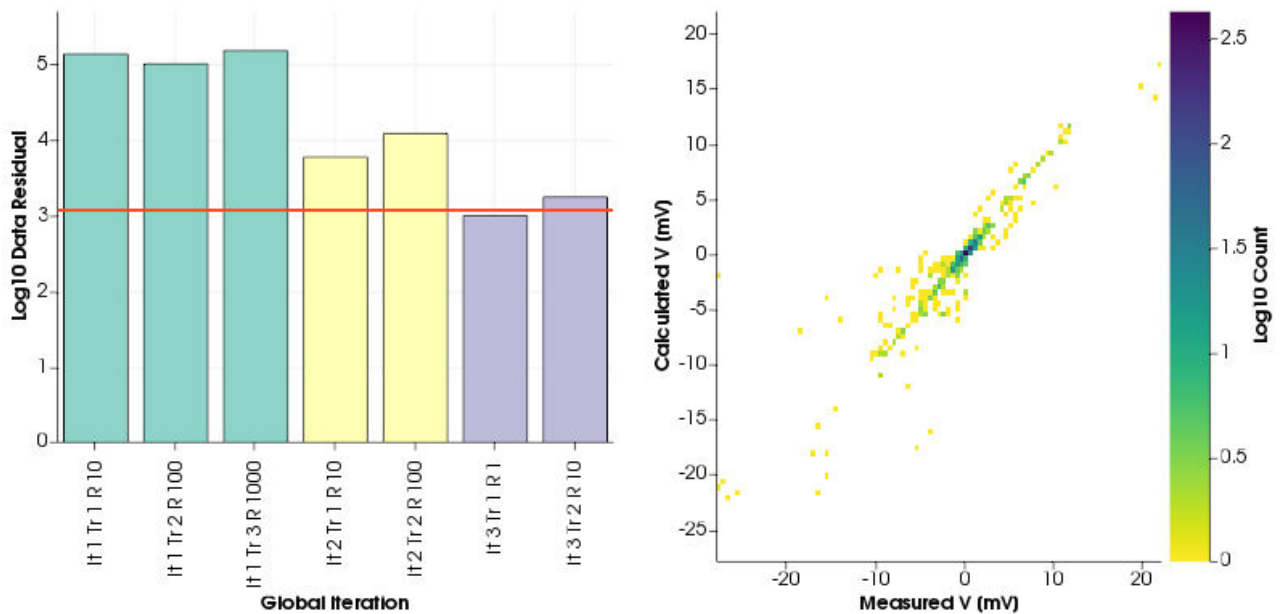


Figure 7. Progress details at the final iteration. Trend of the misfit measures-modeled data, as the iterations proceed (left). *cross-plot* of the modelled data vs measured data (right), at the end of the tomographic inversion.

The results of the inversions are displayed in Figure 8. As expected, the section show very low resistivities in depth, because of the high clay content of the sediments. Note that, at about 13 m depth, the sections indicate the (probable) presence of the sliding surface of a landslide.

Some features of section, characterized by high resistivity, probably indicate the presence of dry sand accumulations at near surface. The section exhibits some features indicating plumes of fresh water eventually mixed with sea water. These features correspond to very low resistivity zones located close to the surface.

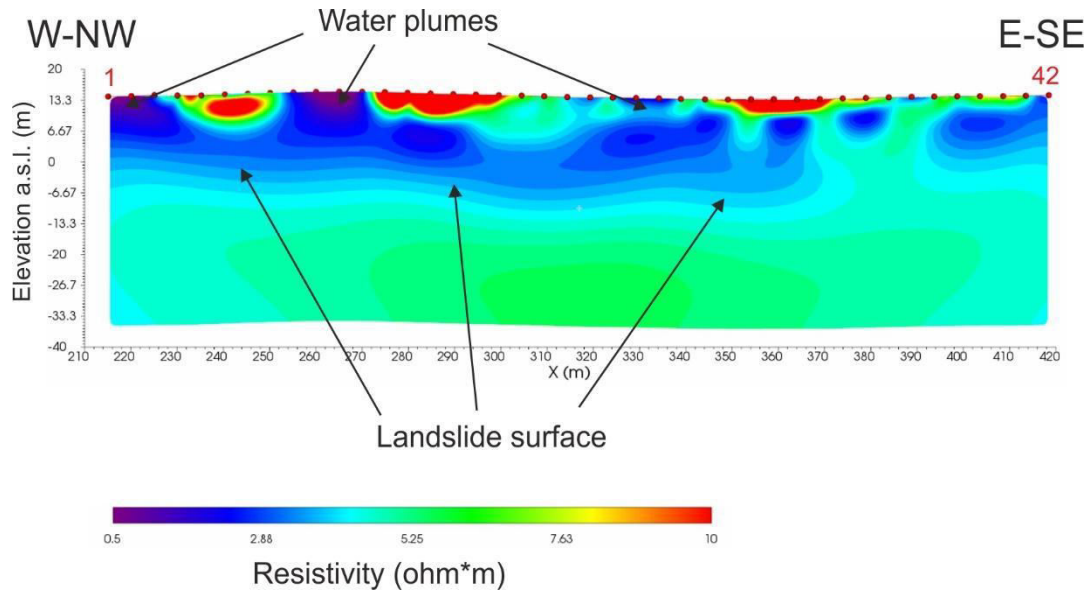


Figure 8. Final tomographic resistivity imaging.

3.2 Marine Data

3.2.1 Interpretation of high-resolution marine seismic data: boomer.

Within the ECOMAP project an interpretation of 18 offshore high-resolution subbottom seismic reflection profiles acquired in 2011 was performed. The seismic lines were acquired using as a source the boomer described in the previous sections. The analysed seismic dataset (Figure 9) consists of:

- 6 WNW-trending, and 1.5 km long seismic profiles that are very close to the coastline. They are roughly parallel to the coastline;
- 10 NNE-trending seismic profiles roughly orthogonal to the coastline. This group includes two over 2 km long profiles (an_12_11 and an_11_11) and other 8 seismic sections between 800 and 1.2 km long;
- 2 NW-trending seismic profiles (an_16_11 and an_24_11). The an_16_11 profile, which is about 1.8 km long, cut all the NNE-trending profiles;

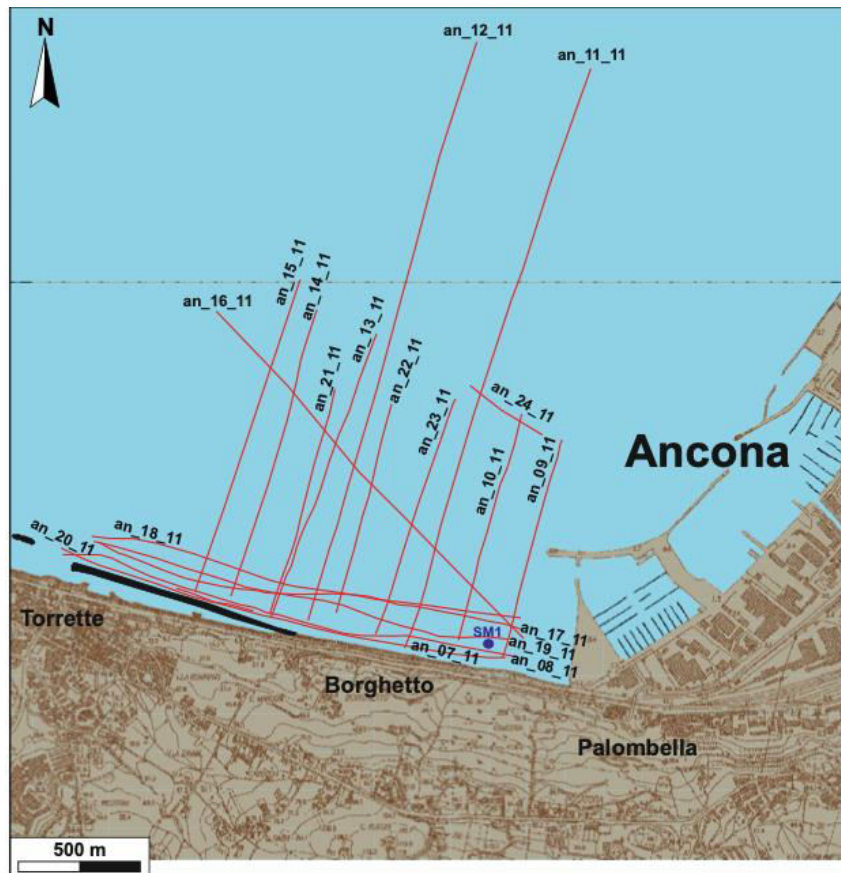


Figure 9. Boomer lines

Moreover, a borehole (SM1), located about 100 m from the coast between the an_19_11 and an_08_11 seismic lines, is available (Fig. 9). This well, positioned at the south-western end of the area covered by the seismic dataset, drilled 80 m of sedimentary succession, consisting of 1,4 m of Holocene bivalve-bearing sandy marine deposits lying on a lower-middle Pliocene succession composed of greysh silty clays and marls containing fine-grained sandy intercalations (Accaino et al., 2019). The contact between these two successions is marked by an erosional surface (ravinement surface).

The interpretation of the high-resolution sub-bottom profiles, which followed the processing phase, has been performed by means of a seismic interpretation software after the loading of the acquired dataset in SEGY format.

The seismo-stratigraphic and structural interpretation consisted of the following phases:

- 1) Analysis of literature data;
- 2) Recognition of key reflectors (generally corresponding to lithological changes and

unconformities characterized by high amplitude and considerable lateral continuity) bounding seismic units, which are characterized by different seismic facies and/or configuration pattern, reflector terminations, depth and thickness;

3) Try to correlate the identified seismic units with known geological formations;

4) Recognition of the tectonic structures (faults and folds) affecting the analyzed succession.

5) Hypothesize a possible evolutionary model for the study area

Six seismic units, separated by five key stratal surfaces (S1-S5), have been identified. They are, from bottom to top: Unit 1, S1 surface, Unit 2, S2 surface, Unit 3, S3 surface, Unit 4, S4 surface, Unit 5, S5 surface, and Unit 6.

Unit 1

Unit 1 is the deepest unit recognized in the study area. This unit generally shows a layered seismic facies characterized by an alternation of parallel high and low-amplitude reflectors that show high frequency and strong continuity in seismic profiles parallel to the coastline, while in the orthogonal ones they are not always clearly recognizable (Figs. 10 and 12-13). The seismic facies can be chaotic in the sectors farthest from the coast. The amplitude variability is related to the alternation of different lithologies, consisting of sand and clay. Unit 1 is outcropping at the seabed in the sectors close to coast (250-300 m from the coastline).

Both along the NNE-trending profiles (Figs. 10 and 12-13) and on the profile an_16_11 (Fig. 14), steeply dipping reflectors inclined 10-15° landward (to the SSW) are recognizable. They delineate the northern limb of a wide WNW-trending syncline mapped onland (Tavernelle syncline, e.g. Agostini et al., 2014), which trends almost parallel to the coastline. The slope of the reflectors increases to the NNE. These reflectors are clearly truncated by the S1 erosional surface (erosional truncation) (Figs. 10-14). Along the WNW-trending profiles located close to the coast, the reflectors are folded forming a gentle syncline outcropping to the seabed (Fig. 11). This syncline has a NNE-trending subvertical axial surface with a more inclined eastern limb. The western limb of this syncline is affected by the offshore continuation of the NNE-trending Torrette fault (Accaino et al., 2019), which is visible in the seismic profiles parallel to the coastline (Fig. 11). This subvertical fault, affecting only the Pliocene succession (Unit 1), shows a modest offset of 1-1.5 m and it does not seem to affect the seafloor. A Pleistocene

to present tectonic phase was responsible for the generation of transverse faults with anti-Appenninic NNE-orientation (Crescenti et al., 1983; Cello and Coppola, 1989; Cello and Tondi, 2013).

The documented tectonic deformation highlights that Unit 1 is probably affected by multiple bending phases, characterized by orthogonal stress directions, produced during the building of the central Apennine chain.

Based on literature information, stratigraphic position and seismic features, Unit 1 is interpreted as the deformed Pliocene substrate of the study area, composed of clays and marls with silty and sandy intercalations. The sedimentary succession lying on the Unit 1 is Quaternary in age.

S1 surface

The S1 surface represents the unconformity bounding the top of the Pliocene succession (Unit 1), and it is clearly recognizable by the truncation of the Pliocene reflectors (Figs. 10-14). This erosional surface crops out close to the coastline (up to 250- 300 m) and gradually dips seaward up to roughly 500 m from the coast, where an abrupt scarp (Scarp 1, see also Curzi and Stefanon, 1986) is recognizable due to the interruption of the underlying succession (Fig. 15). The top of the scarp is at about 10 ms (TWT), and its bottom is at about 25-26 ms (TWT). The total height is about 12 m. The orientation of Scarp 1, reconstructed by the interpretation of the NNE-trending seismic profiles, is parallel to the modern coastline (Fig. 15). The maximum slope of the scarp is 35°-37°. Seaward of the scarp, the S1 surface is seismically expressed by a high amplitude and discontinuous reflector that gradually deepens. Based on literature data and seismic analysis, the S1 surface may be interpreted as a composite surface resulting first by subaerial exposure due to the raising of the Ancona area due to a early-middle Pliocene compressional tectonic phase (Cello and Tondi, 2013), and then by repeated events of wave erosion during late Quaternary time. The early-middle Pliocene tectonic phase generated the major structures of the area, which consist of roughly NW-SE oriented folds (Cello and Coppola 1989) associated with the regional thrusts (Cello and Tondi, 2013). The prominent escarpment (Scarp 1) observed on the seismic profiles and roughly parallel to the coast could be interpreted as a drowned paleo-coastal cliff.

Unit 2

This unit is visible only near the end of the two seismic profiles an_11_11 and an_12_11, (Figs 12-13) where it exhibits a wedge-shaped seismic facies. The internal pattern of the wedge consists of gently seaward dipping reflectors, showing onlap terminations against the basal S1 surface. This wedge-shaped seismic unit includes a semi-transparent upper part, consisting of low amplitude and discontinuous reflectors, and a lower portion composed of sub-parallel, high amplitude, discontinuous and undulated reflectors. This change is probably related to the presence of more fine-grained deposits in the upper part with respect to those present in the lower one. The semi-transparent upper part of Unit 2 seems to be truncated seaward by the S2 surface. The maximum thickness of the unit is about 7-8 m. Unit 2 may be interpreted as a transgressive wedge, probably Pleistocene in age.

S2 surface

This surface represents the top of Unit 2 and merges with the S1 surface landward. The S2 surface is seismically expressed by a high amplitude and continuous reflector that gradually deepens seaward (Figs. 12-13). The deepest part of this reflector shows an articulated configuration characterized by an irregular scarp (Scarp 2, Figs. 12-13)), about 1850-1900 m far from the modern coastline and 5-6 m high in the seismic profile an_12-_11 (Fig. 13). Also the Scarp 2, less prominent than Scarp 1, seems to be oriented parallel to the modern coastline. The distal part of the S2 surface shows a very irregular pattern Scarp 2 might be the result of an incomplete dismantling by waves and/or shelf currents of a previously accumulated prograding wedge, a barrier island or a large-scale bedform in fully subaqueous settings.

Seismic Unit 3

The upper part of t Unit 3 is partially visible along all the sub-bottom profiles orthogonal to the coastline (Fig 10, line an_15_11) and also on the an-16-11 profile (Fig. 14), while its distal part is recognizable only along the two profiles an_11_11 and an_12_11 (Figs. 12- 13). Unit 3 lies both on the Pliocene substrate (Unit 1) and on the wedge-shaped Unit 2. Toward the coast Unit 3 ends against Scarp 1. The top is represented by the S3 surface that is the base of the overlying Unit 4. The thin Unit 3 (up to about 3 m in the distal part of the seismic profiles) consists of parallel, discontinuous, high amplitude and contorted reflectors. These show onlap terminations against the S1 surface in the upper part of the unit, and against Scarp 2 in its deepest part (Figs 10 and 12-13). The distal part of Unit 3, located seaward with respect to Scarp 2, was probably slightly older than the proximal part of the same unit. The distal part of Unit 3 rests on the strongly irregular S2 surface. On the basis of the observed seismic

characteristics, also Unit 3 may be interpreted as a transgressive sedimentary body composed of coarse-grained deposits, probably late Pleistocene in age.

S3 surface

The S3 surface coincides with a high amplitude reflector bounding the top of Unit 3 (Figs 10 and 12-14). It gently dips seaward and onlaps the S2 surface near Scarp 2 (Figs 12- 15). Beyond the scarp, the S3 surface is horizontal.

Seismic Unit 4

Unit 4 is partially visible along all the sub-bottom profiles orthogonal to the coastline (Fig. 10) and also on the an-16-11 profile (Fig.14). It is fully visible only along the two profiles an_11_11 and an_12_11 (Figs. 12-13). This wedge-shaped unit shows an internal configuration consisting of sigmoidal reflectors downlapping the S3 surface with tangential contacts and locally truncated at their upper termination, as highlighted by the irregular configuration of the S4 bounding surface. The sigmoidal reflectors, generally discontinuous and with variable amplitude, onlap the S1 surface landward at Scarp 1. The progressive seaward thinning of Unit 4 is well recognizable in the seismic profiles an_11_11 and an_12_11 (Figs 12-13). The closure of the wedge occurs about 2 km from the coastline, beyond the Scarp 2, and its maximum length along depositional dip is about 1.3-1.5 km. The maximum thickness of Unit 4, close to Scarp 1, is about 10 m. Unit 4 is a clinothem composed of sigmoid clinoforms, resulting from temporary progradation of a sedimentary wedge related to a possible still-stand after the inferred transgressive phase associated with Unit 3. The particular position of the wedge, just seaward of a drowned coastal cliff, suggests that Unit 4 accumulated as a infralittoral prograding wedge (Hernandez-Molina et al., 2000) in fully subaqueous settings.

S4 surface

The seaward-dipping S4 surface is the top of the prograding Unit 4 (Figs 10 and 12-13). The proximal part of this surface is associated with a discontinuous irregular reflector of moderate amplitude, whereas its distal part is a continuous, high amplitude very regular reflector inclined seaward. The irregularity of the proximal part of the surface may be the result of a subaqueous erosion by waves and shelf currents. Landward, the onlap termination of the S4 surface against the relict paleo-coastal cliff Scarp 1 is clearly visible. Seaward, the S4 surface downlaps the S3 surface.

Seismic Unit 5

The Unit 5 lies above the distal part of Unit 4 and is well visible only along in the seismic lines an_11_11 and an_12_11 (Figs. 12-13). The uppermost part of the Unit 5 is visible in the westernmost seismic lines orthogonal to the coast (Fig. 10) and on the an-16-11 profile (Fig. 14). This unit consists of locally contorted, high amplitude and discontinuous reflectors with onlap terminations on the S4 surface and local backlap terminations in the seaward part of the succession. The seismic facies is similar to that of the Unit 3. Unit 5 is up to 4 m thick and progressively thins upslope, although local along-dip thickness changes are found. This unit may be interpreted as a transgressive body probably composed of relatively coarse-grained deposits.

S5 surface

This surface is the top of Unit 5; it consists of a discontinuous, irregular, high amplitude reflector onlapping the S4 surface landward (Figures 10 and 12-14).

Seismic Unit 6

The uppermost unit is wedge-shaped and shows a semi-transparent seismic facies that is locally chaotic. These characteristics suggest that this sedimentary body is mainly composed of relatively fine-grained sediments. The wedge shows a progressive landward thinning, and its maximum thickness, observed near the north-east termination of the seismic lines an_11_11 and an_12_11 (Figures 12-14), is about 13 m. Some thin, high amplitude and discontinuous reflectors onlapping the S1 surface are recognizable in the uppermost part of Unit 6. Moving from proximal to distal locations, Unit 6 rests on the Pliocene succession of Unit 1, on the prograding wedge of Unit 4, and finally on the transgressive body of Unit 5 (Figures 10 and 12-14). The deposits of Unit 6 very probably represent the proximal part of the late Holocene

highstand wedge, which is better developed further seaward

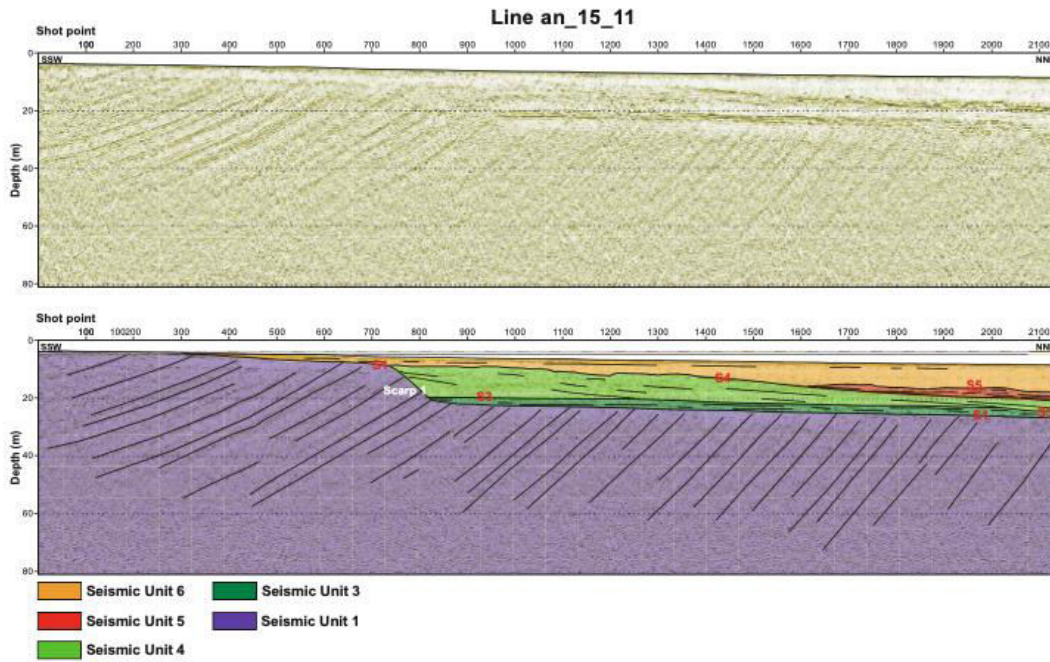


Figure 10. Seismic interpretation of the Line an_15_11 orthogonal to the coast.

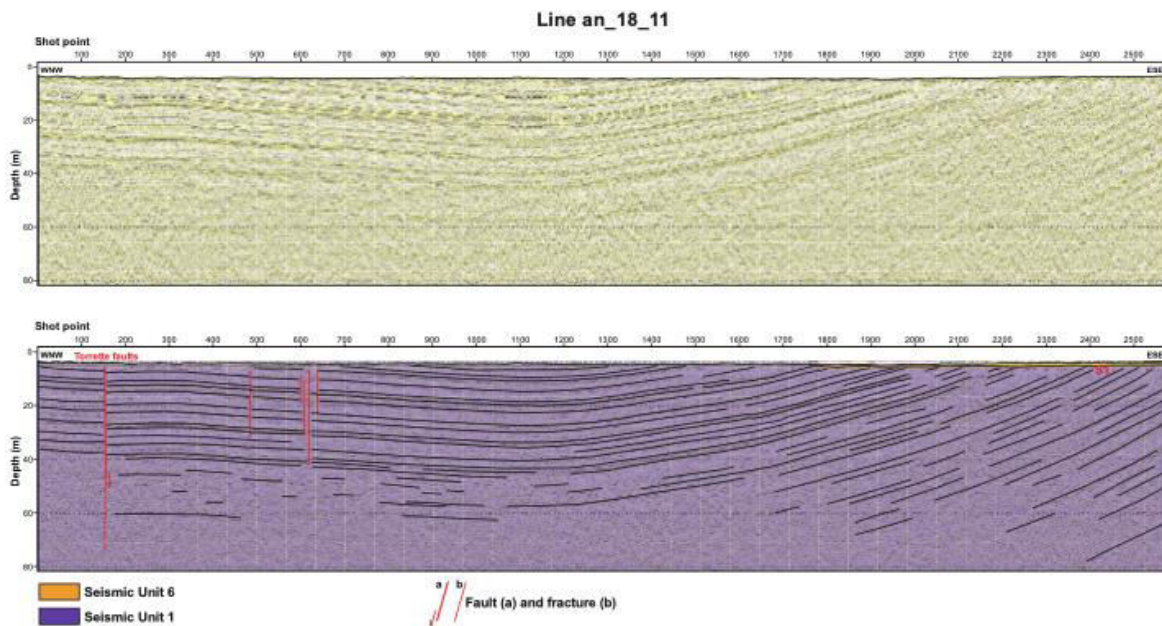


Figure 11. Seismic Interpretation of seismic line an_18_11 parallel to the coast

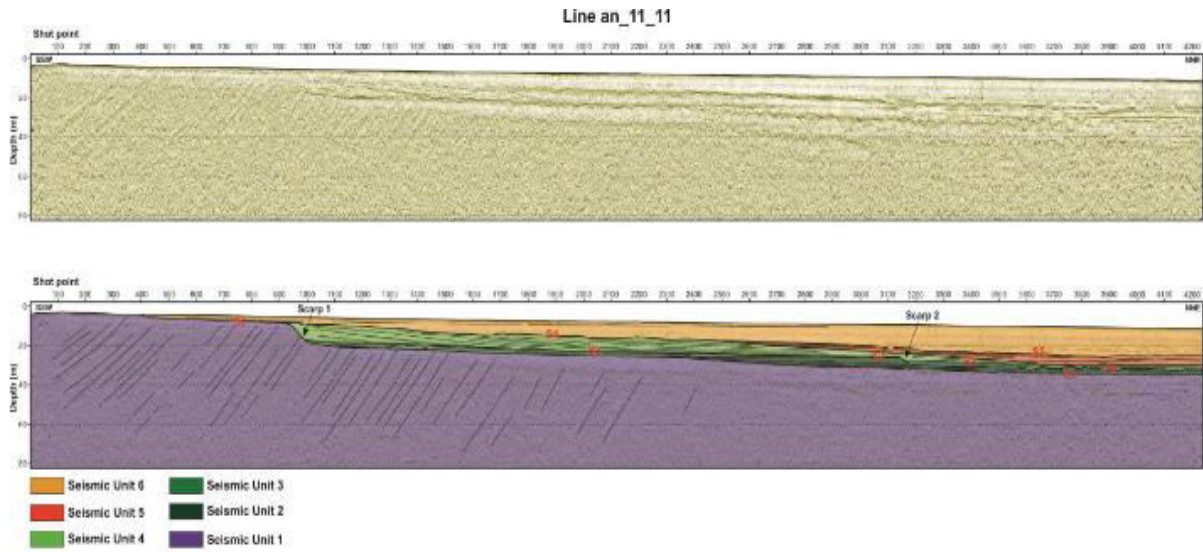


Figure 12. Seismic interpretation of seismic line sn_11_11 orthogonal to the coast

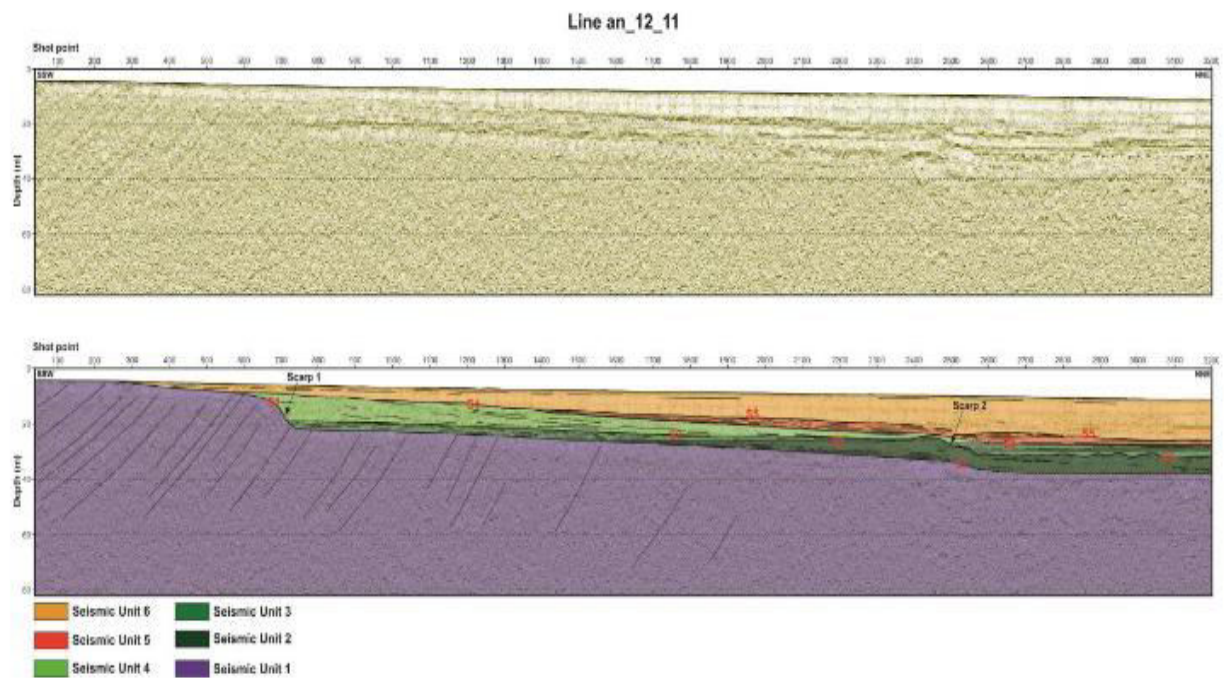


Figure 13. Interpretation of the seismic line an_12_11 orthogonal to the coast.

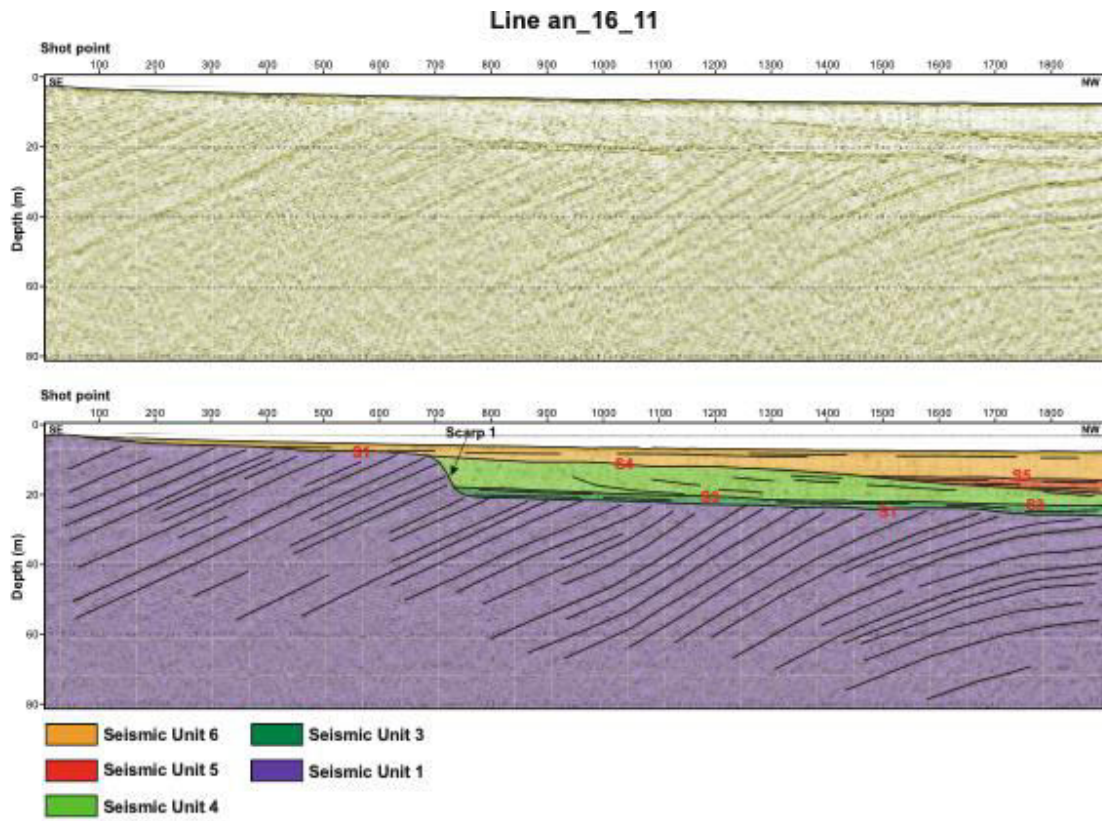


Figure 14. Interpretation of the seismic line an_16_11 (see Fig.1)

Evolutionary model

Overall, Units 2-6 are inferred to record a punctuated transgression followed by a highstand phase, probably associated with the post Last Glacial Maximum (LGM, ca. 20 ks B.P.) glacio-eustatic sea-level rise.

In particular, the S1 surface, recording a first marine transgression in the study area above a Pliocene substrate, consists of a wave-ravinement surface (WRS) reworking an older subaerial unconformity (SU) (e.g., Zecchin et al., 2019). The lower part of Unit 2 very probably consists of a transgressive sand sheet, whereas the present evidence prevents a conclusive interpretation for the upper part of the same unit. It might consist of a remnant of a prograding wedge later mostly eroded, testifying temporary relative sea-level (RSL) still stand or slow rise and modest shoreline regression. The upper part of Unit 2 might alternatively consist of relict large-scale bedforms (e.g., Trincardi et al., 1994), such as transgressive sand ridges, or a barrier island (e.g., Storms et al., 2008). These uncertainties highlight that reconstructing the position of the shoreline during the accumulation of Unit 2 remains uncertain.

The S2 surface and Unit 3 document a further landward movement of the shoreline, which was located near the base of a receding coastal cliff. The S2 surface consists of a newest segment of WRS, which merges with the S1 surface landward. Unit 3 is interpreted as a transgressive sand sheet accumulated in front of the receding coastal cliff. The coastal cliff was later overstepped (Zecchin et al., 2011, 2019), drowned and smoothed by wave action (the currently recognizable Scarp 1) probably during a phase of faster RSL rise (i.e., a melt-water pulse episode; Fairbanks, 1989), which continued to promote shoreline transgression. Probably during an immediately subsequent phase of slower landward retreat of the shoreline or even an episode of slow shoreline regression, possibly associated with decreasing rates of RSL rise, the accumulation of the infralittoral prograding wedge (Unit 4) at the toe of the drowned paleo-coastal cliff started. It should be remarked that the accumulation of Unit 4 does not necessarily reflect regression as it was detached from the local shoreline. The unit accumulated by offshore sediment bypass and/or lateral (along strike) sediment transport by shore-parallel currents as observed for the present day northern Adriatic Sea (Cattaneo et al., 2007).

Unit 5 has the appearance of a transgressive sedimentary body associated with sediment bypass, resulting in the accumulation of a healing-phase wedge on the underlying prograding wedge (Posamentier and Allen, 1999). Finally, Unit 6 is correlatable with the late Holocene highstand subaqueous wedge that characterizes the northern and middle Adriatic off the Italian

coasts (Cattaneo et al., 2007). This implies that Unit 5 represents the latest transgressive deposit, and that the S5 surface, merging landward with the S4 surface, represents a composite maximum flooding surface (MFS).

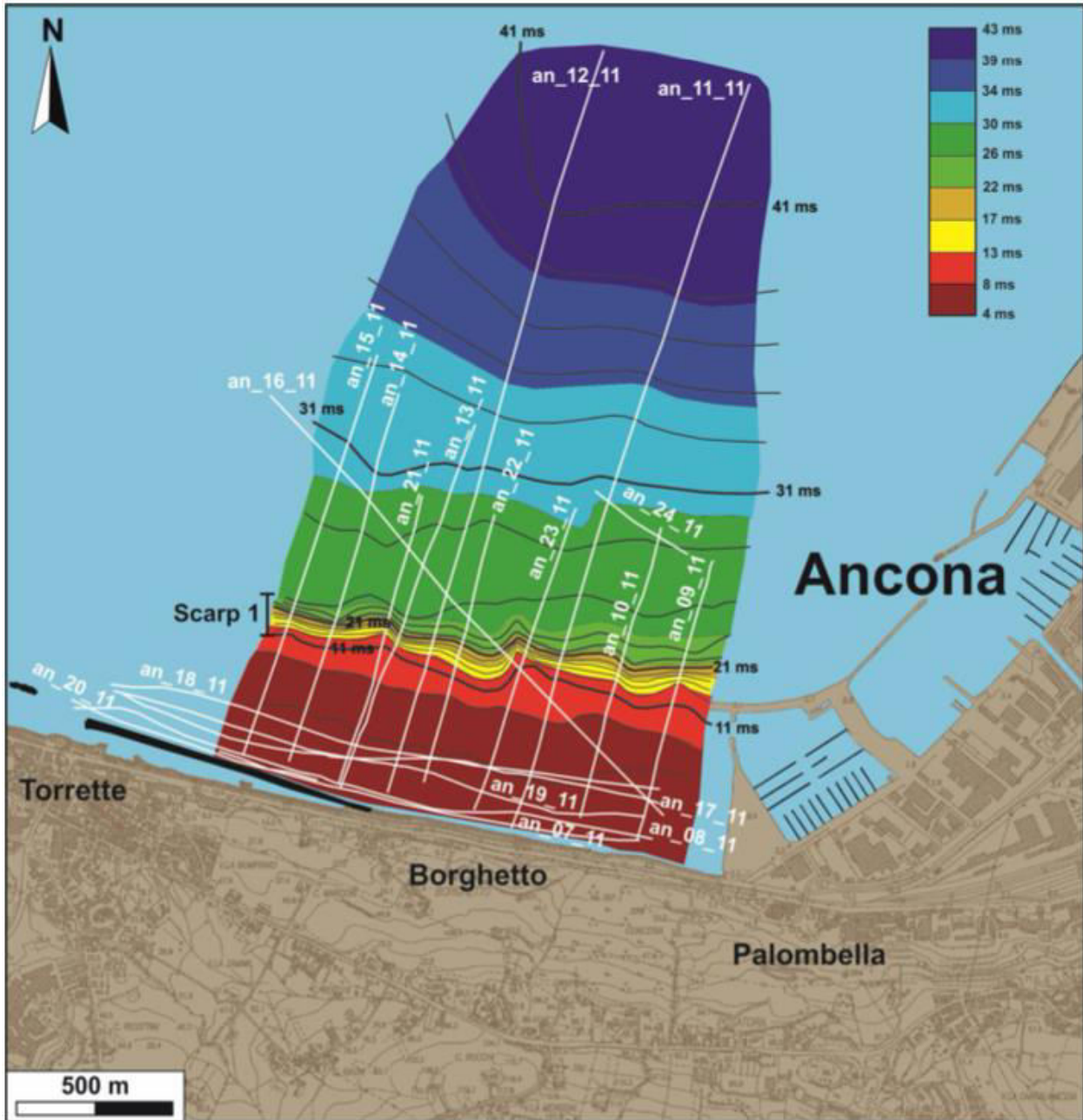


Figure 15. Map of the S1 surface representing the unconformity bounding the top of the Pliocene succession.

3.2.2 Multibeam data

The survey area is a 1 nautical miles long strip along the coast from the touristic harbour “Marina Dorica” toward west. In 1982 along the coast close to this area, there was a strong landslide that created great damage.



Figure 16. Survey area

The "OGS-IRI" boat, owned by the National Institute of Oceanography and Experimental Geophysics – OGS, was used to carry out the survey, duly registered under no. TS550 of the Registers of minor ships of the Port Authority of Trieste. The multibeam transducer (MBES) was installed on a side pole totally aligned with the inertial system (MRU) and the GPS antenna, as described in Figure 17.



Figure 17. OGS-IRI TS550

Model	BSC 50 Colzani Sas
Length	4.93 m
Width	2.29 m
Draft	0.30 m
Engine	Suzuki 40 Hp
Scientific instruments	<ul style="list-style-type: none"> - GPS Topcon NET G3A - Multibeam Reson 7125 - Sound Velocity Profiler Reson SVP 71 - Motion Reference Unit IXSEA PHINS

The multibeam echo sounder has revolutionized the whole bathymetry; few tens of years ago, this kind of survey was performed using single beam echo sounder. In this way a grid of runlines was planned and travelled; the acquired data was subsequently interpolated in post processing to obtain a surface. The final resolution was directly linked to the speed of the vessel and to the thickness of the grid, typically from 10 to 100 meters.

The multibeam allows to obtain a full coverage bathymetric map with pixel side of 10 cm. This is achieved using hundreds of simultaneous beam, equidistant on the seafloor with a swath wide angle of 120-165°.

The along-track resolution is directly connected with the speed of the vessel and the ping rate of the sounder; while the across-track resolution is connected with the nadir-depth and the angle of the swath. Both these resolutions are lower than 10 cm.

In table 1, we show a comparison between the resolutions achievable with the single / multibeam technique.

Hectar area with average depth of 10 m	Single-beam	Multibeam
Number of runlines	20	2
Total lenght (m)	2000	200
Time to go (minutes) at 4 knots speed	16	1.6
Ping rate (Hz)	4	30
Beam number	1	512
Number of point detected	4000 (3883)	1.5 M (1491262)
Along track resolution (m)	0.52	0.07
Across track resolution (m)	10	0.11

Table 1. Singlebeam vs Multibeam

Before starting a multibeam survey there are a lot of parameters to set up in the acquisition software.

Ellipsoid	WGS84
Datum	ETRF2000 (2008)
Projection	UTM33 N

To obtain valid data, the software has to know perfectly the right position of the transducer, Motion Reference Unit and GPS. To do this an XYZ reference system has been chosen with origin in MRU position, vertically projected at waterline level. The X-axis is centered on the MRU, Y-axis coincident with the longitudinal axis of the boat, Z-axis vertical with origin on the water line.

Instrument	X	Y	Z
Multibeam Transducer	-0.02	+0.02	-0.58
GPS	-0.02	+0.16	+2.02
MRU	0.00	0.00	0.73

The sound velocity profiles are used to correct the acoustic pulse trajectory in the water. The profile has been performed with the Valeport SWIFT SVP.

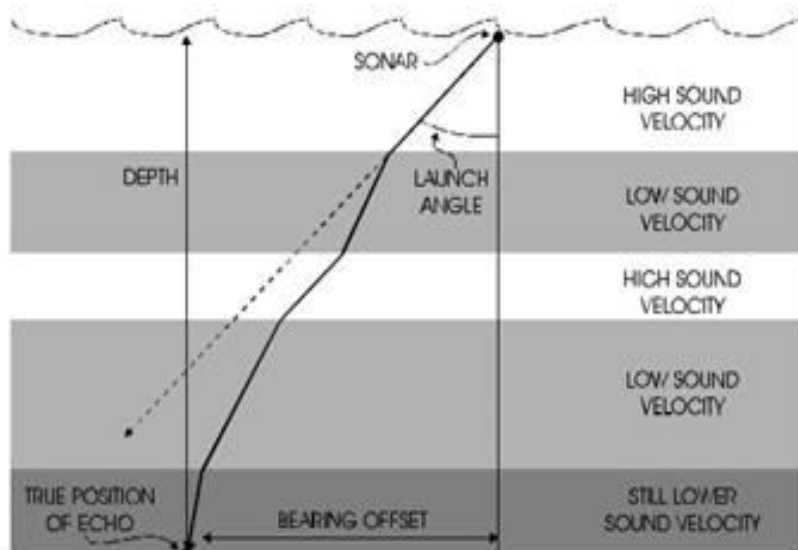


Figure 18. Acoustic pulse path

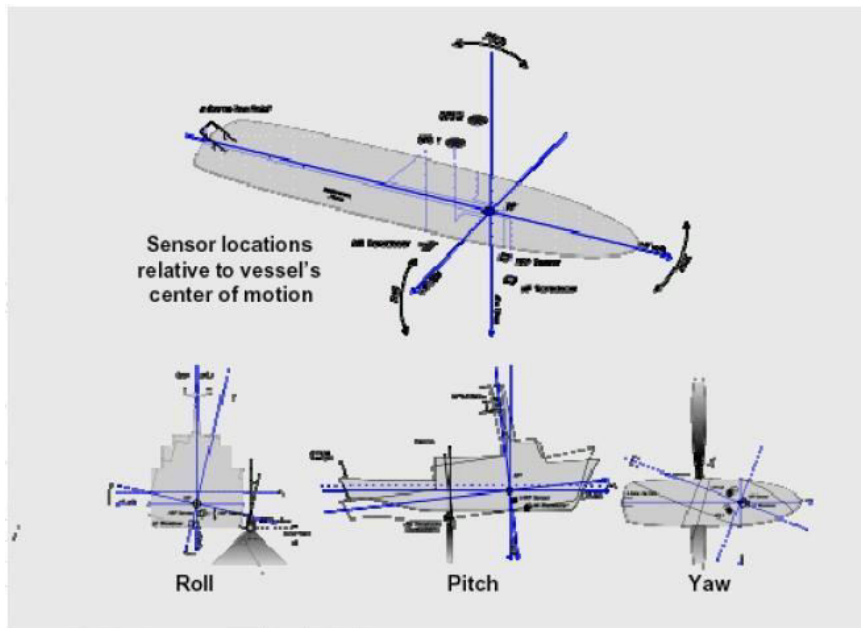


Figure 19. Installation angle in the system XYZ

After setting all the parameters described above, the calibration of the system has to be done. The purpose is to know the installation angles of the transducer, in terms of pitch, roll, yaw, with 0.01° accuracy. To obtain a similar accuracy it is necessary to proceed with an indirect measure. Multibeam data, over a target on the seafloor, have to be acquired along precise runlines. These data are processed by an utility of the acquisition software; different data of the same target are compared so to obtain the mean error. The utility sets an hypothetical angle and then, with successive approximations, generates an error parabolic curve, the minimum value of this curve is the optimal solution for the desired installation angle.

Calibration settings:

Roll	-2.99°
Pitch	$+0.48^\circ$
Yaw	$+0.78^\circ$

In the following figures the software window, with the profiles before and after calibration settings, can be observed; in the right column there are the parabolic errors curves.

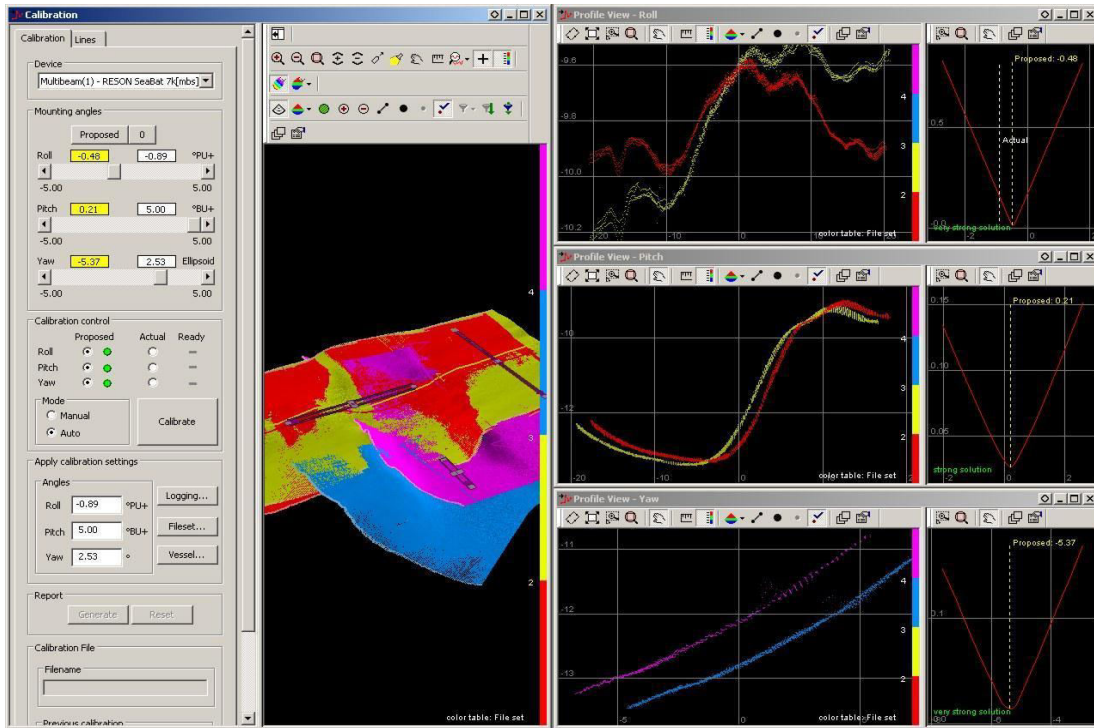


Figure 20. Example: Profiles before calibration - Teledyne PDS

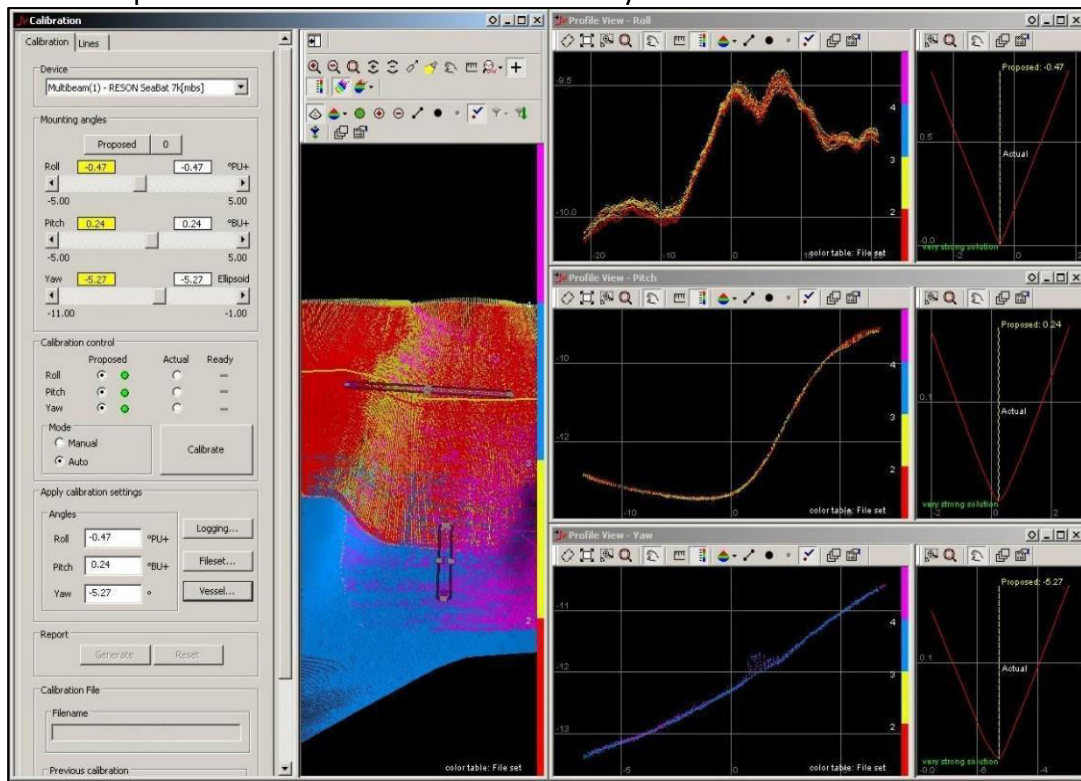


Figure 21. Example: Profiles after calibration - Teledyne PDS

During the data acquisition, the maximum speed of the vessel was always less than four knots, so to get an high along-track resolution of the final data with an overlap, between runlines, constantly above 20%.

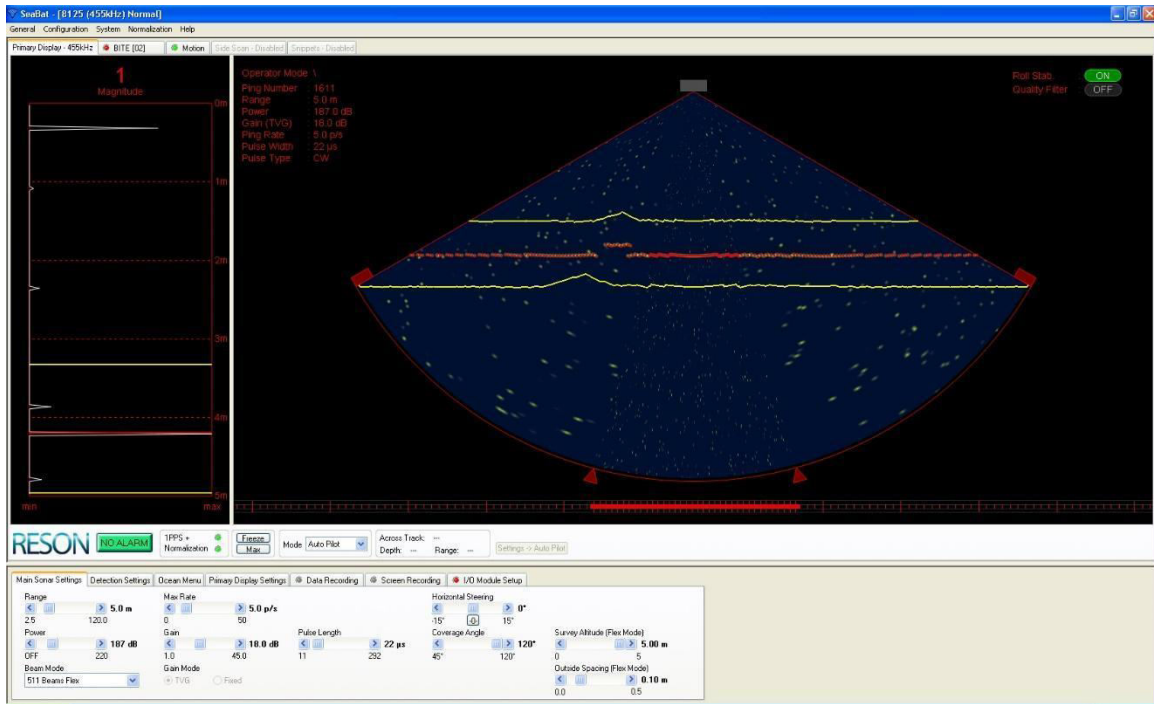


Figure 22. Control system Reson 7125

The barometric data, expressed in hPa, were obtained from the archive of Ancona Station, belonging to the National Tidegauge Network of “Istituto Superiore per la Protezione e la Ricerca Ambientale – Ispra”.

UTC Time	8 th june 2021	9 th june 2021
0	1016.9	1016.2
1	1016.7	1016.0
2	1016.5	1015.9
3	1016.8	1015.8
4	1017.0	1015.7
5	1017.2	1015.9
6	1017.3	1016.2
7	1017.6	1016.3
8	1017.5	1016.6
9	1017.7	1016.9
10	1017.2	1016.9
11	1017.2	1017.1
12	1016.8	1016.8
13	1016.0	1016.4
14	1016.0	1015.7
15	1016.0	1015.6
16	1015.8	1015.1
17	1015.8	1015.2
18	1016.0	1015.4
19	1016.0	1015.6
20	1016.2	1016.3
21	1016.2	1016.6
22	1016.3	1016.4
23	1016.2	1016.3

Table 2. Barometric data

Sound velocity profile.

Date	UTC time	File SVP
8 th June 2021	14:30	20210608SVP01-1430
9 th June 2021	15:27	20210609SVP01-1527
9 th June 2021	16:30	20210609SVP02-1630

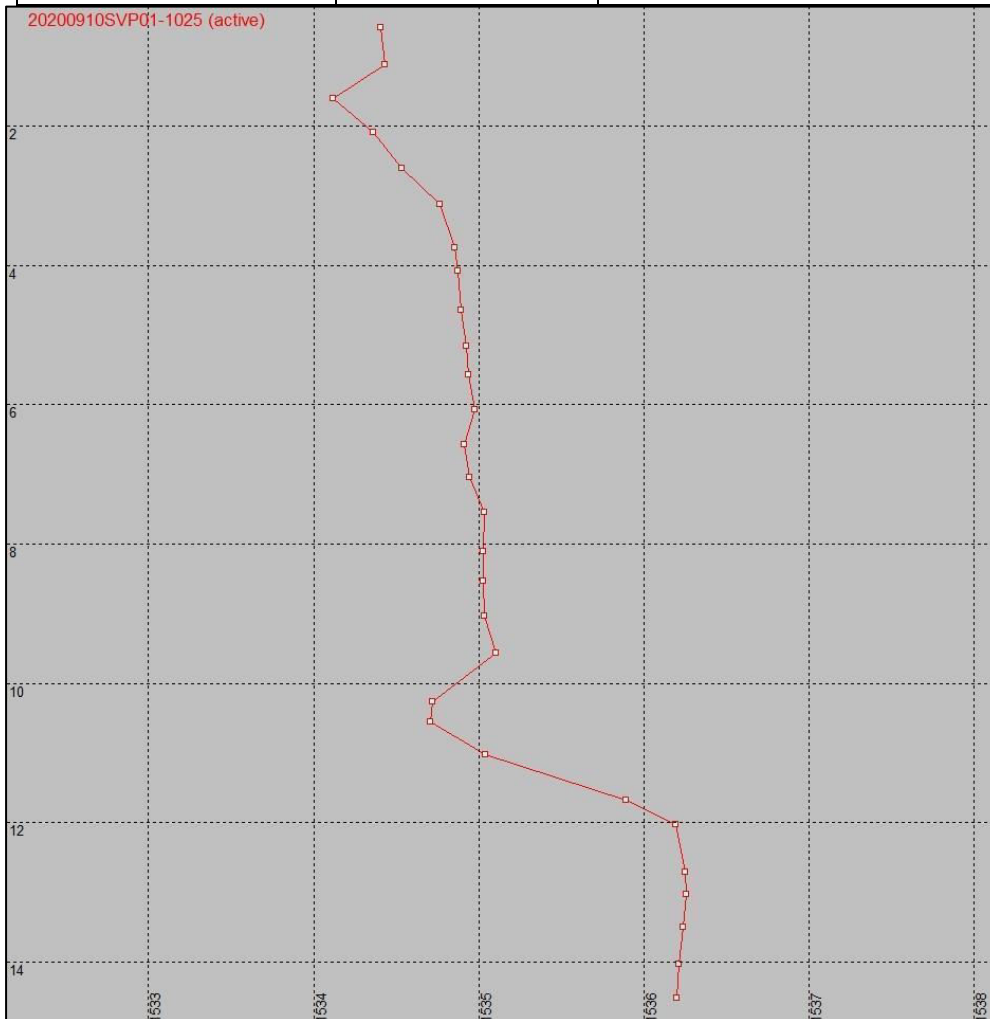


Figure 23. Example of *Sound Velocity Profile*Data Processing

All the bathymetric data have been corrected using official tidal data of Ancona Station, belonging to the National Tidegauge Network of “Istituto Superiore per la Protezione e la Ricerca Ambientale – Ispra”.

The station is located in the “S. Primiano” dock, north pier. The tidegauge station is equipped with altimetric datum. Each datum is referred to the average sea level, measured in Genoa using the ancient Thompson tidegauge. The datums are metallic check tags, used to determinate the altimetric level by means of high precision levelling, following the guidelines fixed by IGM (Italian Military Geographic Institute).







From 16/10/2009 the “hydrometric level” is measured with a new high precision radar sensor SIAP+MICROS TLR .

The data, downloaded from ISPRA web site www.mareografico.it, have been imported in the acquisition software Teledyne PDS, to obtain a full interpolated tidal curve.



Figure 24. Example: tidal correction – Teledyne PDS

Tide station characteristics:

 <p>ISPRA Istituto Superiore per la Protezione e la Ricerca Ambientale</p>	<p>Rete idrografica e mareografica nazionale LIVELLAZIONE DI ALTA PRECISIONE</p>	<p>Rilievi anno 2009 - 2010</p>	<p>Stazione mareografica di Ancona</p>
<p>ORIGINE IGM Csv: 0010_151 Punto GPS: 118705</p>		<p>Annotazioni: il csv mareografico ISPRA è stato misurato utilizzando la stadietta invar da 60 cm. con staffetta di sospensione (vedi foto laterale)</p>	
<p>CSO MAREOGRAFICO Coordinate piane UTM - ETRF 2000 N: 4831293.139 E: 379486.390 Quota s.l.m.: m. 1.5376 quota italgco 2005: m. 2.883 Bullone in acciaio inox murato sullo scalino lato sinistro della cabina</p>			
<p>CSV MAREOGRAFICO Quota s.l.m.: m. 3.5655 Piastra mensolata murata sulla parete a destra della porta di accesso alla cabina mareografica</p>			
<p>STAFFA MAREOGRAFICA Quota s.l.m. 1998: m. 1.5037 Quota s.l.m. 2009: m. 1.5170 Differenza di quota $\Delta = 0,01330$ Staffa in acciaio murata sul boccaforno del pozzo di calma lato destro entrando nella cabina mareografica</p>			
<p>CSO 3 DI LINEA ISPRA Quota s.l.m.: m. 2.4876 Bullone in acciaio inox murato sul cordolo di fondazione della parete ovest di un edificio</p>			

Quality control

The acquisition and processing software has a tool with the following automatic filters, which can be set during the survey, for the data quality control:

Beam Quality, detects and deletes beams with a bad quality level;

Depth, detects and deletes beams out of depth range settings;

Statistic, detects and deletes beams out of statistic settings;

Beam reject, deletes beams;

Range, detects and deletes beams out of range settings;

Nadir, detects and deletes beams out of angle range;

Slope, detects and deletes beams that generate an irregular slope on the seafloor;

Intersect, detects and deletes beams with a not tolerated intersection angle;

Flying object, detects and deletes beams referred to objects too high on the seafloor;

IHO error, detects and deletes beams with not tolerated IHO precision values;

Custom error, detects and deletes beams with vertical propagation errors.

All these filters do not delete or modify the original data, so the operator can always choose and change the filter settings to reach the optimal result.

During acquisition and post-processing only the Beam quality filter has been applied.

Afterwards the data has been manually controlled so to avoid software detection errors.

The manual data process is performed by a slowly data replay, with different points of view so to detect spikes and anomalies.

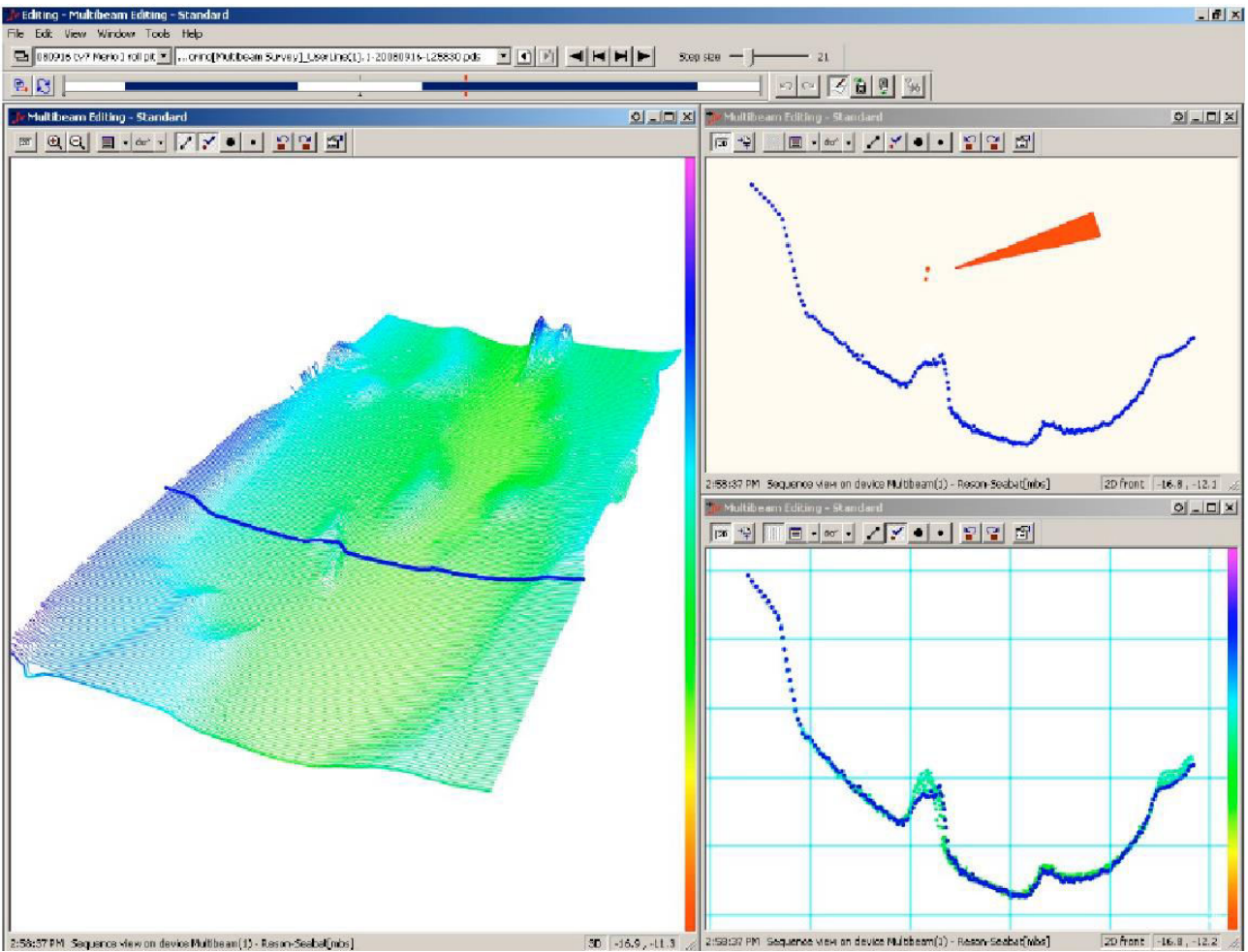


Figure 25. Data manual editing – Teledyne PDS

Data Terrain Model

The last step of post processing is the 3D Data Terrain Model creation. To this purpose a square cell dimension is set and then all the points, inside the square cell, are averaged to obtain a DTM made by a point cloud with constant density.

DTM with square cell of 1 m have been created.

In the following table average depth and density are indicated.

Area (km ²)	Hit count (millions)	Average depth (m)	Average density (points/m ²)
0.91	111	4.8	122

Table 3. Average depth and density

Final results:

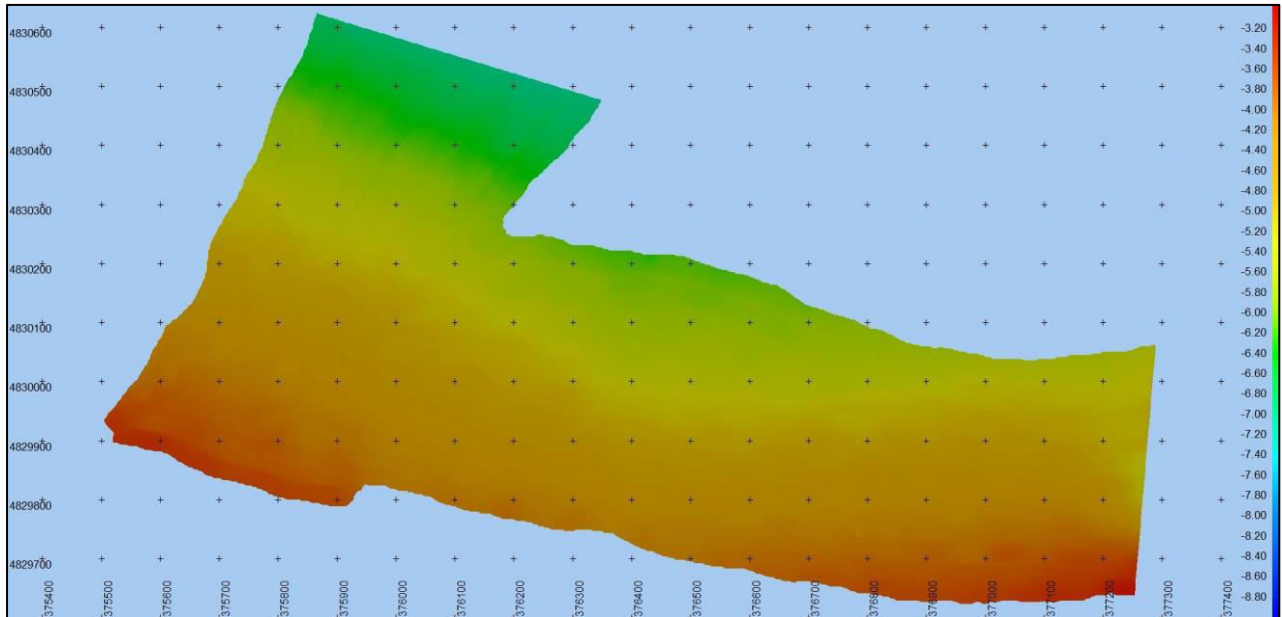


Figure 26. Final DTM cell 1 m

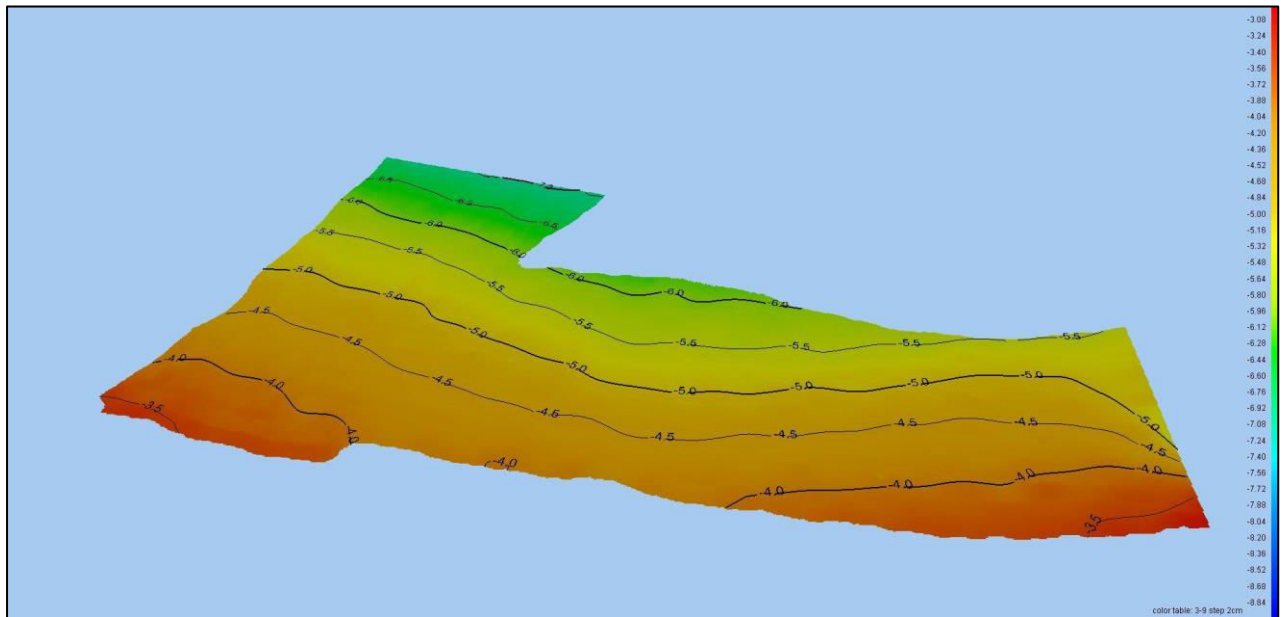


Figure 27. Final DTM 3D

3.2.3 Macropaleontological analysis

For this study we considered samples of sediments taken from two boreholes. The first borehole, **SM1**, is located in Marina Dorica (Ancona) with Gauss Boaga coordinates N 2397134; E 4829501, with an elevation of -0.00 m a.s.l.. The well is 80 m deep. The second borehole ST1 is located in Posatora (Ancona) with Gauss-Boaga coordinates N 239753.075; E 4829010.641 and an elevation of 60.9 m a.s.l.. The well is 150 m deep.

The core sampling was performed in the parts of the well where lithological changes in the sediments occur.

Each sample was taken in 2 cm thick slices. When archiving the samples, information regarding the presence of biogenic (shells, vegetal remains), as well as abiotic material (nodules and mineralisations) was clearly provided on the label as acronyms. Furthermore, structures such as laminations and bioturbations were also detected. Evidence of biogenic material, structures or variations in lithology which identified a lithologic change was captured with digital photos. The laboratory analyses began with the detection of the colour of the sediment samples by means of the *Munsell Soil Chart* (Munsell, 2000). The colour classification was performed on wet sediments. Detecting the colour of the sediments strongly contributes to the recognition of the lithological intervals. Subsequently, per each sample, a lithological description was performed.

Sub-samples from each sediment sample were taken to perform sedimentological and micropaleontological analyses. The remaining part of the samples were preserved to create an archive.

Each sub-sample was put to dry in an oven at 50°C for 24 hours to perform the micropaleontological analysis. The dry samples were weighed and then disaggregated in H₂O₂ (10% vol.) for 12 hours and wet sieved with a sieve shaker (mesh size 63 µm). Finally, also this fraction was dry weighed. The difference between the two weights allowed us to obtain the value in percentage of the sand and silt contents.

The foraminifera were studied in a qualitative way.

We analysed the texture of the samples by computing the percentual composition of the different grain sizes (pipette analysis method). After this, the computed values were compared with the texture triangle (Shepard diagram, Shepard 1954). The results of the granulometric analyses are summarized in Tables 1 and 2, in which the percentages in weight of the main granulometric fractions (clay, silt and mud). In Figures 30 and 31 we show the classification of

the sediments as in Shepard (1954).

For the SM1 core two different stratigraphically subsequent layers were analysed. The first interval ranges from 71.50 to 71.70, while the second one from 73.50 to 73.70. For both intervals, two samples were analysed, the location of which is indicated in Figure 28.

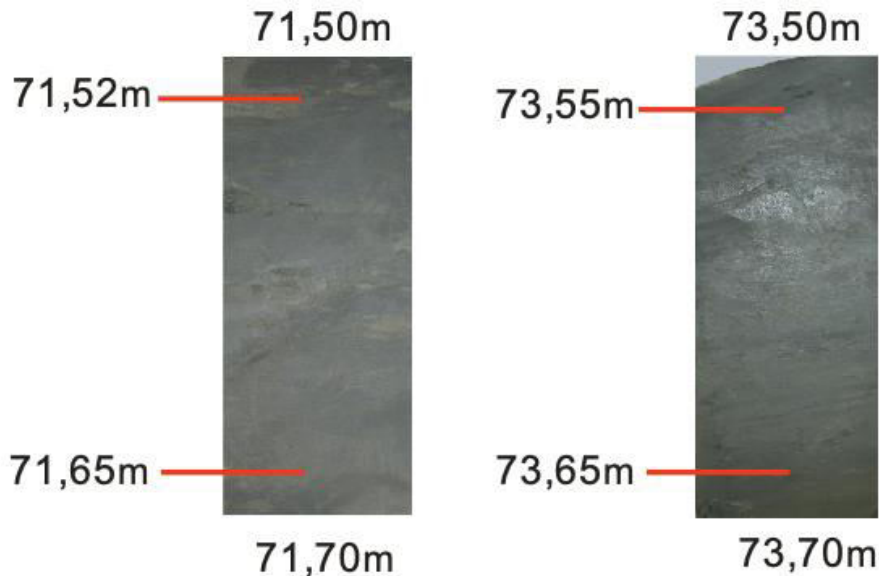


Figure 28. Segments sampled from SM1 core.

Description of the samples from SM1 core.

Interval 71.50-71.70m.

This segment is characterised by silty mud in the base. Above this, sandy mud is present. Furthermore, moving from bottom to top, we observe an increasing presence of levels and light-gray, muddy sand plaques.

Sample at 71.48 m.

Sandy mud, with colour 5Y 3/1 *very dark gray*. Under the microscope, the sediment is characterized by a dominant organic fraction (90%), while the remaining part presents mica and slightly eroded quartz clasts. The organic fraction contains both planktonic and benthic foraminifera, with a dominance of the planktonic one. The main species found for the planktonic family were *Globigerinoides ruber*, *Globigerinoides trilobus*, *Globigerina bulloides*, *Globorotalia scitula* e *Globorotalia bononiensis*. Amongst the benthic are *Bigenerina nodosaria*, *Lenticulina* sp., *Cibicides lobatulus*, *Bolivina dilatata*, *Spiroloculina* sp. e *Melonis* sp..

Furthermore, some fraction of badly preserved, thin and very fragmented lamellibranche and remainders of vegetal frustules.

Age of the sediment: Mid-Pliocene.

Sample 71.65m

Sandy mud, with colour 5Y 3/1 *very dark gray*. Under the microscope, the sediment is characterised by a dominant organic fraction (90%), while the remaining part presents mica and slightly eroded quartz clasts. The organic fraction contains both planktonic and bentonic foraminifera, with a dominance of the planktonic one. Amongst the planktonic foraminifera we identify *G. ruber*, *G. trilobus*, *G. bulloides*, *G. scitula*, *G. bononiensis*, *Neogloboquadrina pachiderma*, *Orbulina universa* e *Hastigerina siphonifera*, while among the bentonic *Bigenerina nodosaria*, *Lenticulina* sp., *C. lobatulus*, *B. dilatata*, *Fursenkoina* sp., *Florilus boueanus* e *Spiroloculina* sp..

Furthermore, abundant vegetal frustules are present. Age of the sediment mid Pliocene.

Interval 73.50-73.70m.

This segment is characterized by sandy mud at the base transitioning to silty mud moving upwards. Furthermore, from bottom to top we observe and increasing presence of levels and light-gray, muddy sand plaques.

Sample at 73.55 m

Silty mud, color 5Y, 4/1, *dark gray*. Under the microscope, the sediment is characterized by a dominant organic fraction (90%), while the remaining part presents mica and quartz clasts. The organic fraction contains both planktonic and bentonic foraminifera, with a dominance of the planktonic one. Amongst the planktonic foraminifera we identify *G. ruber*, *G. trilobus*, *G. bulloides*, *G. scitula*, *G. bononiensis*, *O. universa* e *N. pachiderma*, while among the bentonic we identify *B. nodosaria*, *Lenticulina* sp., *Cibicides* sp., *B. dilatata*, *Textularia conica*, *Fissurina* sp., *Spiroloculina* sp. e *Melonis* sp..

Furthermore, few ostracods and remainders of vegetal frustules are present. Age of the sediment: mid.Pliocene.

Sample at 73.65m

Sandy mud, color 5Y, 5/1 gray. Under the microscope the sediment appears well classified with 20% organic fraction. The remaining fraction presents mainly mica and quartz clasts. The organic fractions contains small-size foraminifera. Among the planktonic family we identify *G. bulloides*, *G. scitula*, e *N. pachiderma*, while among the bentonic, which are quite scares, we identify *B. nodosaria*, *Cibicides* sp., *B. dilatata*, *T. conica*, *Fissurina* sp., *Spiroloculina* sp. e *Melonis* sp..

Due to the overlap of the age of the microfossils it is not possible to estimate an exact age of the sediment. We can assume it is Mid-Pliocene.

For core ST1 three lithological segments were taken, in stratigraphic succession, from which we extracted two samples, as shown in Figure 29.

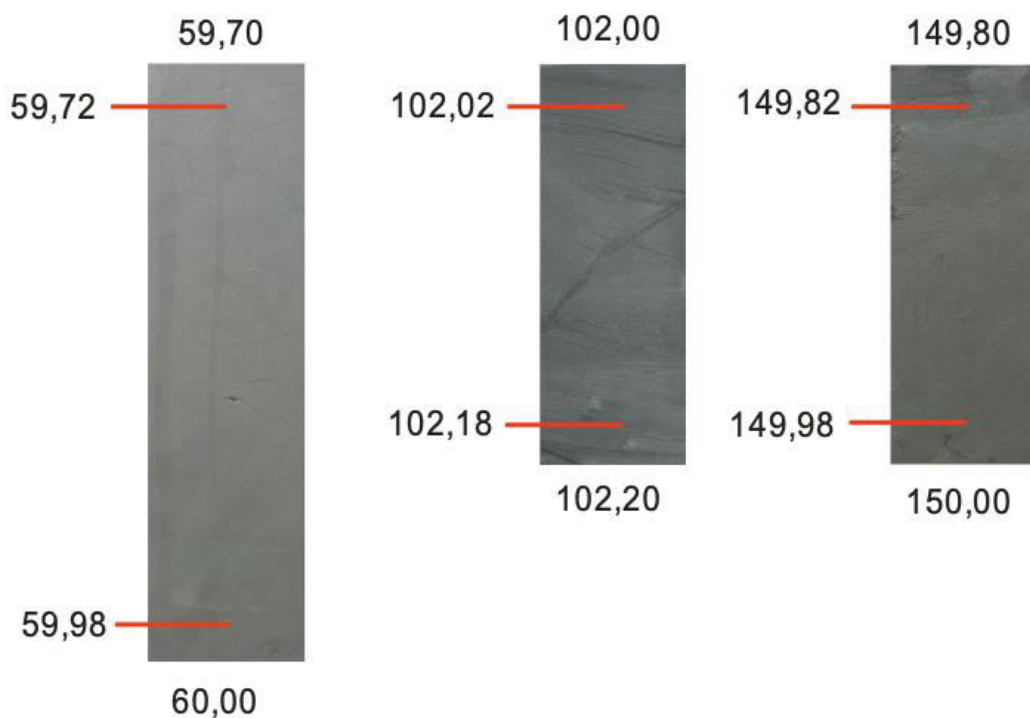


Figure 29. Three segments from core ST1. The first is 30 cm long, while the other two 20 cm long.

Description of the samples from core ST1.

Interval 59.70-60.00 m.

This segment is characterized by homogenous silty mud, with small plaques of sandy mud.

Sample at 59.72 m.

Silty mud, color 5Y 4/1 *dark gray*. Under the microscope, the sediment is characterized by an organic fraction of 30%. The remaining inorganic part is composed mainly of mica and quartz clasts. In the organic part the component of planktonic foraminifera prevails on the bentonic one. Among the planktonic foraminifera we identified: *G. bulloides*, *G. ruber*, *G. trilobus*, *Globorotalia scitula* e *O. universa*, while among the bentonic we identify *Bolivina alata*, *Lenticulina* sp., *C. lobatulus*., *B. dilatata*, *Florilus* sp., e *Melonis* sp.. Furthermore, small aggregations of fromboidal pyrite and remainders of vegetal frustules are present.

Age of the sediment: Lower Pleistocene. Sample at 59.98 m.

Silty mud, color 5Y 4/1, *dark gray*. Under the microscope, the sediment is characterized by a very scarce organic fraction, composed mainly by planktonic foraminifera. The organic fraction is also generally strongly mineralized and we detected fromboidal pyrite.

The sample is characterized by insufficient micropaleontological markers to state a precise age.

Interval 102.00-102.20

This segment is characterized at the base by muddy sand / sandy mud which towards the top transitions to sandy mud. Furthermore, from bottom to top we see an increasing presence of crossed laminations, locally subject to convolutions. Furthermore, in the upper part, small worm-shaped bioturbations are present.

Sample at 102.02 m.

Sandy mud, colo 5Y 4/1, *dark gray*. Under the microscope, the sediment shows an organic fraction of 60%. The remaining inorganic part consists mainly of mica and quatz clasts. The organic component consists mainly of small foraminifera. Among the planktonic foraminifera we identify *G. bulloides*, *G. ruber*, e *G. trilobus*, while among the bentonic we identify *B. nodosaria*, *Cibicides* sp., *B. alata*, *B. dilatata*, *T. conica*, *Florilus* sp., *Elphidium complanatum*, *Elphidium advenum* e *Melonis* sp..

Due to the rehashing of the microfossils and the evident sorting of the sediment, we are unable to state a precise age of the sediment. Possibly, Mid- to Lower-Pleistocene.

Sample at 102.18 m.

Sandy mud / muddy sand, color 5Y 4/1 *dark gray*. Under the microscope, the sediment is characterized by an organic fraction of more than 90%. The remaining inorganic part consists of mica and generally slightly eroded quartz clasts. In the organic component, the fraction of planktonic foraminifera prevails on the bentonic one. Among the planktonic foraminifera we identify *G. ruber*, *G. trilobus*, *G. bulloides*, *G. scitula*, *G. bononiensis*, *N. pachiderma*, *O. universa* e *H. siphonifer*, while among the bentonic *Bigenerina nodosaria*, *Lenticulina* sp., *C. lobatulus*, *B. dilatata*, *Fursenkoina* sp., *F. boueanus*, *T. conica*, e *Spiroloculina* sp..

Furthermore, abundant remainders of vegetal frustules are present.

Age of the sediment: Mid-Pliocene.

Interval 149.8-150.0 m

This segment is characterized by sandy mud with levels of silty mud. In the upper part of the segment small fragments of thin shells of unidentifiable mollusca are present.

Sample at 149.82 m

Muddy sand, color 5Y 4/2 *olive gray*. Under the microscope, the sediment is characterized by an organic fraction of 60%. The remaining inorganic fraction is composed of mica (30%) and quartz. In the organic part, we observe a prevalence of planktonic foraminifera. Among the planktonic foraminifera we observe: *G. ruber*, *G. trilobus*, *G. bulloides*, *Globorotalia crassaformis*, *G. bononiensis*, *Globorotalia* cf. *aemiliana*, *O. universa* e *H. siphonifera*, while among the bentonic *B. nodosaria*, *Dentalina* sp., *C. lobatulus*, *B. dilatata*, *Fursenkoina* sp., *F. boueanus*, e *T. conica*.

Furthermore, abundant remainders of vegetal fructules are present. Age of the sediment: Mid-Pliocene.

Sample 149.98 m

Sandy mud, color 5Y 4/1, *dark gray*. Under the microscope the sediment is characterized by an organic fraction larger than 90%. The remaining inorganic part is composed of mica and slightly eroded quartz clasts. In the organic component we observe a predominant planktonic foraminifera fraction. Among the planktonic foraminifera we observe *G. ruber*, *G. trilobus*, *G. bulloides*, *G. scitula*, *G. bononiensis*, *Globigerinoides obliquus*, *Globorotalia* cf. *aemiliana*, *Globorotalia crassaformis*, *N. pachiderma*, *O. universa* e *H. siphonifera*, while among the

bentonic *B. nodosaria*, *Lenticulina* sp., *C. lobatulus*, *Pullenia quinqueloba*, *B. dilatata*, *Fursenkoina* sp., *F. boueanus* e *Siphonina reticolata*.

Furthermore, abundant remainders of vegetal fructules are present. Age of the sediment: Mid-Pliocene.

Granulometric Analysis

The results of the granulometric analysis of both cores SM1 and ST1 are summarized in Figures 30 and 31 and in Tables 1 and 2. In the latter, for each core, we write the fractions (%) of the main granulometric components (sand, silt, clay) and, finally, the classification as in Shepard (1954).

SM1 Core				
Sample	SM1-A	SM1-B	SM1-C	SM1-D
Depth. m	71.52	71.65	73.55	73.65
Total weight g	76.89	70.50	68.87	46.54
Sand g	4.18	1.25	0.37	2.55
Silt g	47.03	40.22	34.68	31.32
Clay g	25.68	29.03	33.82	12.67
%Sand	5.44	1.77	0.54	5.48
%Silt	61.17	57.05	50.36	67.30
%Clay	33.40	41.18	49.11	27.22

Sample	Classification (Shepard, 1954)
SM1-A	Clay silt
SM1-B	Clay silt
SM1-C	Clay silt
SM1-D	Clay silt

Table 1. Granulometric fractions and classification of the sediment for SM1 core.

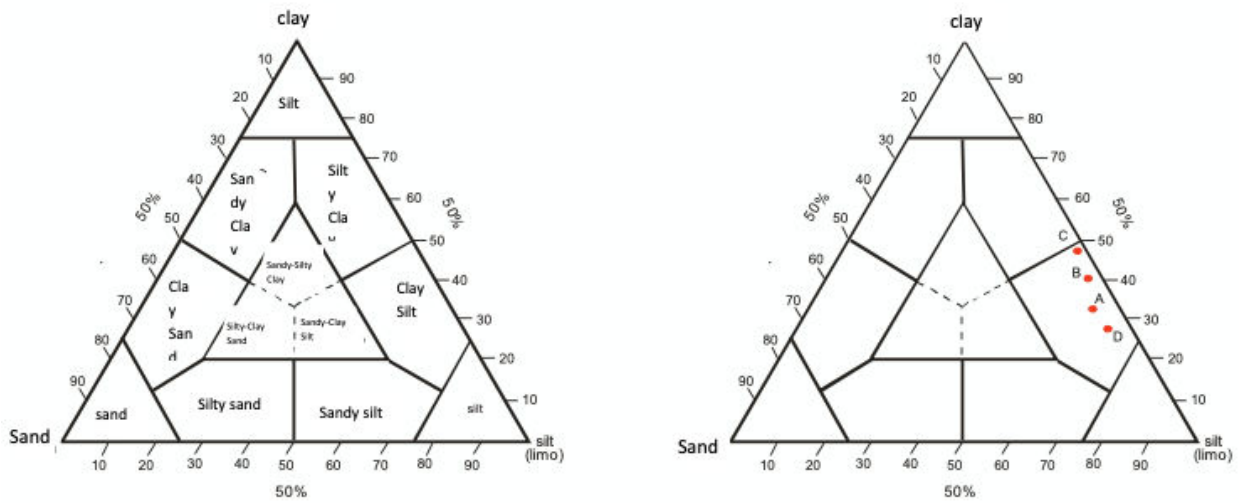


Figure 30. Shepard diagram for the classification of the sediments in SM1 core.

ST1 Core							Sample	Classification (Shepard, 1954)
Sample	ST1-A	ST1-B	ST1-C	ST1-D	ST1-E	ST1-F		
Depth. m	59.72	59.98	102.02	102.18	149.82	149.98		
Weight g	40	40	40	40	40	40		
Sand g	0.41	0.47	2.21	3.13	1,44	1,56		
Silt g	23,22	21,45	22,55	25,41	23,28	22,07		
Clay g	16,37	18,08	15,24	11,46	15,28	16,37		
%Sand	1,03	1,18	5,53	7,83	3,60	3,90		
%Silt	58,05	53,63	56,38	63,53	58,20	55,18		
%Clay	40,93	45,20	38,10	28,65	38,20	40,93		

Table 2. Granulometric fractions and classification of the sediment for ST1 core.

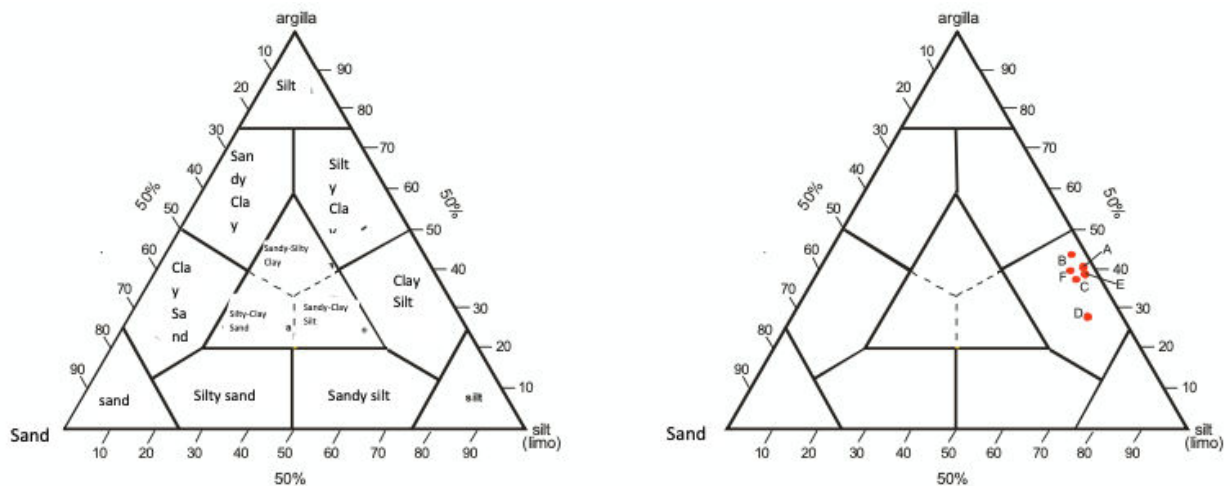


Figure 31. Shepard diagram for the classification of the sediments in ST1 core.

Final Remarks

Even though the examined material represented only a small part of the stratigraphic sequence of the two cores, the analysis of the samples allowed us to define the age of the sediments. In ST1 core, the sample at depth 59.72 m was dated to the Lower-Pliocene. The analysis of the microfossils was accurate enough to also determine levels like the Placentian and the Gelasian. This is an important detail in order to obtain a larger chrono-stratigraphic differentiation. Furthermore, in samples ST1 59.98 and ST1 102.02, the microfossils were subject to rehash. This indicates that the sedimentation environment was quite dynamical and that small landslides and/or turbidity currents occurred. Results of the granulometric analysis show that all the samples can be classified as clay silt. However, a few interesting dispersions are present, like in sample SM1-D, caused by the presence of sandy levels. Also, these analyses allow us to recognise along the sedimentary sequence an evolution in the deposition of the sediments which are subject to small inputs from turbidity currents and small landslides.

References

- MUNSELL COLOR COMPANY (BALTIMORE). 1988. Munsell soil color charts. *Macbeth*.
- Shepard, F.P.. 1954. Nomenclature based on sand-silt-clay ratios. *Journal of Sedimentary Petrology*, **24**, 151-158.

4. Bibione – Italy

4.1 Land data

4.1.1 Electrical resistivity data

This section contains a summary description of the processing activities of two-dimensional electrical resistivity tomography (ERT) measurements acquired during the spring 2020 exploration campaign in the two Bibione sites (Italy – Figure 1).



Figure 1. Map of the two investigated areas in Bibione (Export from G.E. Pro)

The data processing involved a total of two data sets acquired with different electrode configurations:

1. Dipole-Dipole measurements acquired on a surface 2D profile of 45 electrodes spaced 5 meters. The Line is approximately N-S oriented and orthogonal to the shoreline (ERT1 - Figure 2a).
2. Dipole-Dipole measurements acquired on a surface 2D profile of 60 electrodes spaced 3 meters. The Line is approximately N-S oriented and orthogonal to the shoreline (ERT2 - Figure 2b).

The data consists of a total of approximately 3060 measures (ERT1) and 5100 measures (ERT2). Resistivity data were collected using a new-concept georesistivimeter Multi-Source System (MSS)

a)



b)

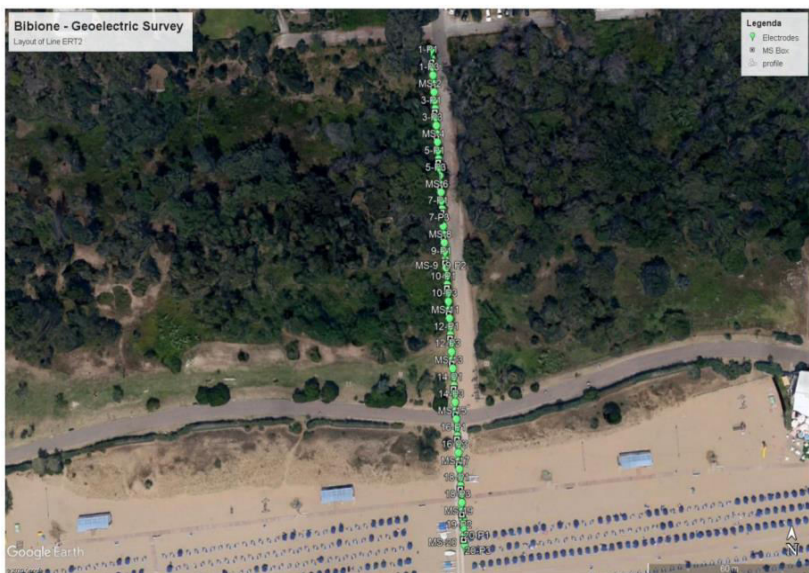


Figure 2. Map of the ERT surveys in Bibione: ERT1 (a) and ERT2 (b).

(<http://www.mpt3d.com> – Multy-Phase Technology). The MSS System comprises several stand-alone transceivers synchronized via GPS timing and controlled via a 900 MHz radio signal (Wireless Protocol). Each transceiver (indicated as MS Box in Figure 2) is capable of handling a maximum of three electrodes. It is worth to notice that with this peculiar design transmitting and receiving dipoles must belong to different units. The peculiar and innovative feature of this system, beyond the wireless communication between units, is its capability of transmitting the current simultaneously with multiple dipoles, each one connected to a different transceiver.

Both profiles were designed gathering the units in different blocks each one comprised of 5 units. Figure 3 shows the blocks-scheme of the acquisition for both profiles. The profile ERT1 was acquired using 3 blocks (three shifts), while 4 blocks were used for profile ERT2 (four shifts). The total survey length was of 220 m for ERT1 and 177 m for ERT2. The surveys were designed to image the shallow structure of the subsoil, providing a maximum theoretical depth of investigation of about 40 m and 30 m, respectively.

a)

ERT 1

TX-RX	Box Block #1					Box Block #2					Box Block #3				
b1-b2	1	2	3	4	5	6	7	8	9	10					
b1-b3	1	2	3	4	5						6	7	8	9	10
b2-b3						1	2	3	4	5	6	7	8	9	10
Distance (m)	10	25	40	55	70	85	100	115	130	145	160	175	190	205	220

b)

ERT 2

TX-RX	Box Block #1					Box Block #2					Box Block #3					Box Block #4				
b1-b2	1	2	3	4	5	6	7	8	9	10										
b1-b3	1	2	3	4	5						6	7	8	9	10					
b2-b3						1	2	3	4	5	6	7	8	9	10					
b2-b4						1	2	3	4	5						6	7	8	9	10
b3-b4											1	2	3	4	5	6	7	8	9	10
Distance (m)	6	15	24	33	42	51	60	69	78	87	96	105	114	123	132	141	150	159	168	177

Figure 3. Blocks scheme adopted during the acquisitions. The block distance is computed using a spacing of 5 m for ERT1 (a) and a spacing of 3 m for ERT2 (b).

The geoelectric datasets show good values of the measured electric potentials. The average apparent resistivity value is around 11.8 Ohm*m for ERT1 and 75.4 Ohm*m for ERT2. This difference is mainly due to the different settings of the two surveys. Both Lines are located close to the shoreline, as shown in Figure 1. However, the former is located at the extremity of the peninsula, and the sea is very close at both sides, north and south. For the latter, instead, the shoreline is present only on the south.

Preliminarily to the inversion procedure for the production of the resistivity model (imaging), the dataset must be subjected to a quality control. We removed approximately 47% of the total quadrupoles of Line ERT1, and approximately 43% of the total quadrupoles of Line ERT2.

- | | | |
|--|----------|-----------|
| Removal | criteria | included: |
| - Removal of the reciprocal measurements. | | |
| - Elimination of measurements with instrumental standard deviation (obtained through multiple measurement stacks) larger than 10%. | | |
| - Removal of the receiver potentials V lower (in absolute value) than 0.01 mV. | | |
| - Filtering of negative apparent resistivity values. | | |

Figure 4 shows the histogram of the statistical distribution of potentials, currents and the same apparent resistivities after filtering the noisy and the reciprocal measurements. The negative apparent resistivities, admitted only in 3D surveys, were filtered.

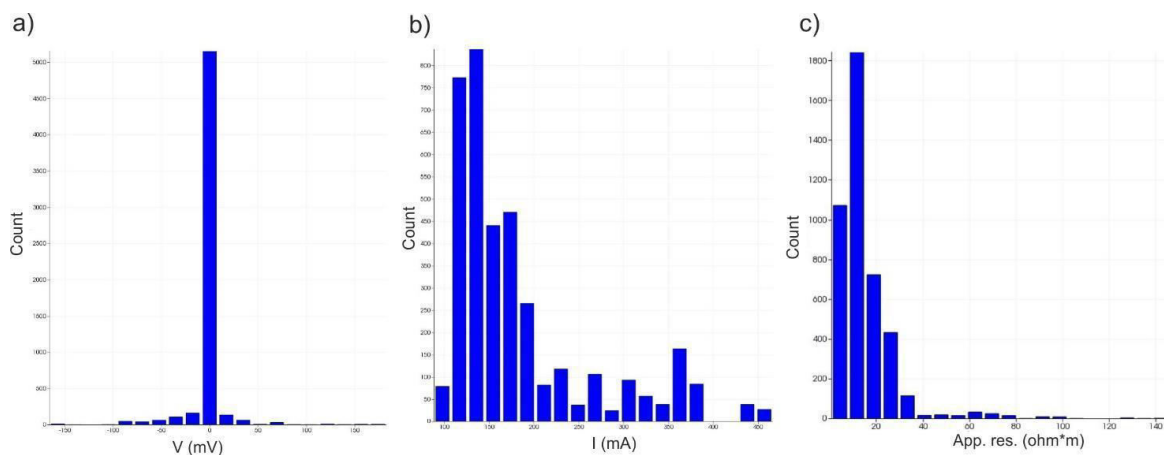


Figure 4. Histograms of potentials (a), currents (b) and apparent resistivities (c), corresponding to ERT 1 profile.

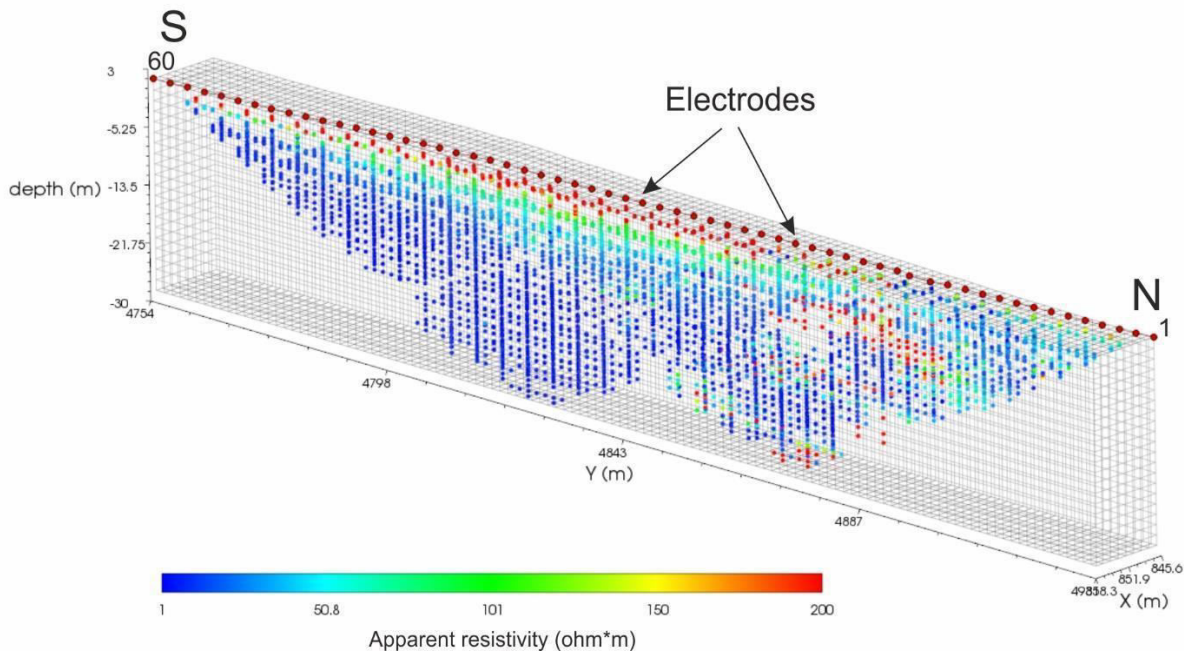


Figure 5. Pseudo-plot of the apparent resistivity measurements after the quality control, corresponding to ERT 2 profile. The mesh used for the inversion procedure and the electrodes are also represented.

The apparent resistivity values of Line ERT1, after filtering the noisy measurements, are characterized by the following statistical behavior:

- minimum value around 0.62 Ohm*m;
- maximum value around 145.6 Ohm*m;
- average value of 11.8 Ohm*m;
- median value of 7.3 Ohm*m;
- average standard deviation equal to 13.5 Ohm*m.

The currents injected at the transmission electrodes have an average value of about 177 mA. The statistical behavior of the apparent resistivity values for Line ERT2 is the following:

- minimum value around 0.12 Ohm*m;
- maximum value around 492.4 Ohm*m;
- average value of 75.4 Ohm*m;
- median value of 30.8 Ohm*m;
- average standard deviation equal to 105.8 Ohm*m.

The currents injected at the transmission electrodes have an average value of about 268 mA.

Figure 5 shows the point cloud 2D distribution of the apparent resistivities acquired along the ERT2 profile.

Electrical resistivity tomography (ERT) was performed using the VIEWLab Studio software, after removing inaccurate measurements. The entire set of measures was inverted in order to perform the imaging and characterize the correct resistive behavior of the subsoil.

The three-dimensional inversion of the measures is based to the following configuration:

- - *mesh* size in the x, y, and z directions of space: 2.5 m for ERT1 and 1.5 m for ERT2, equal to half electrode spacing.
- - Starting resistivity close to the average of the apparent resistivities.
- - Estimated noise on the data equal to 3%

The tomographic inversion converged after a maximum of 8 iterations, for all the considered datasets. The concordance of the modeled measures with respect to the measured values is very good, as evidenced by the example of Figure 6, which shows the progress details at the final iteration for the profile ERT 1

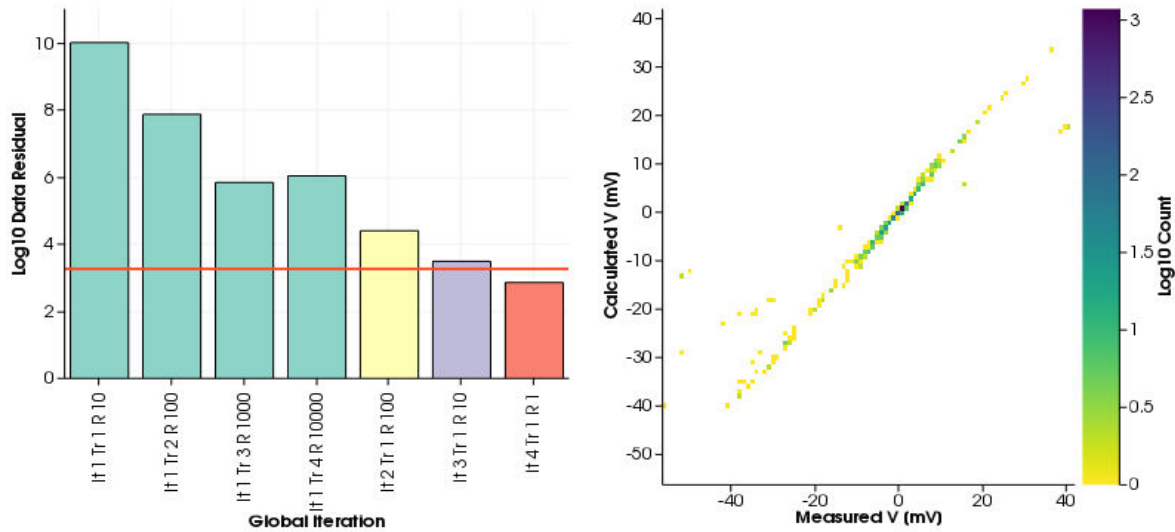


Figure 6. Progress details at the final iteration for the profile ERT 1. Trend of the misfit measures-modeled data, as the iterations proceed (left). *cross-plot* of the modelled data vs measured data (right), at the end of the tomographic inversion.

The results of the inversions are displayed in Figures 7-8. As expected, both sections show very low resistivities in depth, because they are located very close to the shoreline. Note that, at about 13 m depth, bot sections indicate the (probable) presence of salt water. Some features of ERT1 and ERT2 sections, characterized by high resistivity, probably indicate the presence of dry sand accumulations at near surface. ERT2 section exhibits some features indicating plumes of fresh water eventually mixed with sea water. These features correspond to low resistivity zones located at about 100 m from the beach (i.e., at the beginning of the line, see Figure 8), close to the surface.

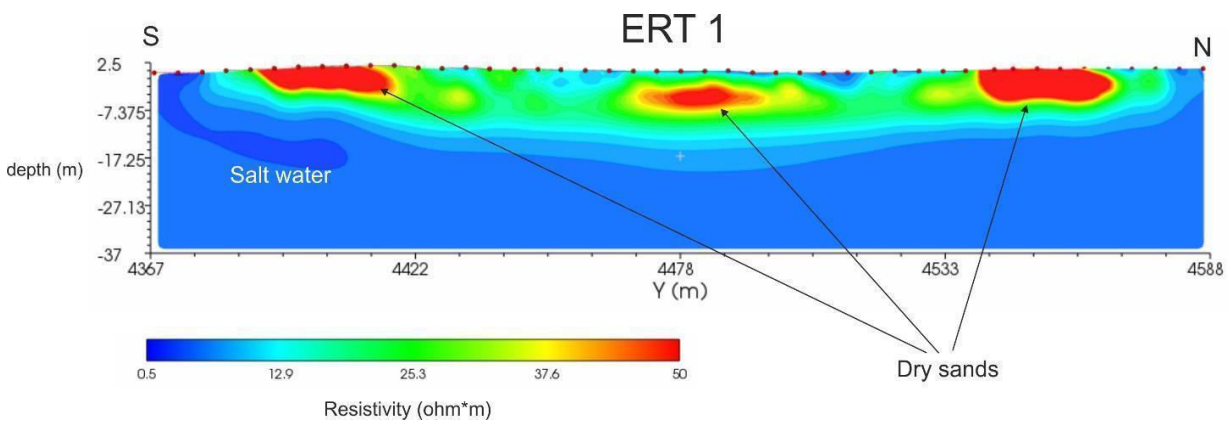


Figure 7. Tomography resistivity imaging corresponding to ERT 1 profile.

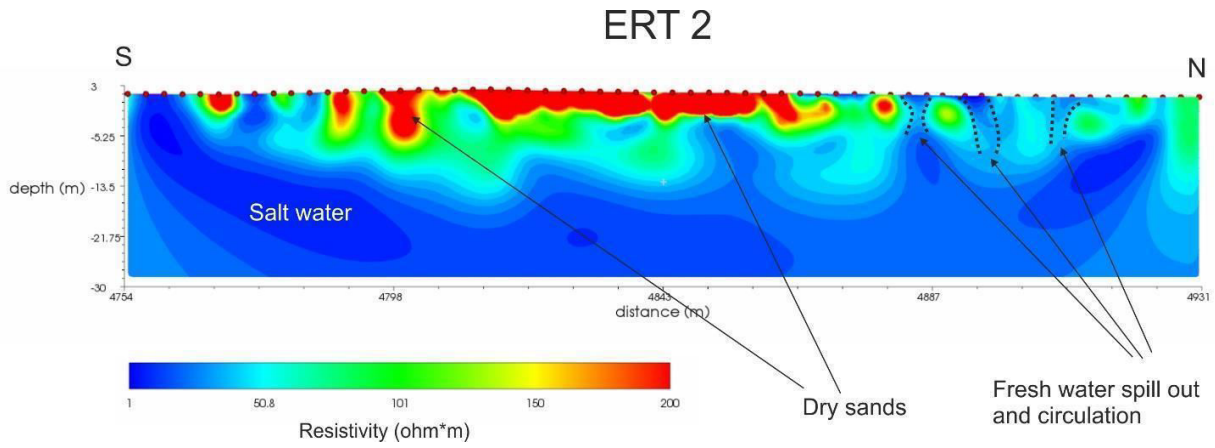


Figure 8. Tomography resistivity imaging corresponding to ERT 2 profile.

Another geoelectrical survey was carried out by Eureka, to investigate the underwater sediments in proximity of the shore where the OGS survey were performed. The goal was to map geological variations, salt and fresh water saturation and any unconformities in the first 5 meters of the subsoil. The investigation campaign was carried out on June 16th 2021.

EUREKOS' profiles have been recorded following the alignment of OGS' profile. To reach the sea it was necessary to insert a gap of 20 meters between the end of OGS profile and start of EUREKOS' measurements (electrode1) of EUREKOS Profile Bibione 1. Details are visible in the below picture (Figure 9).

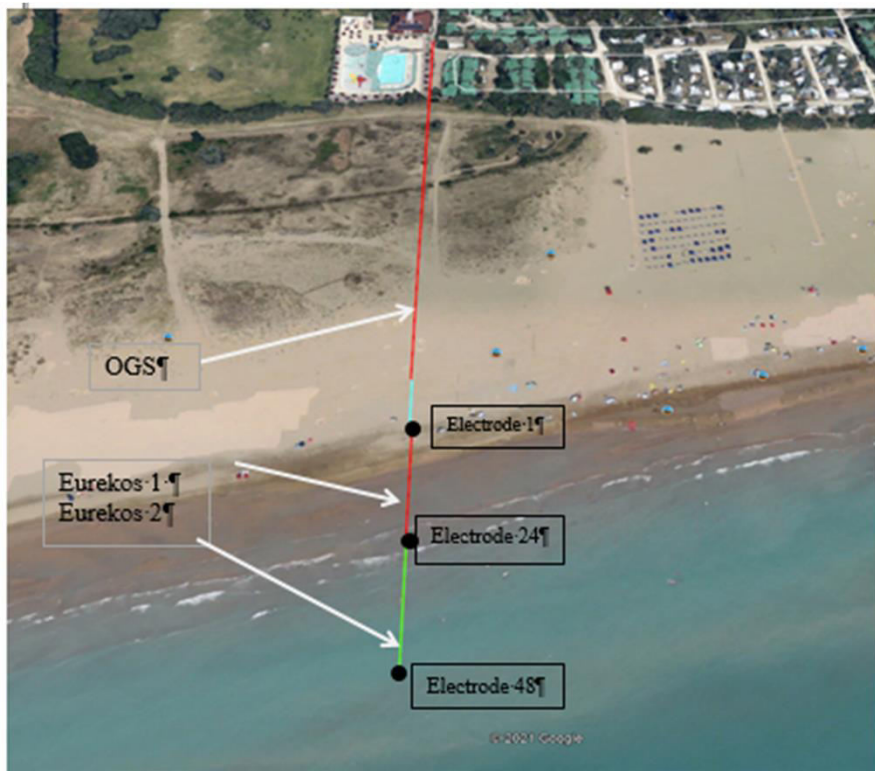


Figure 9. Survey area with geoelectric profiles

The coordinates of Eureka's profiles are:

Electrode 1: 342894.82 N 5054350.79 E, Z = 0 (N 45°37.495', E 12°59,077')

Electrode 24: 342883.65 N 5054303.34 E, Z = -40 cm (N 45°37.469', E 12°59,078')

Electrode 48 (24+24) 342895.74 N 5054254.04 E, Z= -80 cm (N 45°37.443', E 12°59,079')

Investigations have been carried out using the following equipment, configurations and procedures (Figure. 10).



Figure 10. Examples of Equipment used for the geoelectrical acquisition.

Equipment:

- Geoelectric automatic control unit LIPPMAN 4PK HP controlled by a Panasonic Toughbook laptop;
- Array: Dipole-Dipole, Wenner and reciprocal
- Submersible cable, electrode spacing 2 metres, 24 electrodes; Software for data acquisition:
- GETOTEST (Lippman-Rauen) Software for data processing:
- ResInv 2

Data quality is displayed during the data acquisition in the pseudosection matrix. If the data quality for the given point is not satisfactory, that measurement could be repeated with different settings at any moment during data acquisition.

When all data is recorded, it is possible to cancel the ones with low quality or to exclude them from the data processing.

Acquired data have been processed by the program RES2DINV 3.55 (GEOTOMO SOFTWARE) for Windows based on Resistivity & IP inversions by application of least-squares method. Data processing package RES2DINV is a computer program that automatically determines a two-dimensional (2-D) resistivity model from the recorded data, by a series of iterations and removal of bad data it is possible to reach a inverse model having an acceptable statistical error. (Griffiths and Barker 1993).

Figure 11 shows an example of the electrodes arrangement and measurement sequence that can be used for a 2-D electrical imaging survey. The 2-D model used by the inversion program, which consists of a number of rectangular blocks, is shown in Figure 12. The arrangement of the blocks is loosely tied to the distribution of the data points in the pseudo section. The distribution and size of the blocks is automatically generated by the program, using the distribution of the data points as a rough guide.

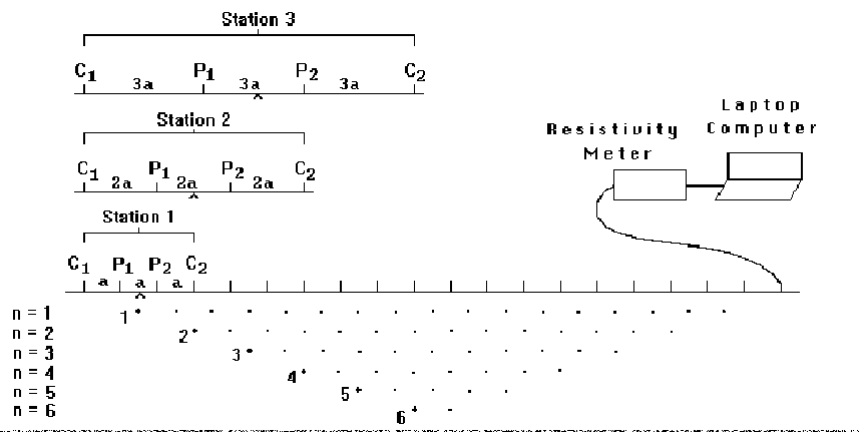


Figure 11. Sequence of measurements to build up a pseudosection

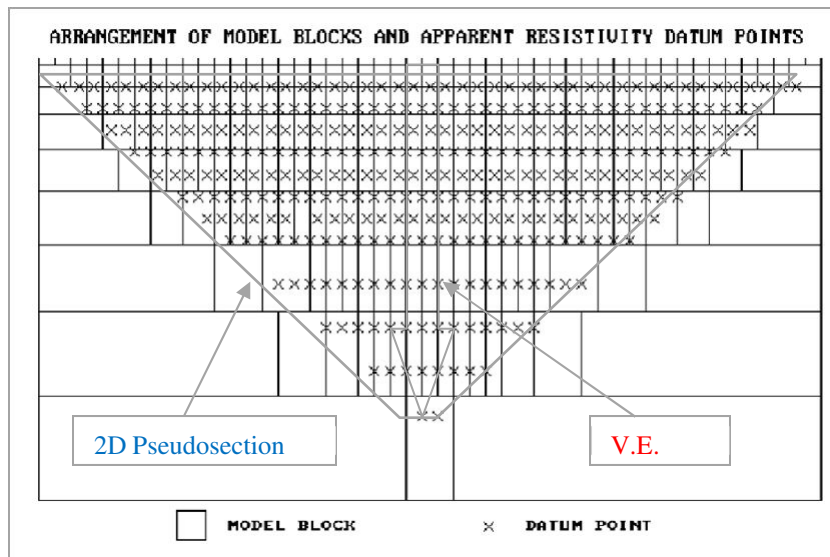


Figure 12. Arrangement of the blocks used in a model together with the data points

The final products are resistivity and I.P. (Induced Polarization, not presented in Report), pseudo sections are shown below (Figures 13-15).

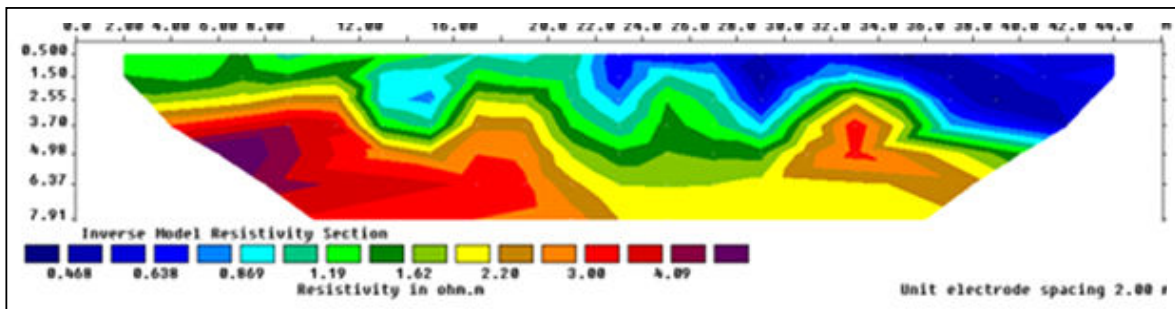


Figure 13. Profile Bibione1-Wenner

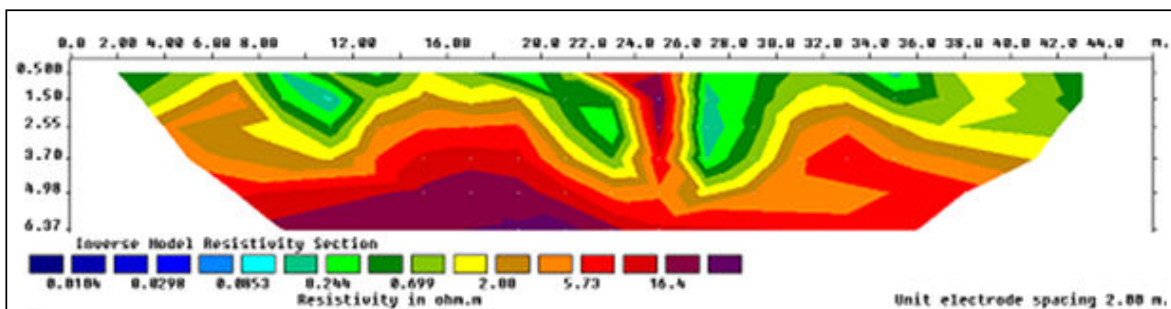


Figure 14. Profile Bibione 2- Wenner reciprocal

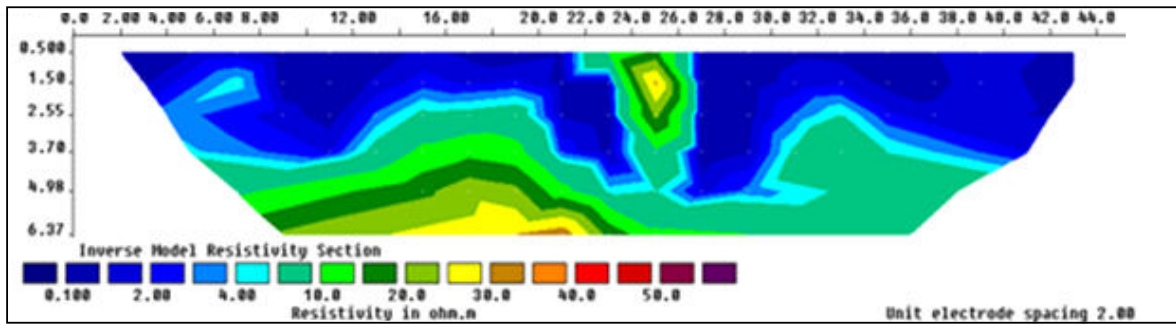


Figure 15. Profile Bibione 2 -Dipole-Dipole- Linear scale

The application of geoelectric tomography, has permitted to point out the main features of the first meters of sediments below the sea floor in front of Camping Capalonga.

As expected, the sediments present very low values of electric resistivity, but below 2,5-3 m from the bottom the resistivity increases, that could be associated to a harder layer of sediments known as “caranto”.

There are no evidences of freshwater venues or freshwater water bearing layers.

4.1.2 Seismic data – P-waves

In 2020 two land seismic high resolution seismic lines were acquired in the Bibione test site. In Figure 16 the location map of the two lines, having a length of approximately 200 meters, is shown.

The aim of the acquisition was the definition of the very shallow geological structures of the area. Along the two seismic lines, also two geoelectrical profiles were acquired, which will make it possible to associate the geological structures to the presence of water in depth.

The two lines were acquired positioning 10 Hz geophones every 4 meters and shooting every two meters. The source was a vibrator mounted on a wheelbarrow.



Figure 16. Position map of the two seismic lines acquired in Bibione

The first step of the processing of the seismic data was the application of the geometries. This step consists in inputting the coordinates of the geophones and shots in the trace headers. Then, with this information, static corrections and binning were applied in order to obtain the CDP gathers. Then, with the aim to increase the signal/noise ratio, a butterworth filter, a trimmed mean dynamic dip filtering, a spiking deconvolution, and an automatic gain control (AGC) were applied. Then normal move out correction and a stacking of the CDP gathers were applied. The resulting stacked , sections are shown in Figures 17 and 18.

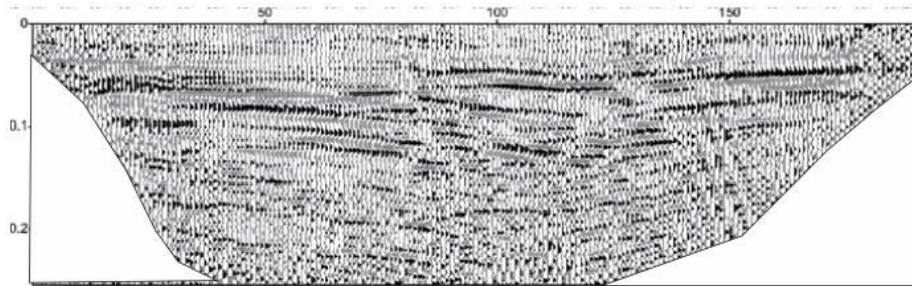


Figure 17. Stacked section of Line 1

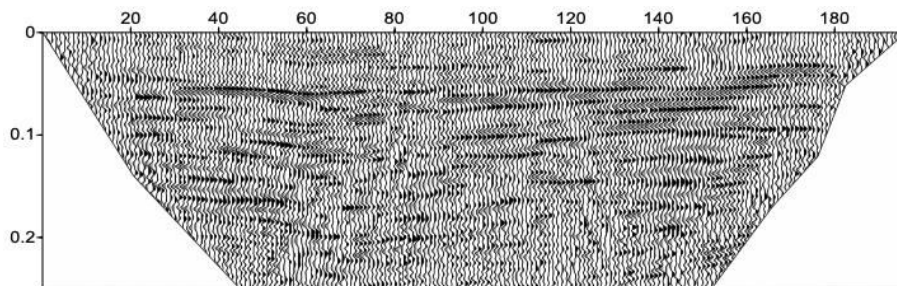


Figure 18. Stacked section of Line 2

The same procedure was applied to the data acquired along Line 2 and the final result is shown in Figure 18. In both sections, the presence of a clear reflection at about 50 ms TWT (about 7-8 meters) is evident. In line 1, a clear discontinuity in the main reflection is evident at about CDP 80.

To better characterize the sediments of the subsoil from a petrophysical point of view, also a tomographic inversion of first arrivals of the seismic data was performed. An example of picking of first arrivals in the shot domain is shown in figure 19.

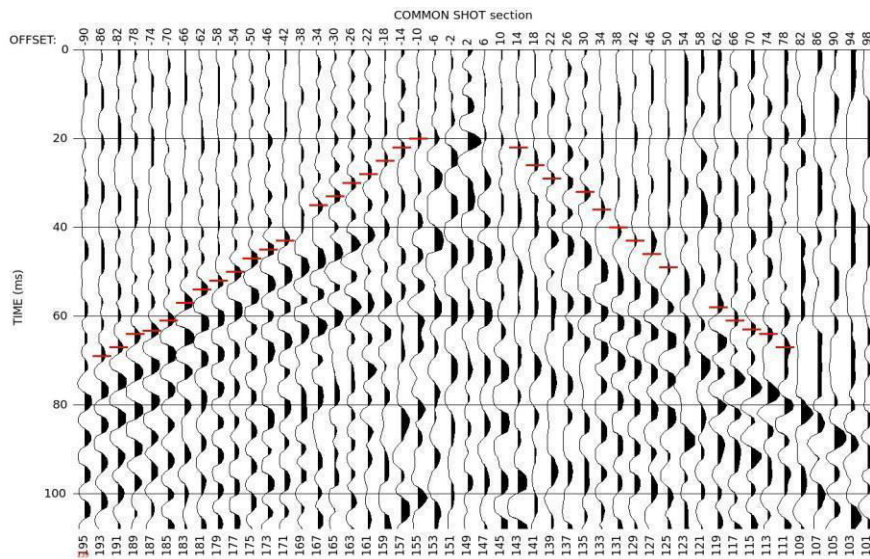


Figure 19. Example of first arrivals picking in the shot domain
P VELOCITY

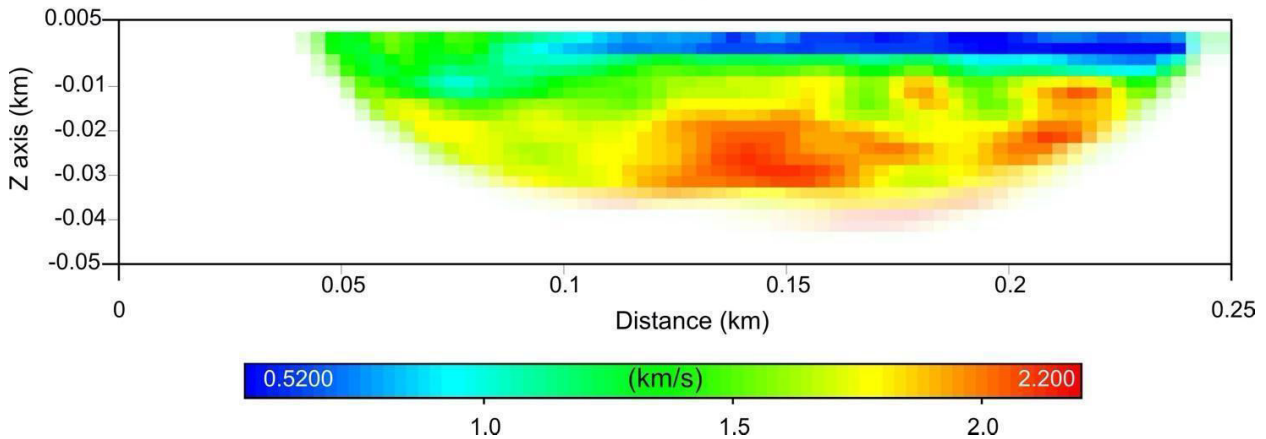


Figure 20. Velocity field obtained by inversion of first arrivals. The section starts at X=0.45.

The final tomographic velocity field of Line 1, obtained by the inversion of the first arrivals, is shown in Figure 20. Similarly to the stacked section shown in Figure 17, there is an evident difference in the thickness of the shallow sediments, characterized by low velocity, between the north and south part of the line.

A time residual analysis was also calculated to define the goodness of the inversion procedure (difference between picked times and times calculated from the final velocity field). The RMS was equal to 1,1 ms, corresponding to an error of 2,8% with respect to the real values. Tomographic analysis highlights the presence of two discontinuities. A discontinuity at about 2

meters in depth (not clearly visible in the seismic section) and another one at about 7-8 meters, which is also evident in the stacked section.

As for Line 2, a different approach was adopted. The tomographic inversion of the first arrivals was performed considering the first arrivals both as head waves and as diving waves. The velocity model obtained using the head waves is more reliable (the RMS value is lower compared to the inversion of the diving waves).

However, the diving wave inversion provides a similar and smoother velocity field with almost equal reliability. For a comparison between the results of the two lines we show the velocity field of the diving waves in Figure 21.

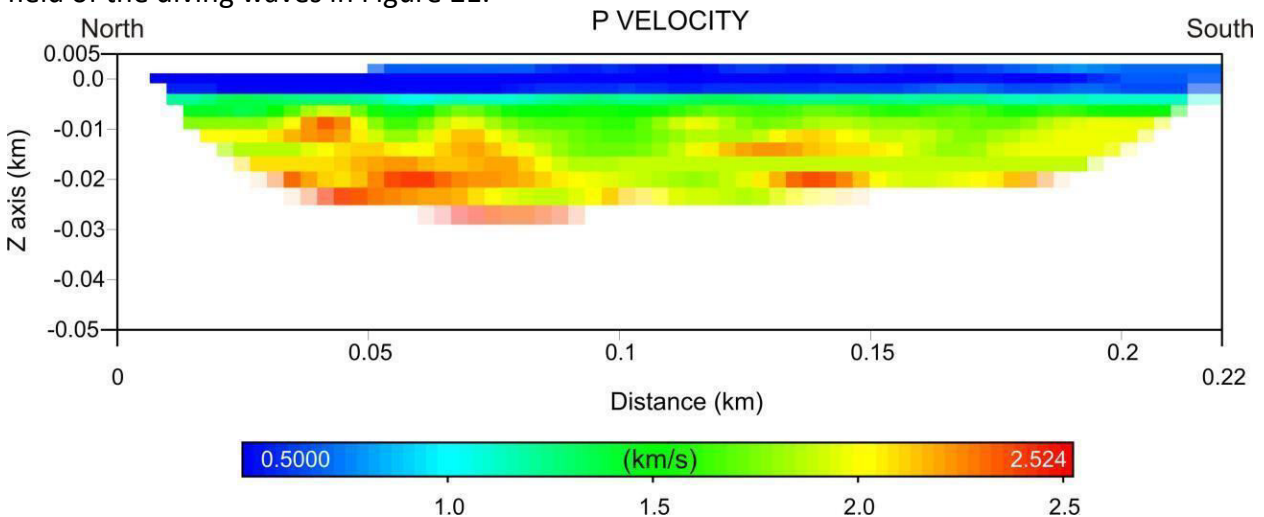


Figure 21. Velocity field of the line 2 obtained by inversion of first arrivals as diving waves.

The resulting velocity profile (Figure 21) shows more or less the same velocity changes at 2 and 7-8 meters as in Line 1. In the central part, the depth of the discontinuity at 7 meters increases and consequently also the thickness of the shallow sediments.

The results obtained by the reflection-seismic processing of the seismic data, together with the inversion of first arrivals, provided valuable information regarding the buried structures of the sediments in the proximity of the coast. In fact, the seismic sections show the geometries of the structures, while the velocity field furnished information regarding the characteristics and the petro- physical properties of the sediments.

4.1.3 Seismic data – S-waves

The area interested in this study covers the same area as the first line of the first survey areas, on the Bibione’s shore, on the left side of Figure 16, a zoom can be seen in Figure 22.

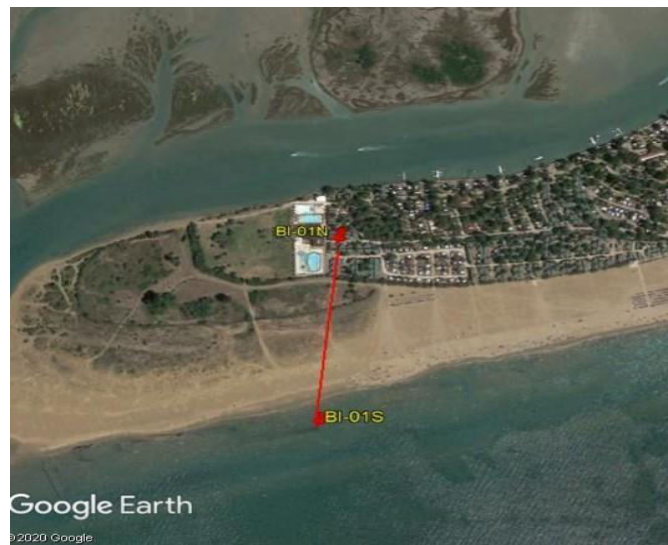


Figure 22. Overview of the extent of the survey area

As is the previous survey, the source employed in one small handly-operated vibrator, producing S and P-waves.

Basing on the project's targets requirements, the main acquisition aspects taken into consideration are:

1. Instrumentation
2. Acquisition parameters
3. Source points
4. Data management

These are described in this chapter.

The instrumentation required for the survey can be divided in two groups:

1. Sensors
2. Acquisition system
3. Seismic source

The scheme in figure 23 shows the interconnections between each instrument involved in the whole survey operations

Horizontal mount 10 Hz geophones were used as seismic receivers during both SV and SH configurations. When in SV configuration, the oscillating axis of the sensor is oriented along the line's direction, while in SH configuration it is oriented perpendicularly to the line's direction

The whole acquisition equipment includes one laptop PC that runs the acquisition control interface, as well as the digitizer's interface, and has QC capabilities (data visualization and inspection). The digitizer employed is Summit XONE from DMT, driven by its proprietary software, which handles the acquisition settings, records and exports the SEG2 data

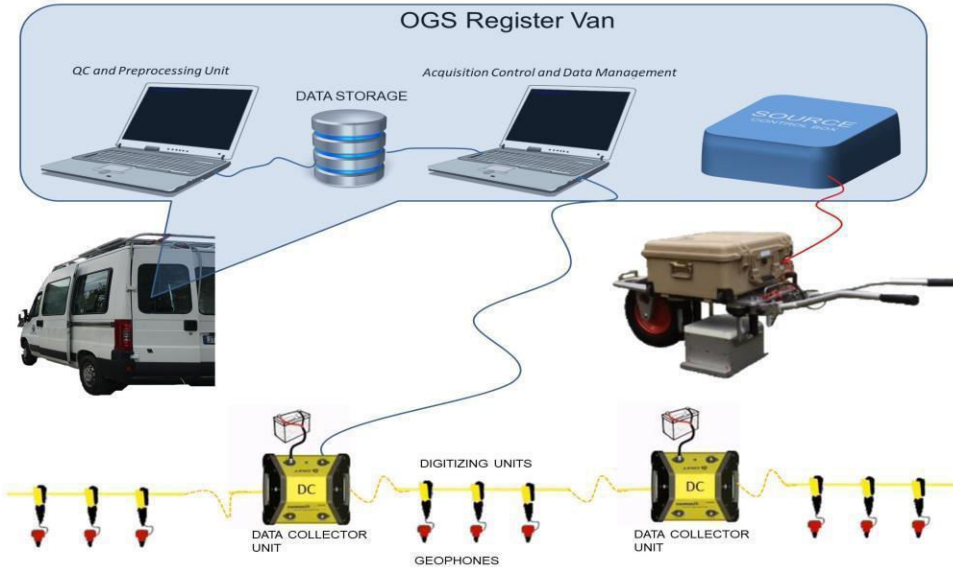


Figure 23. Instruments and connection scheme



Figure 24. Vibroseis source Elvis VII from Geosym

The vibrating source for this survey is an Elvis VII from Geosym GmbH. The vibrating mass is entirely mounted, together with its battery and the electronic power amplifier, on a light and robust wheelbarrow so that can be handled easily. The controller offers manual triggering capability, providing a timebreak signal to the acquisition system. The source has been operated in both SV and SH modes, after having oriented the sensors accordingly.

The following parameters have been set as a result of the tuning phase:

Sweep type: linear

Frequency range (Hz): 20 - 160 Taper type: cosine

Start taper (s): .100

Load force (Kg): 112

Sweep length (s): 15 2 Acquisition design and set-up

In order to maximize the information content of the data to match the investigation purposes, at first the following survey parameters have to be tuned: record parameters acquisition channels vibration points source parameters

Record parameters

record length (s): 16.0 sampling interval (ms): 1 cross-correlation listening time window: from -0.1 to 1.0 s.

The spacing between the sensors is always fixed to 2 m. For vibroseis operations, the reference (pilot) signal trace is always identified by track number 90, which has been previously recorded by a high resolution, low-noise A/D converter in OGS laboratory. The line's layout changes slightly when the source operated is the accelerated mass, since in that case some of the p-geophones sensors have been added, or moved along the line. The seismic receivers are placed along paths mostly straight and perpendicular to the sea shore. The receiver stations numbering starts with 101, and proceeds in ascending order from North to South. See the next chapter for a detailed description of each receiver station, for each of the acquired lines. Typically the source points have been designed to fall in the middle point of two subsequent receivers, every two receivers couples thus resulting in 4 m. source spacing. The rule for the numbering is that each VP is numbered as the stake of the next receiver (in numeric terms), incremented by 1000. So, for instance, VP 1143 is placed 1 m. behind stake/receiver 143 (taking into account the direction of the increment is from North to South), which is 1 m. ahead of stake 142 as well.

The records files produced by the X-One are automatically gathered, managed and preprocessed by OGS custom-made acquisition software 'PyACQ'. This application software interfaces the user to the records database and computes the first quality control on the acquired data, by means of checking the incoming data consistency, includes information in each trace header, then cross-correlates each trace with the pilot. The system also allows the user to insert comments about each individual record, enabling the software to automatically discard bad or noisy records from later re-processing. Finally both correlated and uncorrelated raw data are secured in a safe storage.

The records set produced has been organized as follows. The main data folder contains the correlated data (RAW uncorrelated will always be available in the OGS data storage system). This contains several sub-folders, named after the source type.

Each record is related to a specific position (numbered as described in the previous section) of the Vibroseis along the line.

The file name is formatted as in the following example: "F005 S1101.corr" means the record has been acquired on VP 1101, corresponding to Field Record number 5. The file format is Seismic Unix SU, with inner standard SEG-Y trace headers, explained in detail in the next paragraph.

Most of the acquisition information are recorded in the header of the SEG-Y files, such as source and receiver position, start time, trace identification codes, etc. The meaning and the position of the header fields follows the SEG-Y standard definition. The most relevant subset of the header parameters is reported in detail in table 2.1.

SEG-Y header parms		
Name	Description	byte
fldr	field record number	9-12
ns	number of samples	115-116
dt	sample interval in microseconds	117-118
tracf	field trace number	13-16
offset	distance between source and receiver	37-40

Table 2.1. SEG-Y header Parameters

After moving the register van onto a suitable position along the survey line, while preparing and connecting all the instruments and equipment, the technicians coupled the geophones to ground, then deployed the line cable and the data collector units. The topographic survey took place a few days after, given the stakes left on the ground. Figures 25 show details of these different steps. After a few tests, the optimal number of records per shot point has been set to two.

It took the first few records to tune some of the acquisition and sweep parameters. The number of records for each EP has been set to 2. The first Source configuration used is SH, then SV and finally the Weight Drop. Moreover, for testing purpose, a few shots have been recorded with P vibroseis source and SV geophones configuration. These have fldr number ranging from 218 to 221. In the following paragraphs, start - stop time, field record number range and remarks are reported.

SH configuration

Start time: 26-09-20 15:23:41

Stop time: 26-09-20 15:12:06

Field records range: 5 - 110

Notes:

fldr 5 - 21: sensor tracf 114 has inverted polarity fldr 5 - 89: sensor tracf 180 has inverted polarity fldr 57, 58: actual source position is about 1/2 meter away from the line.

SV configuration

Start time: 27-09-20 11:12:44

Stop time: 27-09-20 12:30:15 Field records range: 112 - 217 Notes: fldr 146 - 217: starts raining
fldr 162 - 217: changed source's vibration polarity

Weight drop configuration

Start time: 27-09-20 14:51:58

Stop time: 27-09-20 15:24:05

Field records range: 224 – 232



(a) deploy sensors and digitizers



(b) coupling geophones to ground



(c) deploy wirelines



(d) crossroads

Figure 25. Line set-up steps

4.1 Marine data

4.1.1 Sparker data

Specific objective of this data acquisition in Bibione was to evaluate the thickness of the near shore sediments by means of the acquisition of a series of multichannel seismic profiles, in

order to obtain information at greater depths with respect to other geophysical methods that will be used to better define the geometries of the very shallow sediments. The line plan was designed taking in account the departure location, the length of profiles, and mainly the weather conditions. The original work plan is indicated in Figure 26. The work started on August 31st with the MOB operations in Porto Baseleghe (Bibione Pineda, VE), and the acquisition started on September 1 . Further details of the timeline can be found in the Cruise diary.

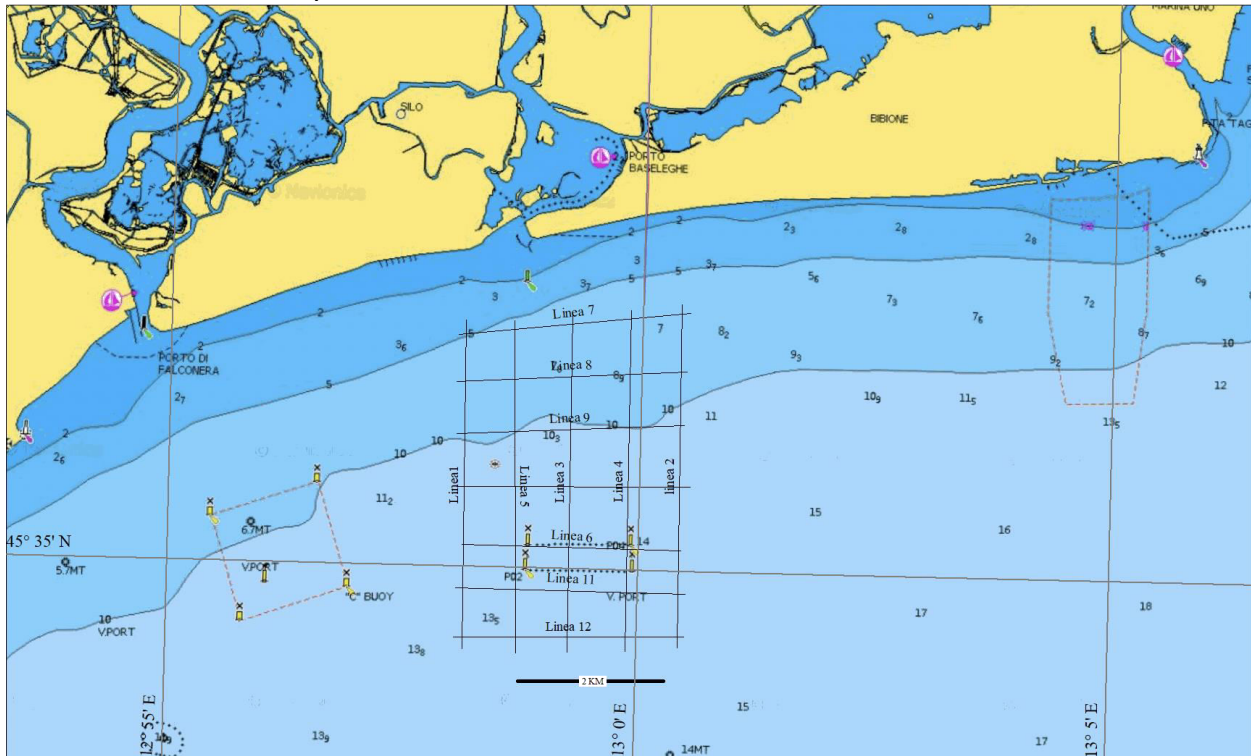


Figure 26. Original work plan.

The navigation has been managed by using the “Teledyne Reson - PDS2000” software, configured to send the fire commands (fix) at 6.25 m (two times the Hydrophone distance 3.125m) shot point distance to trigger both the source and the recording system.

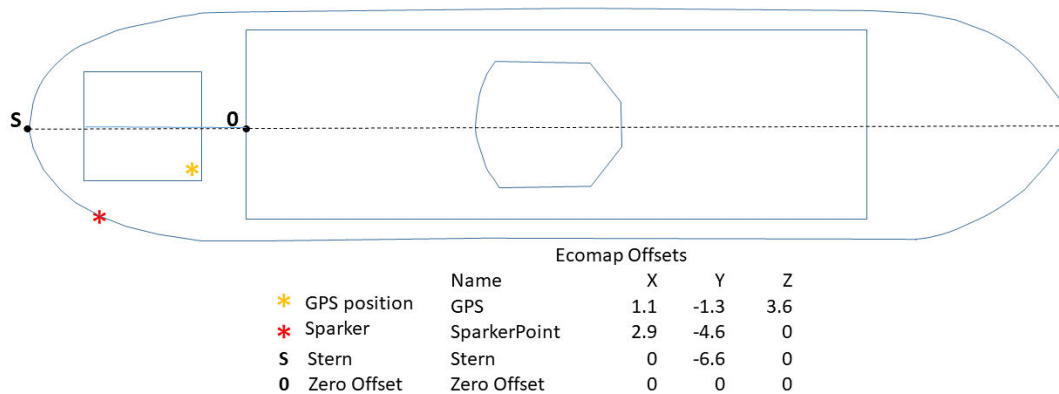


Figure 27. Offset list.

Acquisition parameters

The choice of the acquisition parameters was driven by the target depth.

The source consisted of one Dura-Spark 400 Applied Acoustic sparker system, coupled to a CSP-Nv charge condenser by means of a HV3500 cable. The shot point distance was set to 6.25 m, corresponding to a time interval of about 3.5 seconds at 3.8 knots of ship speed.

The array was towed to the surface thanks to its four buoys.

The data were collected by 64 channels, 200 m long digital streamer, with a channels distance of 3.125 m, corresponding to an effective horizontal sampling of 1.5625 m in the stacked section.

With 6.25 m shot point interval, the fold coverage attainable was 16 traces / CDP.

The distance between the source and the first channel (near offset) was kept at 33,7 m, large enough to prevent saturation (data clipping).

The streamer was towed at a depth of 0.5m-1m m below the sea surface (Figure 28).

To keep the streamer at the target depth 4 depth levelers (birds) have been used. The bird controller receives from the birds the information relative to the depth, and send commands to the wing to keep the birds at the target depth.

The general acquisition parameters are summarized in Table 4. A more detailed description of the seismic equipment can be found in Annex B. The SEG-D format recorded data were logged on the acquisition computer hard disk and on an external hard disk. Backup copies were stored at the end of each line on an extra external USB HD.

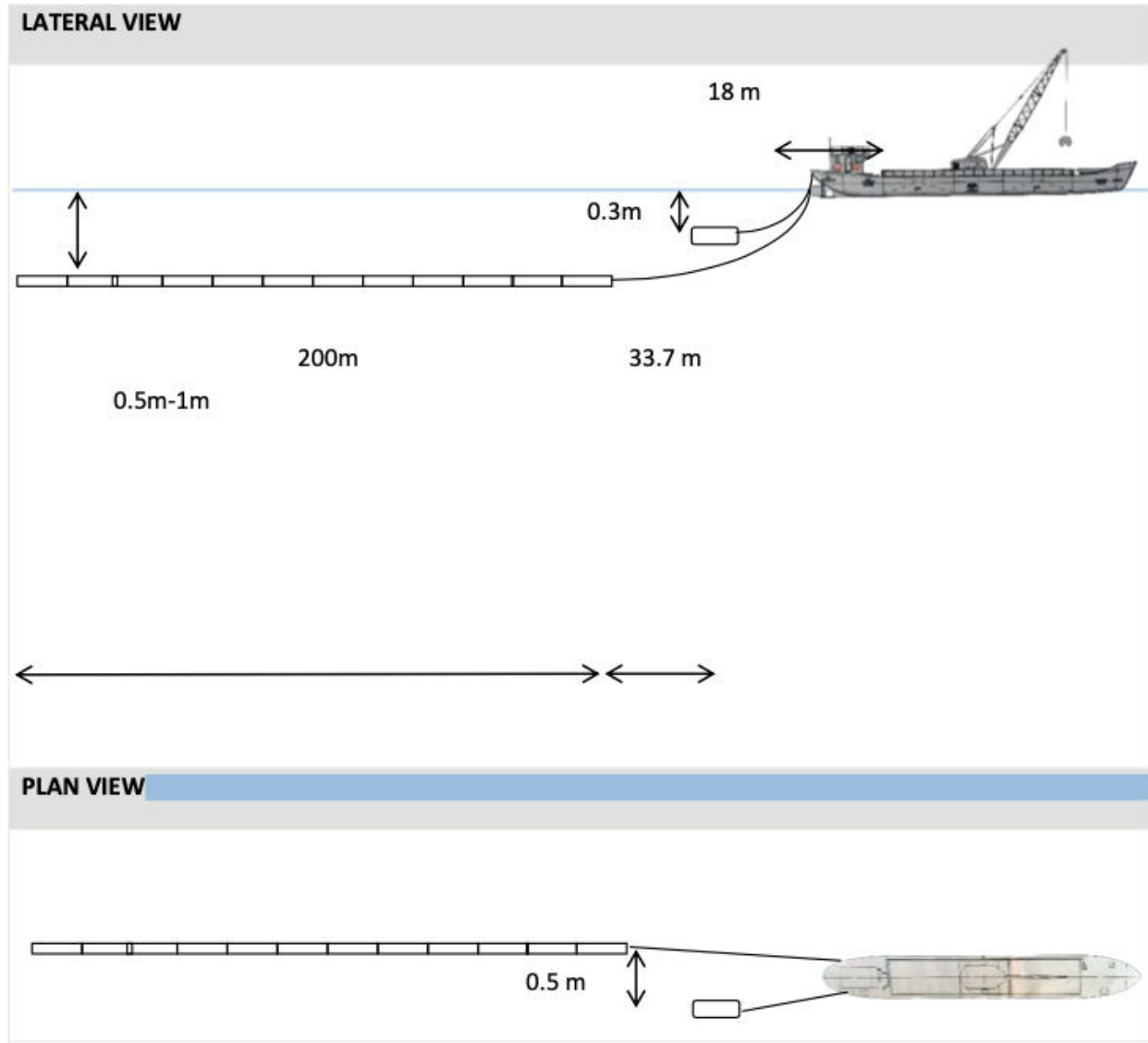


Figure 28. Acquisition geometry.

		ACQUISITION PARAMETERS			
SOURCE		STREAMER		RECORDING	
Model	Dura-Spark 400	Model	Geoeel	Model	Geometrics CNT-1
Power Unit	CSP nV	Length	200 m	Samp. rate	125 μ s
Shot Interval	6.25 m	Ch. No.	64	Rec. length	1.2 sec
Power	750 – 1000 J	Ch. Dist.	3.125 m	LC filters	3 Hz (LC)
Depth	30 cm	Depth	1 m – 0.5 m	HC filters	Antialias
		Min off.	33.7 m	Aux ch.	Ch.2
		Max off.	233.7 m		

Table 1. Acquisition parameters.

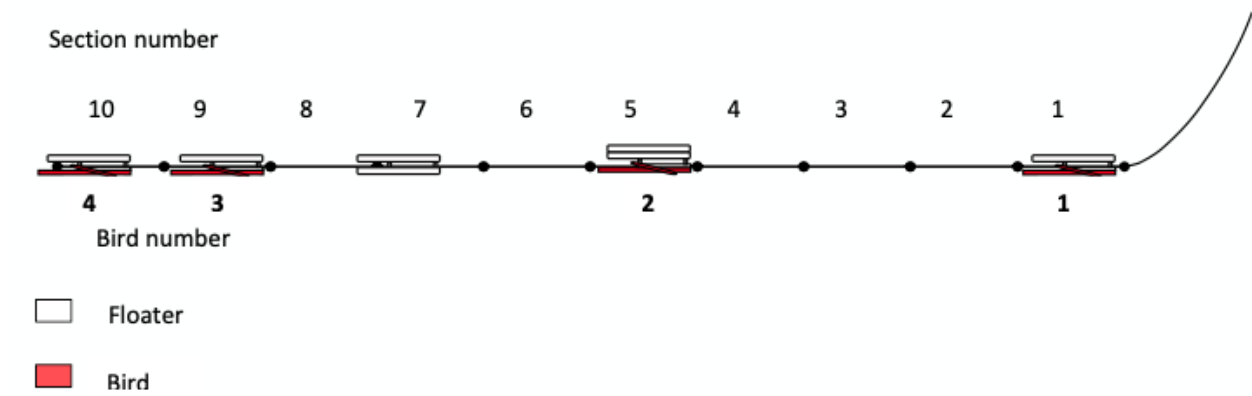


Figure 29. Streamer and birds configuration

Data quality control

The objectives of the field quality control are as follows:

- to check the overall quality of the data by single shot and near trace screen display;
- to verify that the data contain all the necessary information;
- to identify the nature of the noise (if any) affecting the data. In detail:
- to identify the origin of the noise (environmental or artificial - electric, mechanic, etc.);
- to study the characteristics of the noise (such as dominant frequency, apparent velocity and wavelength, etc.) and possibly suggesting a strategy to reduce its effects.

The quality control was performed during the acquisition through the Schlumberger Vista software, version 2019.000.12093 (64 bit), installed on a laptop.

The data were first transferred from the external backup HD to the processing laptop. The SEG-D raw data were reformatted to SEG-Y and loaded in the Vista processing package.

With reference to Figure 30, the first remarkable element is the presence of the seafloor reflection at a more than 250 ms two way time. This is obviously not possible, because with an assumed sound speed of 1520 m/s the corresponding depth would be around 190m, in an area where the seafloor is as shallow as 15-20m.

The second element is an apparently sub horizontal signal just a few milliseconds above the seafloor reflection, that has been interpreted as the trigger signal.

The trigger signal, that marks the beginning of the record and always occurs at zero time, is in this case offset by around 250 ms on the first channel. Even more strangely, it exhibits an offset dependent linear upward trend; that means that the larger the offset, the earlier the zero time. The arrival is in fact at 250.75 ms on the 1st channel and at 242.75 ms on the 64th channel, with a total difference ΔT of 8 ms between the near and the far offset (Figure 31, zoom on the left).

To correct for this effect, and given the linearity of the trend, it has been applied an offset dependent downward static correction, given by:

Static = Channel No. / 8, so as the correction will increase with offset.
 Given this formula, even the 1st channel will receive a small correction (1/8 ms=125 μs) but this can be considered negligible, being equivalent to a single sample. The result of such a correction is provided in Figure 31 (on the right) where the trigger signal is now (almost) perfectly aligned and parallel to the offset axes. To achieve an exact alignment, however, it could be considered the application of residual static corrections.
 After this, a negative bulk static correction of 250 ms can be finally applied to bring the trigger signal to zero time. The results are displayed on the right side of Figure 32

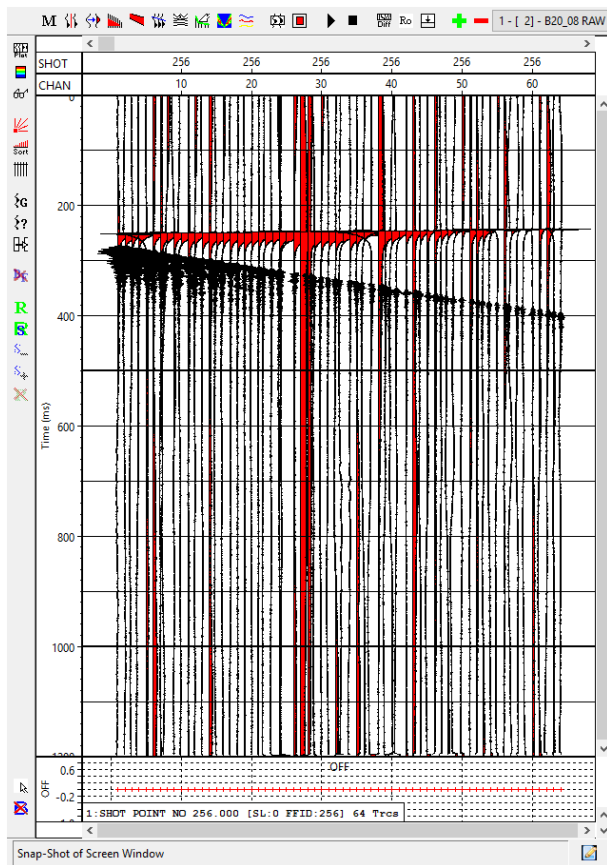


Figure 30. Example of raw shot record.

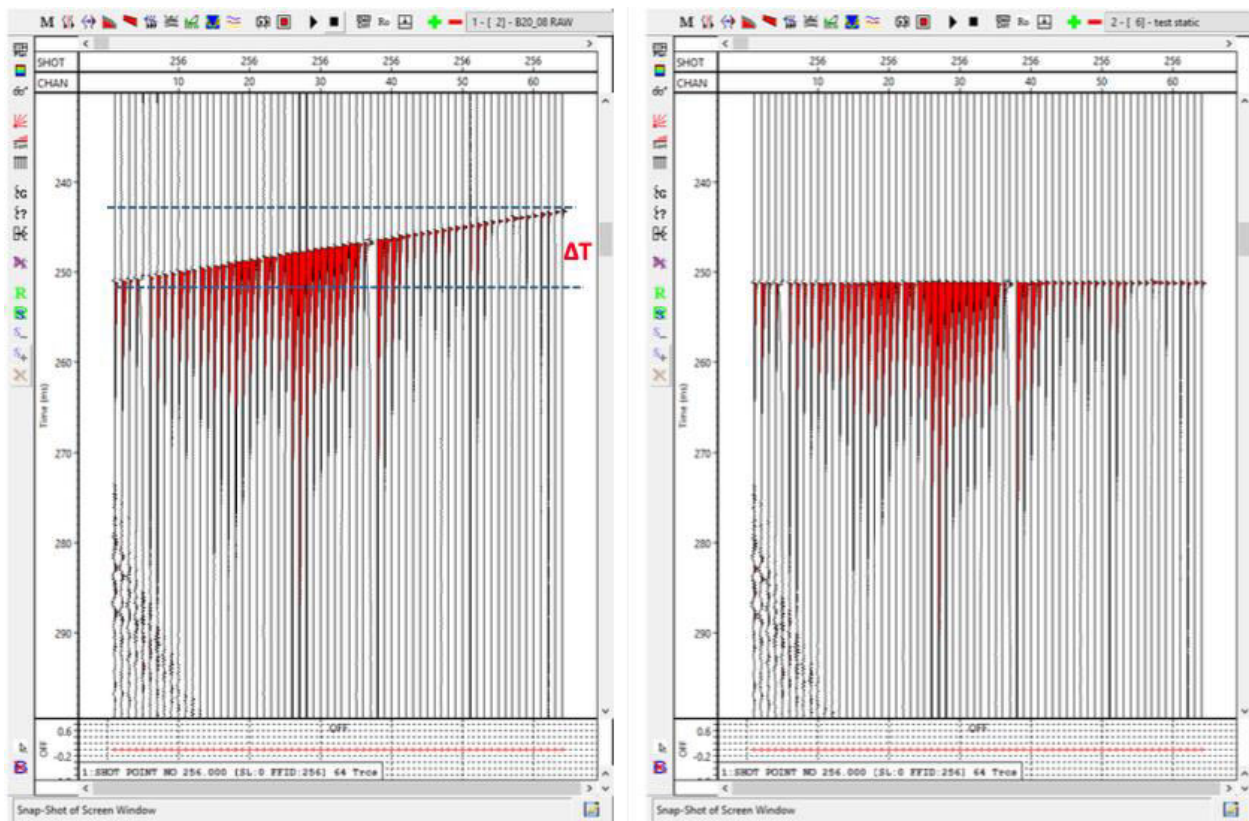


Figure 31. On the left, a zoom on the first portion of a raw record. The trigger signal, usually occurring at zero time, appears at around 250 ms. Even more strangely, it exhibits an upward, offset depending linear trend; that means that the recording starts in advance as the offset increases. The difference in starting recording time ΔT has been estimated in 8 ms between the 1st and the 64th channel.

On the right, the same record with an offset dependent static correction applied. The trigger signal is now perfectly aligned and parallel to the offset axis.

In both of the record, the very first part of the seafloor reflections are visible in the lower left corner.

See text for further details.

Noise characteristics

A general noise analysis has been performed on the window ahead of the trigger signal in the raw version (orange frame); the corresponding amplitude spectrum is displayed in Figure 30 (on the left).

The record is dominated by a not organized, very high amplitude and very low frequency (less than 10 Hz) noise component. Some DC is probably present as well. Given the nature of the

survey, this noise does not pose any concern because it can be easily removed by the application of a low cut filter.

Another noise component can be found in the very right part of the spectrum, at around 3 kHz. It is probably an electronic noise component that can be removed by applying an high pass filter. Both of the components have been pointed by the orange arrows in Figure 33.

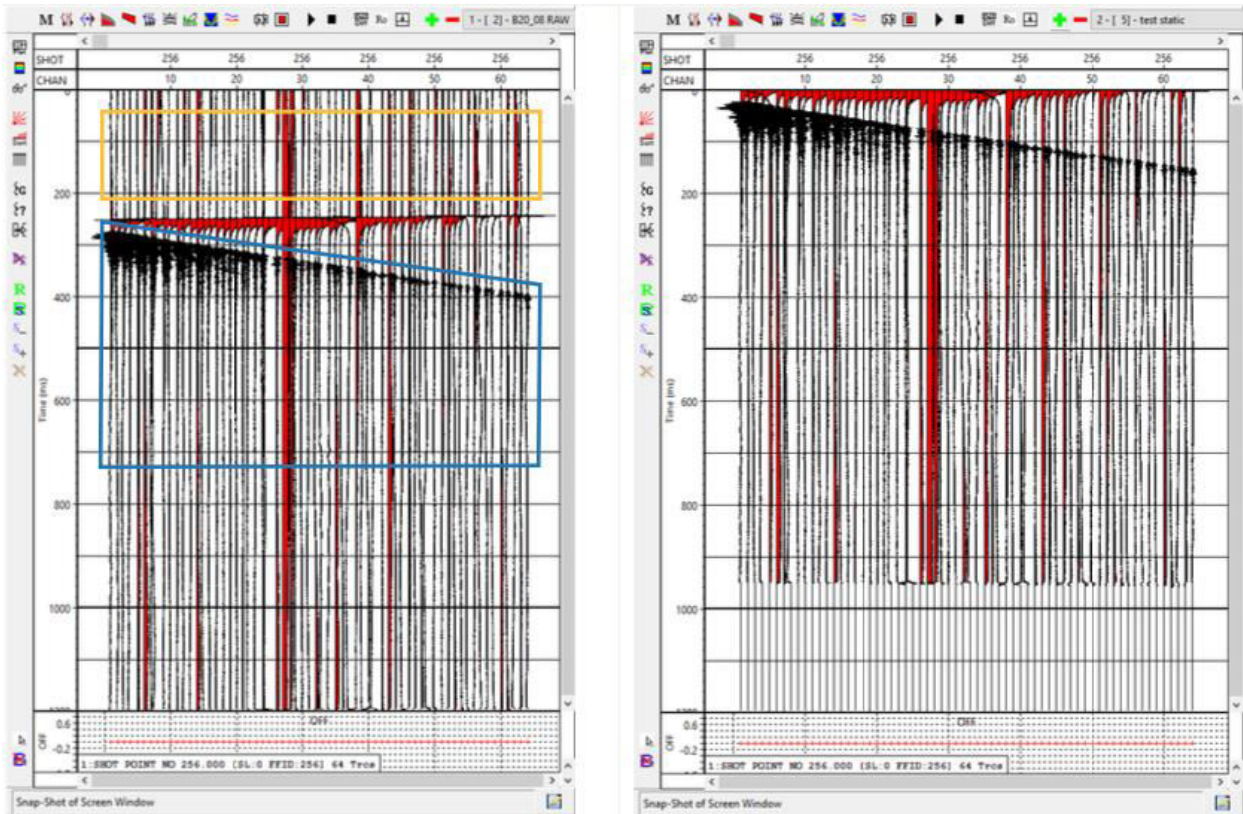


Figure 32. Raw record (on the left) and with statics applied. The static is constituted by two components: the offset dependent static (which is given by $\text{Ch. No} / 8 \text{ ms}$) and the upward bulk static, common to all the channels (which is 250.875 ms). Notice that the deeper part of the data (250 ms, on the right hand side record) has been lost due to this procedure.

A second analysis has been performed in a window containing both the reflected signals and the noise.

In Figure 34 (on the right) the corresponding spectrum has been displayed for a comparison with the noise spectrum.

The band of the signal is roughly limited between 80 Hz and 1 kHz; a secondary band, characterized by high amplitude and centered in the interval 2.5-3.5 kHz, appears on the record.

Although it could be arguable to say whether this part is related to the signal or not, on the basis of previous experiences with this source we conclude that this part of the spectrum represents the noise previously described and somehow reinforced by the recording system.

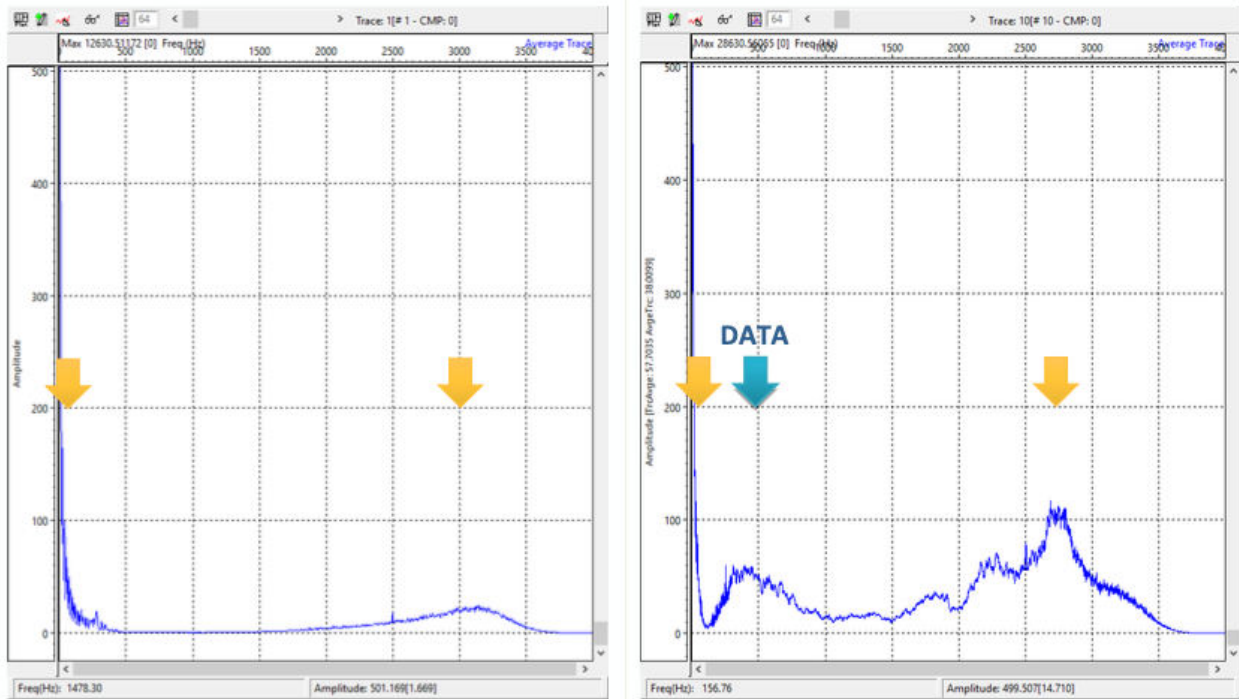


Figure 33. Amplitude spectra of the raw record. On the left, the spectrum representing the window of record ahead of the first arrivals: only the noise is present on this spectrum (primary and secondary peaks are highlighted by the orange arrow). On the right, the spectra with the additional contribute of the data is shown (light blue arrow). The windows where the analyses has been performed are shown in Figure 35 and are represented by the orange frame (for the noise) and the light blue frame (data + noise) respectively.

On the basis of these considerations, a large Ormsby trapezoidal pass filter has been applied to the data with the following characteristics: $F1 = 30$ Hz, $F2 = 60$ Hz, $F3 = 1000$ Hz, $F4 = 2000$ Hz. The results are shown in Figure 35.

Following the application of the filter, some linear noise appears on the record, and especially in its deeper portion (red arrow in Figure 35). This noise exhibits a constant apparent velocity (actually the speed of sound in the water) and is part of what is usually defined as cable noise: this noise is in fact most of the times caused by the tugging of the cable, that cause it to propagate from the point where it submerges. Just like the direct wave, this noise is usually removed by the stack of the traces. In alternative, a linear noise removal can be attempted but care must be taken to avoid affecting the signal.

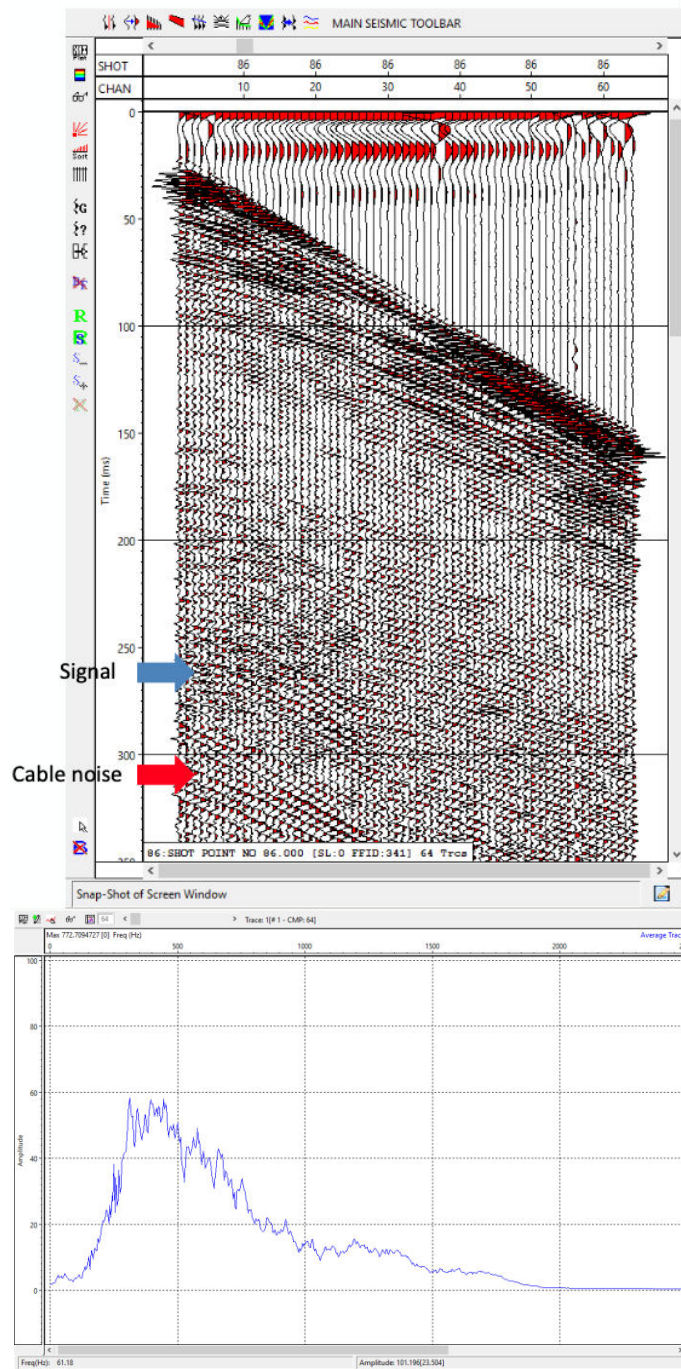


Figure 34. Filtered record (above) and corresponding spectrum (below). A band-pass Ormsby filter 30-60 / 1000-2000 Hz has been applied to the raw record. Linear noise appears starting from around 300 ms.

Signal characteristics

Although in this very first phase of analysis it is difficult to identify all the signals in the section, it looks evident that even with just a wide band pass filter application it is possible to spot some reflected energy.

It must be said, however, that a lot of reverberations (due to the waves being trapped within the water layer, which is very thin) are clearly present in the data, and sometimes their signals may be erroneously attributed to primary reflections; specific deconvolution techniques will have thus to be adopted to spot the primary energy only.

However, the deepest primary reflection that is possible to see at this stage occurs at about 250 ms roughly corresponding to a depth ranging between 200 m and 250 m.

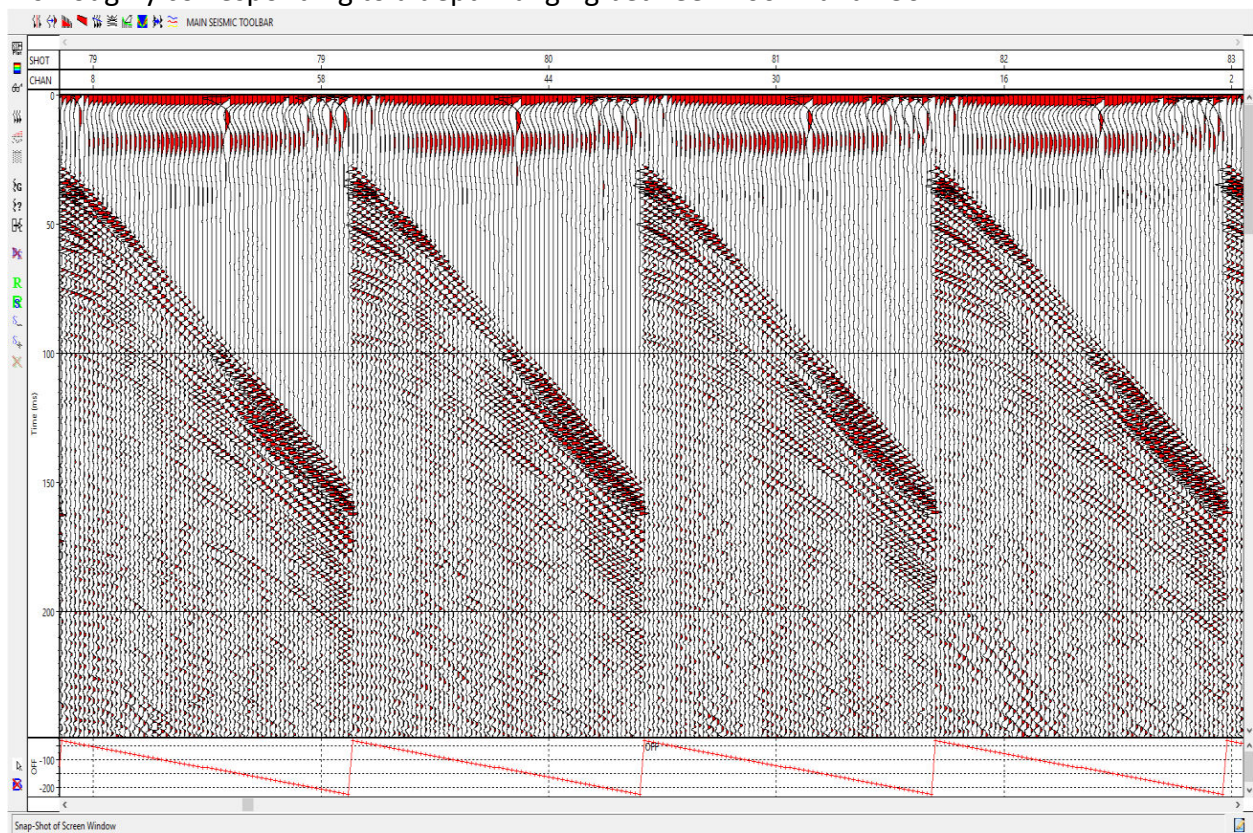


Figure 35. A series of adjacent shot records.

Geometric parameters

The first geometric parameter to verify is the near offset, that is the distance between the source and the first channel. For doing this, a good approximation of the speed of sound in the water is mandatory.

The speed of sound in the water can be calculated from the steepness of the direct wave trajectory, displayed in Figure 36.

The very first arrival of the direct wave occurs at **21.875 ms** and at on the 1st channel, and at **149.750 ms** on the 64th channel.

The speed of sound can be calculated by the simple relation:

$$\text{Speed of sound} = \frac{[(\text{channel No.} - 1) + \text{channel distance}]}{\text{transit time}}$$

where the numerator represents the distance covered by the direct wave.

In our case, the channel distance is 3.125 m and the channel No. is 64. With a transit time of 149.750 ms – 21.875 ms = 127.875 ms, the calculated speed of sound is **1539.5 m/s**.

This result, which is quite realistic, confirms also that the method adopted to correct for the static shift of the zero time was acceptable.

At this point, the near offset is easily calculated by multiplying the first arrival time (**21.875 ms**) of the direct wave by the speed of sound (**1539.5 m/s**), that is:

$$\text{Near Offset} = \text{First arrival time} * \text{speed of sound}$$

The result is **33.7 m**.

In this Figure 36 it is also possible to note that channels 5, 37, 55, 60 and 63 have their polarity inverted.

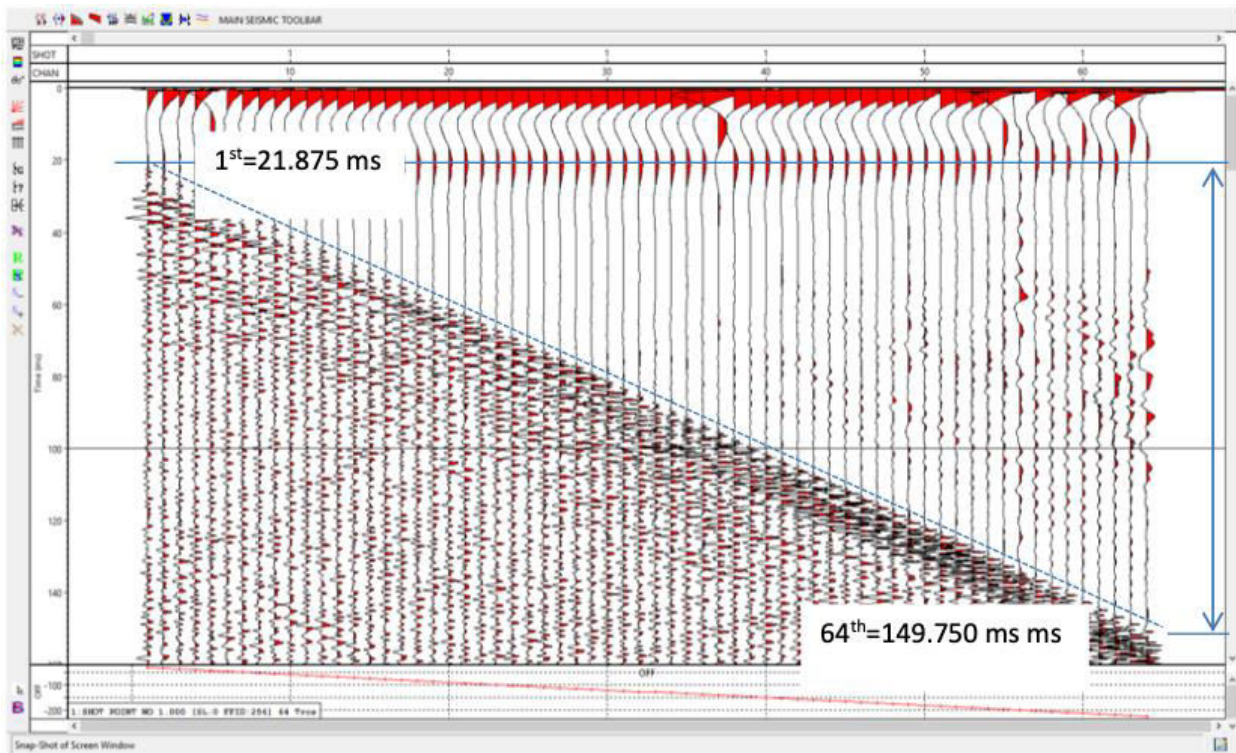


Figure 36. Measurement of the speed of sound from the direct wave arrivals of the first and the last channel. The light blue dotted line represents the trajectory of the direct wave.

The second element that is possible to verify from the data themselves is the depth of the streamer and the source, by inspecting the amplitude spectra in search for the notches caused by the ghost effect.

The notch frequency, in its simplest formula, is given by the relation:

- - $f_{ns} = \text{speed of sound} / 2 * \text{source depth}$;
- - $f_{nr} = \text{speed of sound} / 2 * \text{receiver depth}$;

In our case, with a source depth of around 0.3 m and a streamer depth between 0.5 and 1 m, the two notch frequencies should be 2.56 kHz for the source and somewhere between 770 and 1540. The source frequency notch is beyond the amplitude spectrum limit (2 kHz), the second one is not easily detectable in the spectrum

Near trace

1. A further check of the data quality, extended to an entire profile, can be conducted by plotting a succession of single traces extracted individually from each record, to form a single trace section. It is usually common to extract the first trace (that is, the near offset trace) because the corresponding section will be the one that resemble most the stack section.

Moreover, displaying the single trace section is useful to monitor the performance of a source like the sparker, whose signature quality can be subjected to degradation with time.

In the following figures, the single section for the 1st, the 32nd and the 64th channel are shown.

The quality of the data appears to be constant over the entire profile, no degradation of the source signature is seen over time.

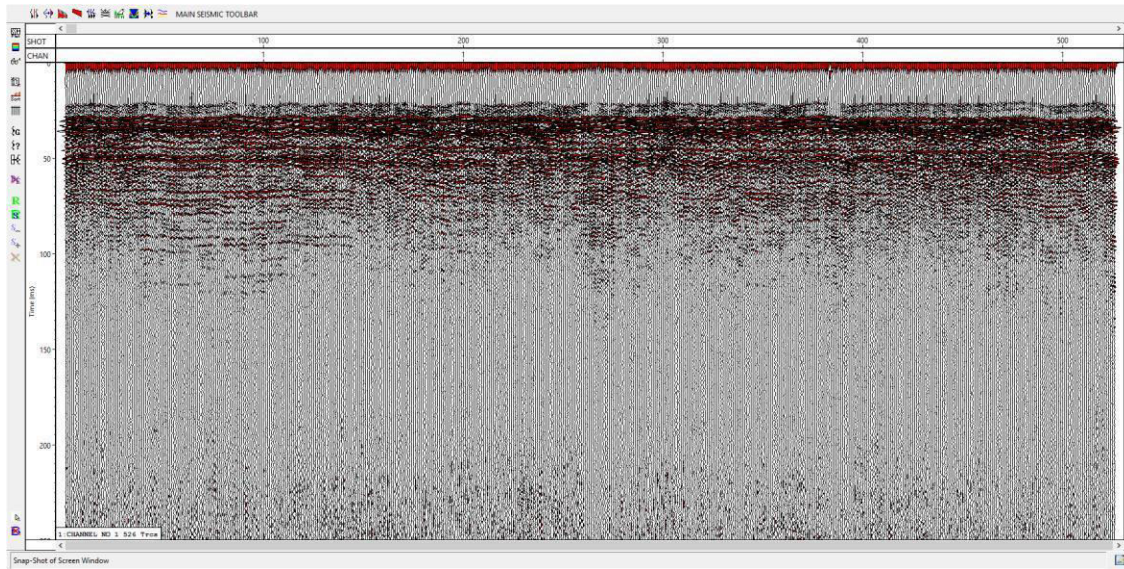


Figure 37. 1st trace (near trace) profile of line B20_08

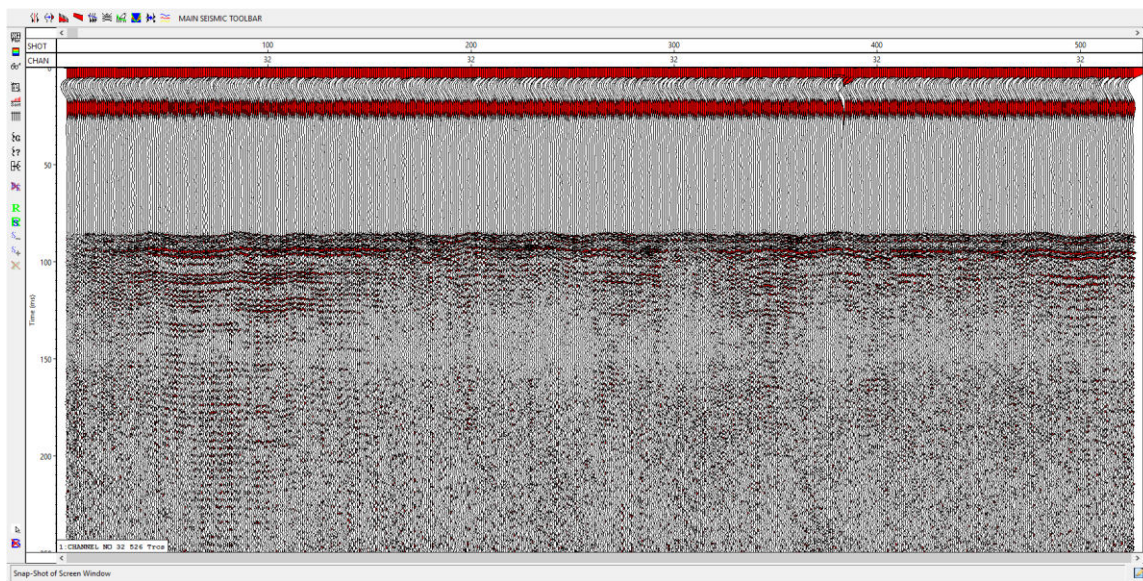


Figure 38. 32nd trace profile of line B20_08

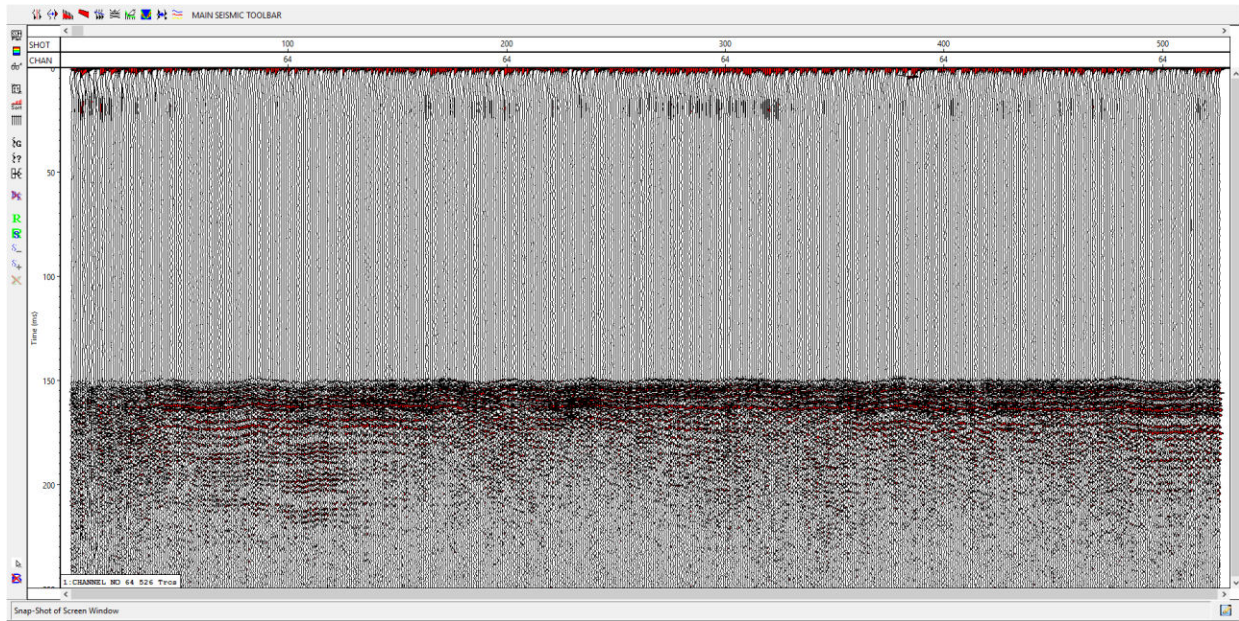


Figure 39. 64th trace profile of line B20_08

Cruise summary

The mobilization started on Monday 31st August at 07:10 UTC and involved seismic equipment installation, PDS2000 project configuration, and pre-cruise meeting to plan the activities. The operations started on Tuesday 1st September 07.30 UTC. The survey ended on Wednesday 2nd w As a whole, **36.4 km** of multichannel seismic were recorded.

4.1.2 Boomer data

The present section describes the Boomer survey (HRS) performed by OGS in Bibione (VE) on September

9th 2020, in the frame of ECOMAP project.

The objective of the HRS survey is to characterize the stratigraphy of the subsurface sediments. The principal goal is to detect where eventually fresh water gushes.

In this survey, a High Resolution Seismic (HRS) acquisition has been planned at sea in front of Bibione Pineda. The seismic survey has been carried out with a boomer system. The grid survey is constituted by 3 lines with N-S direction and 5 lines with E-W direction. The M/B Medusa was used for the acquisition of the lines.



Figure 40. N/R Medusa

Classe 500	
Type	Pilothouse
Length	9.10 m
Width	2.95 m
Draft	0.86 m
Engine	2 x AIFO Diesel 155 HP

Table 1. boat features

The survey started with the MOB operations in Muggia (TS) bay and then after a travel of one hour we arrived at the survey area and began to acquire immediately.

RS reflection profiles have been acquired using a Boomer source (an electro-dynamic transducer mounted on a catamaran frame) and a mono-channel receiver (a pre-amplified streamer composed of 8 piezoelectric elements connected in series). This source, suspended at a constant depth of 40 cm, produces a short impulsive energy every 0.5 second.

The acquisition has been carried out at a speed of about 3-4 knots, so obtaining an inter-trace < 1 m.

In order to minimize the noise and the spatial filtering produced by the hydrophones array, the streamer has been towed near the source with a 15 m longitudinal offset and a 3.5 m lateral offset. We have been kept it as shallow as possible to avoid destructive interference between reflected signals and multiple events from the air/water (ghost). The plate produces a theoretical minimum phase wavelet with an amplitude spectrum between 400 and 4000 Hz. With this frequency range, under favourable conditions, we can obtain data with decimetric resolution (See Appendix for the description of the instruments). The weather condition didn't affect the boomer data: the sea waves were long and not very high, so was not necessary apply tidal corrections to the data.

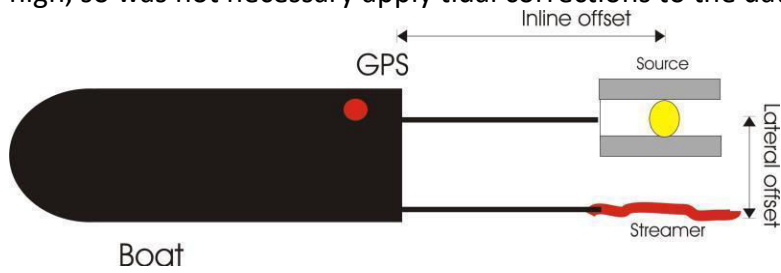


Figure 41. Acquisition geometry: 15 m inline offset, 3.5 lateral offset.

Eight seismic profiles were acquired with the following characteristics. The first and the last shot for every line are indicated (see map in Figure 42).

All profiles (for a total of more 20 km) were acquired with a sample rate of 0.05 and a time length of 100 ms. The plate worked at 300 J Low mode.

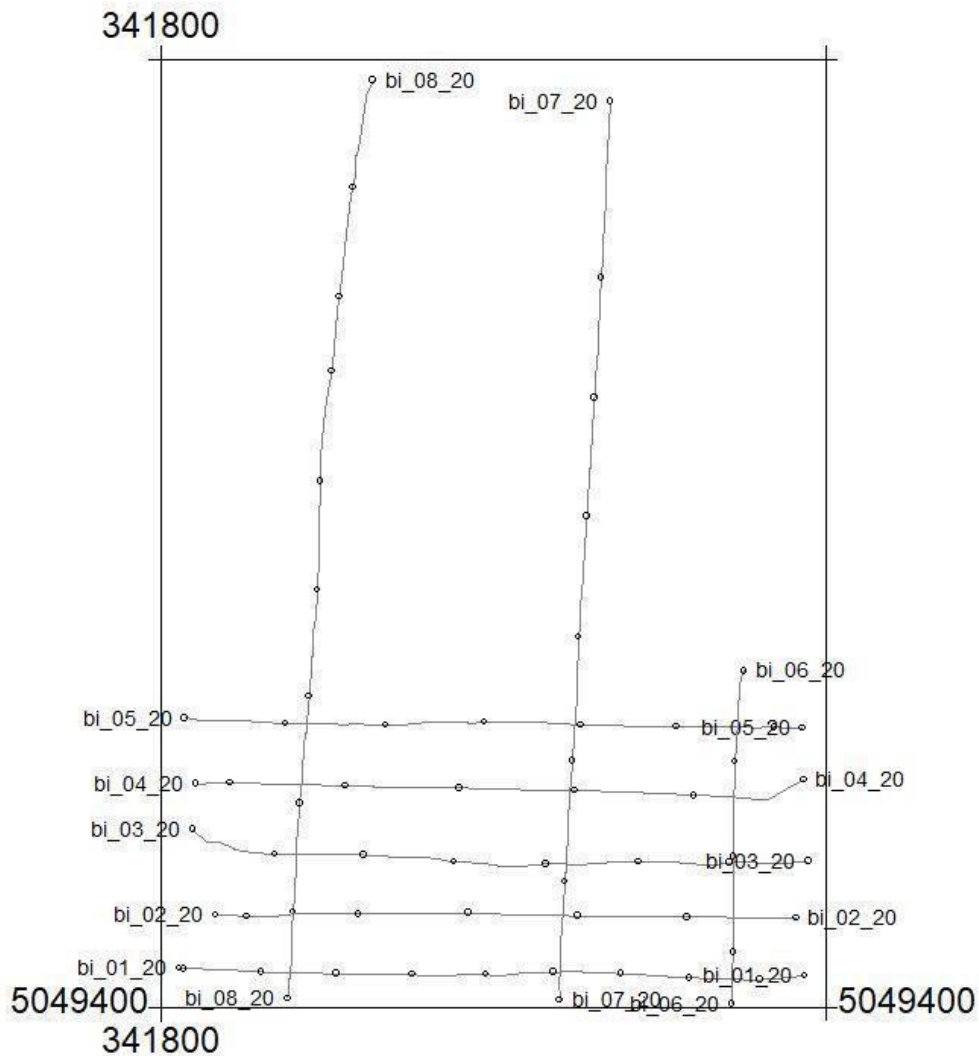


Figure 42. Map of the survey (UTM33).

Boomer data has been processed with a conventional single-channel processing sequence with Echos 2011.3 (PARADIGM) on workstation. The sequence includes:

1. 1) Geometry (we need to calculate the X and Y of every trace from DGPS data);
2. 2) DC removal (marine data often has a continuous noise from electrical devices);
3. 3) Filter (time variant band-pass in a range 100-6000 with slope in dB/octave)

4. 4) Gain (spherical divergence and balance gain obtained by inverse of amplitude decay curve);
5. 5) Predictive deconvolution (improving vertical resolution);
6. 6) Enhancing seismic signal with algorithms ad hoc;
7. 7) Noise eddy currents suppression via time-frequency transform;
8. 8) Mute 2-5 ms on bottom

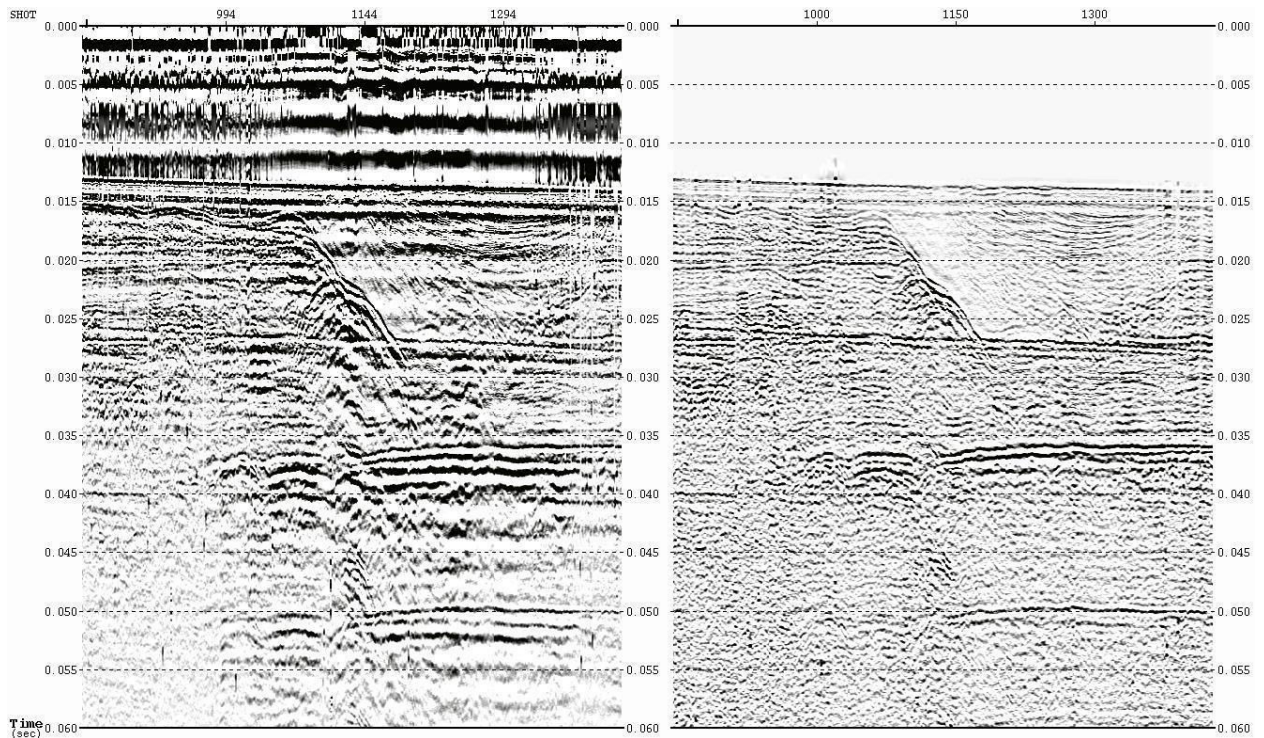


Figure 43. Example of processed profile (right) and raw data (left) [part of B1_08_20]

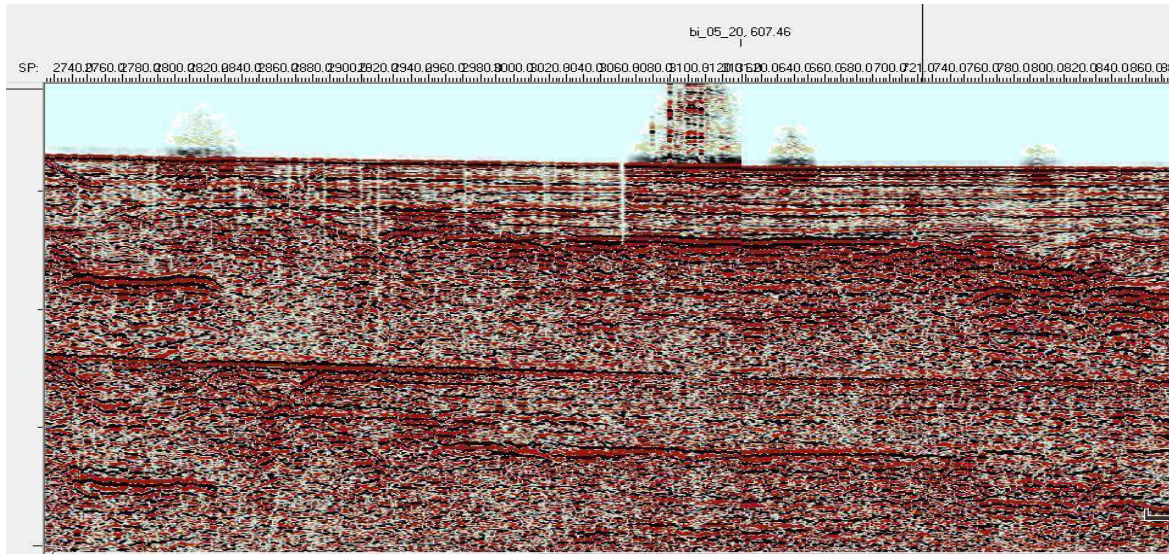


Figure 44. Crossing (see vertical line in the right part of the figure) between two lines (b1_05_20 and bi_08_20).

Boomer data collected during survey in Bibione sea detected and identified several subsurface discontinuities. All seismic profiles have been imported into IHS Kingdom and verified that in their intersections the reflected signals are coherent.

The Boomer signal has a good penetration with good resolution. In some profile, signals associated with puffs are visible above the sea bottom (Figure 44).

4.1.3 Multibeam data

The bathymetric data was processed following the scheme included in the "Technical Regulations for the construction of coastal and port hydrographic surveys" issued by the Hydrographic Institute of the Italian Navy.

The survey area is under a maritime state concession for the construction of an artificial submerged maritime barrier for naturalistic purposes. The area is located 2.3 nautical miles off the coast of Bibione with access regulated by the order 24/2015 of the Caorle Maritime District Office.



Figure 45. Survey area.

The "Medusa" boat owned by the National Institute of Oceanography and Experimental Geophysics - OGS was used to carry out the survey, duly registered under no. TS575 of the Registers of minor ships of the Port Authority of Trieste.



Figure 46. Medusa TS575

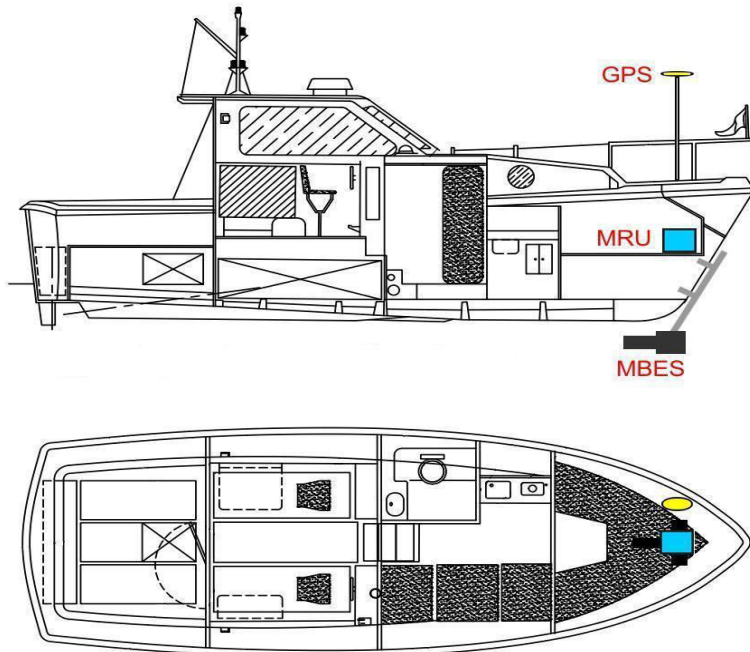


Figure 47. Multibeam system on MEDUSA TS 575

The multibeam transducer (MBES) was installed on a suitable support in the bow of the boat, in a position where it can be aligned with the inertial system (MRU) and relatively close to the GPS antenna.

The multibeam echo sounder has revolutionized the whole bathymetry; few tens of years ago, this kind of survey was performed using single beam echo sounder. In this way a grid of runlines was planned and travelled; the acquired data was subsequently interpolated in post processing to obtain a surface. The final resolution was directly linked to the speed of the vessel and to the thickness of the grid, typically from 10 to 100 meters.

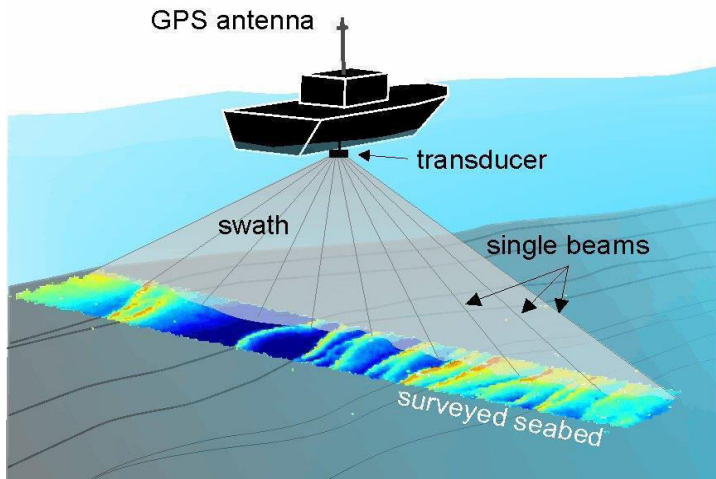


Figure 48. Multibeam coverage.

The multibeam allows to obtain a full coverage bathymetric map with pixel side of 10 cm. This is achieved using hundreds of simultaneous beam, equidistant on the seafloor with a swath wide angle of 120-165°.

The along-track resolution is directly connected with the speed of the vessel and the ping rate of the sounder; while the across-track resolution is connected with the nadir-depth and the angle of the swath. Both these resolutions are lower than 10 cm.

In the table 1, there is a comparison between the resolutions achievable with the single / multibeam technique.

Hectar area with average depth of 10 m	Single-beam	Multibeam
Number of runlines	20	2
Total lenght (m)	2000	200
Time to go (minutes) at 4 knots speed	16	1.6
Ping rate (Hz)	4	30
Beam number	1	512
Number of point detected	4000 (3883)	1.5 M (1491262)
Along track resolution (m)	0.52	0.07
Across track resolution (m)	10	0.11

Table 1. Singlebeam vs. Multibeam.

System's components.

A complete multibeam system is made by six fundamental components, each one basic to have a good final data.

1. The sonar Processor

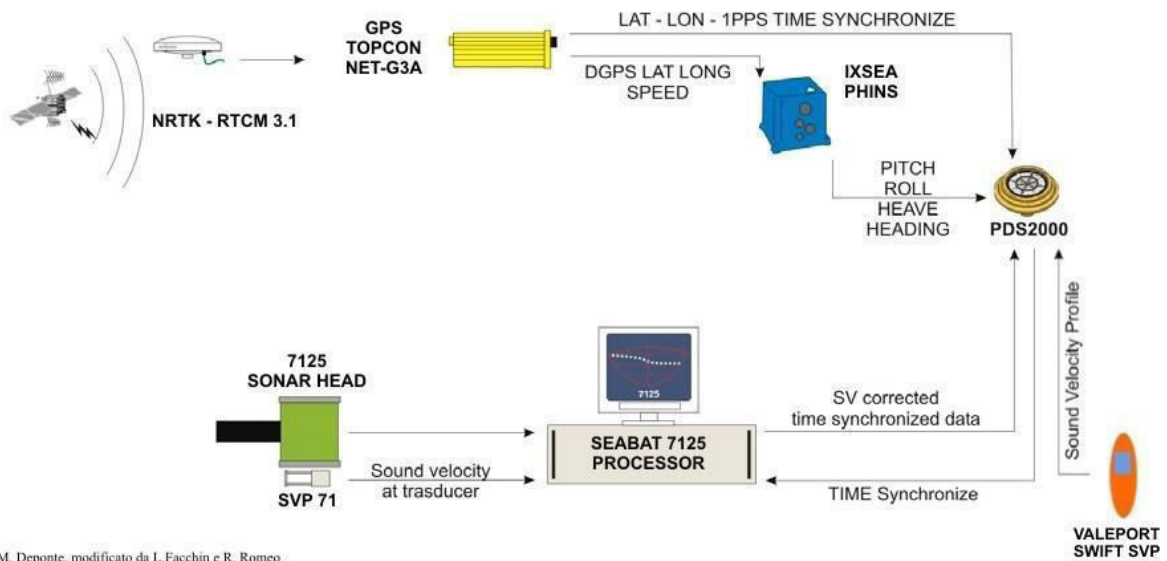
2. The transducer
3. The Motion Reference Unit and Gyrocompass
4. The differential GPS
5. The speed of sound probe
6. The acquisition software

The *sonar processor* Reson Seabat 7125 is the main core of the system; it generates the electric pulse that is converted by the transducer in acoustic pulse. The transducer is made by two parts: projector and receiver; the return-echoes are converted by an hydrophone array to electrical signals that are decoded by the sonar processor to obtain, thanks to a beam forming technique, the final data: 512 points. To correct these points the system has to know precisely, for each pulse, the vessel attitude in terms of pitch, roll, heave, yaw; this is the task of the motion reference unit model PHINS, produced by IXSEA. The roll value is also used to steer the acoustic pulse so to insonify always the nadir area of the seafloor.

The maximum ping rate of the Reson 7125 is 50 Hz so all the data have to be perfectly synchronized by the electric pulse 1 pps (1 ping per second - 5 ns length) generated by the differential GPS model NET G3A produced by Topcon. The differential GPS provides a centimetric position, using the Italpos NRTK service, for an accurate georeference of the final data.

To know the correct path of the acoustic pulse in the water, it is important to measure the local speed of sound of the water. For this purpose, there is a real time probe that continuously measures and sends the speed of sound close to the transducer, beside, at the beginning of the survey there is the necessity to measure this speed along the water column with a profiler probe.

The final data are sent from sonar processor to the acquisition software Teledyne PDS for georeference and vessel's attitude correction.



M. Deponte, modificato da L.Facchin e R. Romeo

Figure 49. Multibeam system's components.

System operation

Before starting a multibeam survey there are a lot of parameters to set up in the acquisition software

Geodetic settings

Ellipsoid	WGS84
Datum	ETRF2000 (2008)
Projection	UTM33 N

Geometry

To obtain valid data, the software has to know perfectly the right position of the transducer, Motion Reference Unit and GPS. To do this an XYZ reference system has been chosen with origin in MRU position, vertically projected at waterline level. The X-axis is centered on the MRU, Y-axis coincident with the longitudinal axis of the boat, Z-axis vertical with origin on the water line.

Instrument	X	Y	Z
Multibeam Transducer	0.00	-0.12	-0.89
GPS	-0.73	-0.17	2.79
MRU	0.00	0.00	0.44

Sound Velocity Profile

The sound velocity profiles are used to correct the acoustic pulse trajectory in the water. The profile has been performed with the Valeport SWIFT SVP.

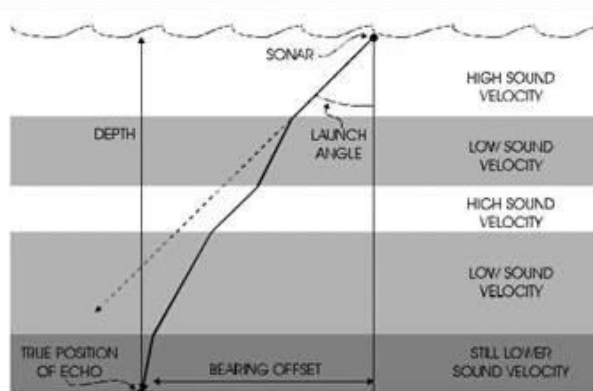


Figure 50. Acoustic pulse path.

Calibration

After setting all the parameters described above, the calibration of the system has to be done. The purpose is to know the installation angles of the transducer, in terms of pitch, roll, yaw, with 0.01° accuracy. To obtain a similar accuracy it is necessary to proceed with an indirect measure. Multibeam data, over a target on the seafloor, have to be acquired along precise runlines.

These data are processed by an utility of the acquisition software; different data of the same target are compared so to obtain the mean error. The utility sets an hypothetical angle and then, with successive approximations, generates an error parabolic curve, the minimum value of this curve is the optimal solution for the desired installation angle.

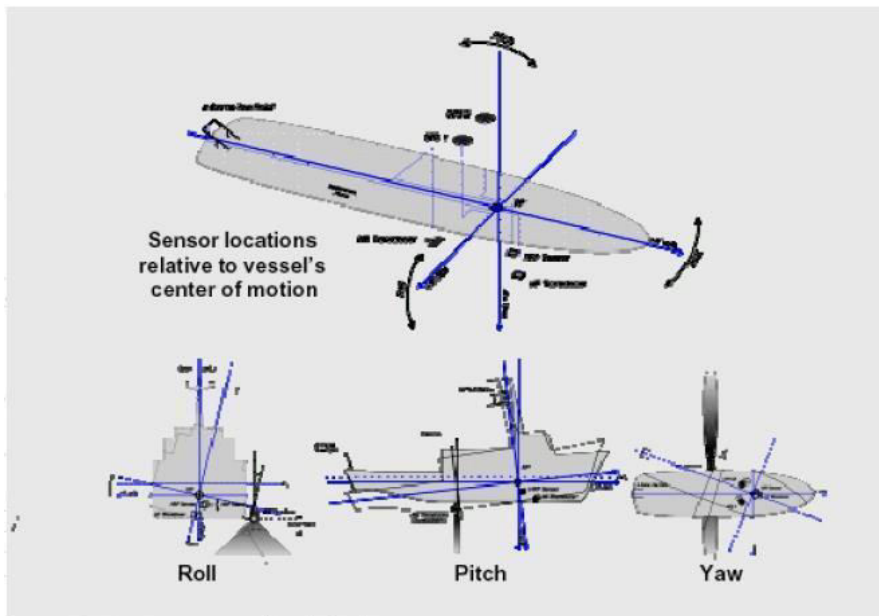


Figure 51. Installation angle in the system XYZ.

Calibration settings:

Roll	-1.55°
Pitch	+3.63°
Yaw	+0.19°

In the following figures the software window, with the profiles before and after calibration settings, can be observed; in the right column there are the parabolic errors curve

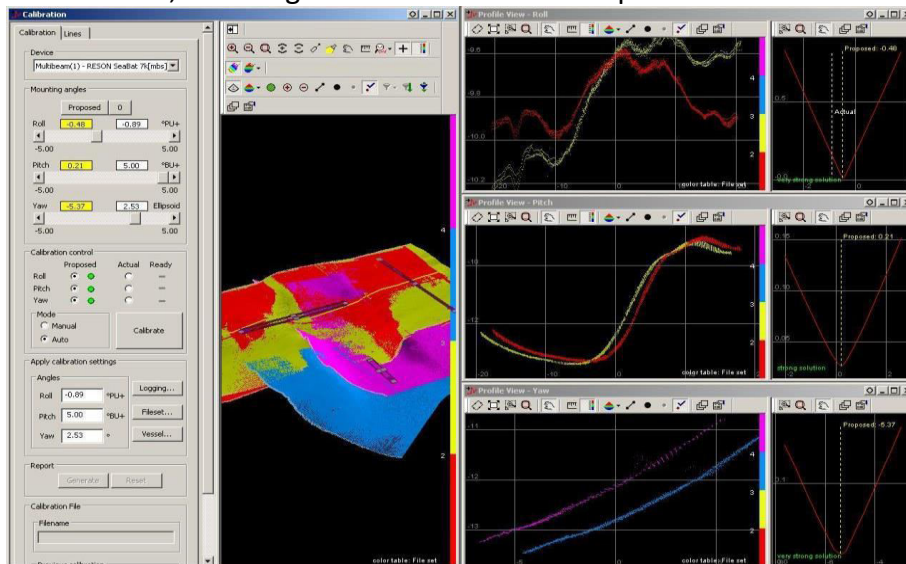


Figure 52. Example: Profiles before calibration - Teledyne PDS

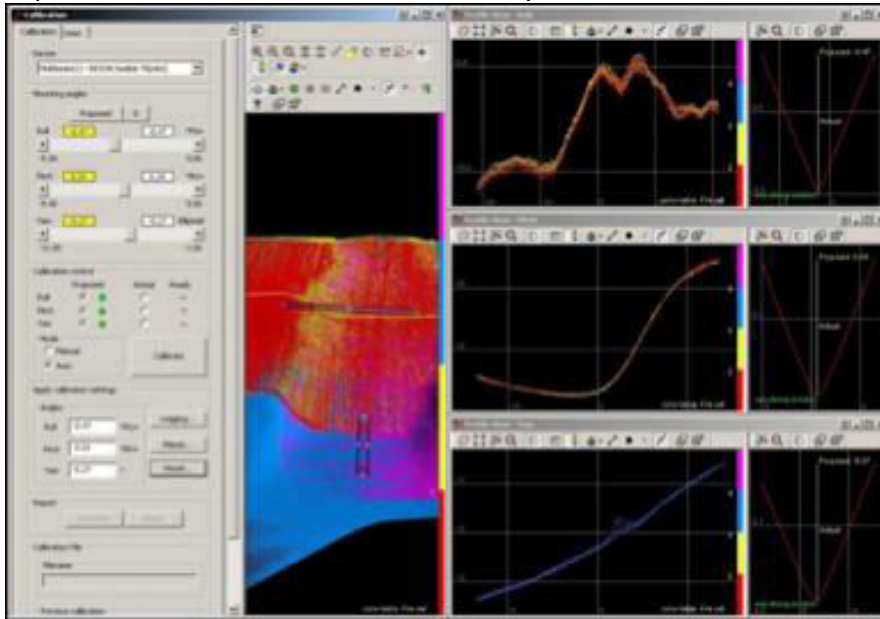


Figure 53. Profiles after calibration - Teledyne PDS

Acquisition parameters

During the data acquisition, the maximum speed of the vessel was always less than four knots, so to get an high along-track resolution of the final data with an overlap, between runlines, constantly above 20%.

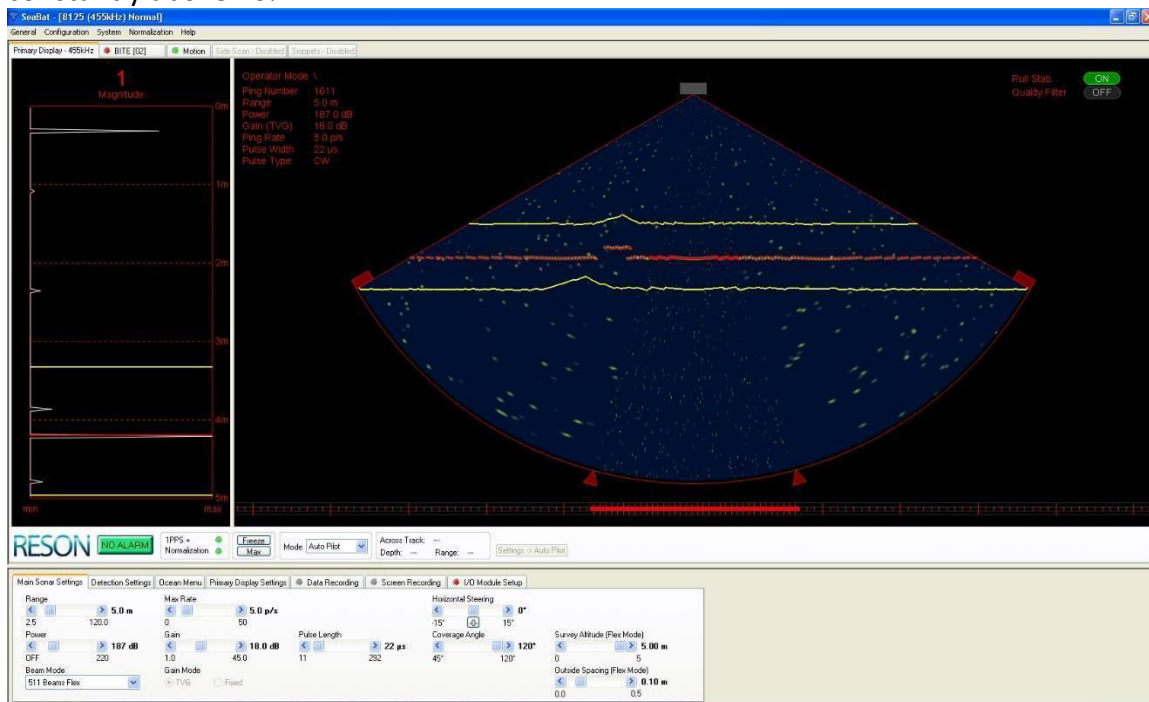


Figure 54. Control system Reson 7125

Barometric data:

The barometric data, expressed in hPa, were obtained from the archive of the Osmer Regional Meteorological Observatory - FVG, Lignano Sabbiadoro (UD) station.

UTC time	10 th september 2020
1	1016.6
2	1016.1
3	1016.2
4	1015.8
5	1015.9
6	1015.7
7	1015.9
8	1016.4
9	1016.3
10	1016.0
11	1015.3
12	1014.8
13	1014.0
14	1013.0
15	1012.4
16	1011.9
17	1011.4
18	1011.7
19	1012.4
20	1012.6
21	1012.5
22	1012.5
23	1012.2
24	1011.9

Table 3. Barometric data.

Sound velocity profile:

Date	UTC time	File SVP
10 th September 2020	10:25	20200910SVP01-1025

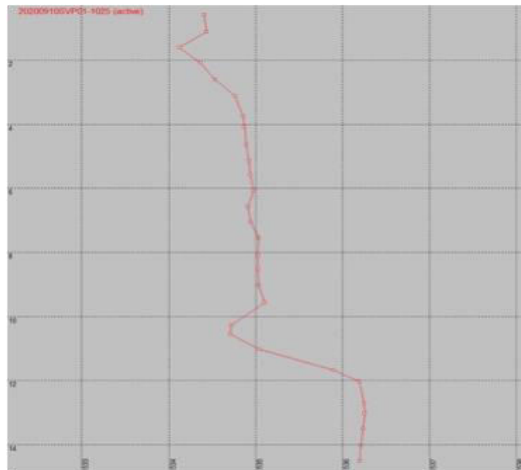


Figure 55. Sound velocity profile.

Data Processing

Tide correction

All the bathymetric data have been corrected using official tidal data of Venice Station, belonging to the National Tidegauge Network of “Istituto Superiore per la Protezione e la Ricerca Ambientale – Ispra”.

The station is located in lido of Venice, near the south dam. The tidegauge station is equipped with altimetric datum. Each datum is referred to the average sea level, measured in Genoa using the ancient Thompson tidegauge. The datums are metallic check tags, used to determinate the altimetric level by means of high precision levelling, following the guidelines fixed by IGM (Italian Military Geographic Institute).






From 16/10/2009 the “hydrometric level” is measured with a new high precision radar sensor SIAP+MICROS TLR .

The data, downloaded from ISPRA web site www.mareografico.it, have been imported in the acquisition software Teledyne PDS, to obtain a full interpolated tidal curve.



Figure 56. Example: tidal correction – Teledyne PDS.

Tide station characteristics:

 <p>ISPRA Istituto Superiore per lo Studio e la Ricerca Ambientale</p>	<p>Reti idrografica e mareografica nazionale LIVELLAZIONE DI ALTA PRECISIONE</p>	<p>Rilievi anno 2009 - 2010</p>	<p>Stazione mareografica di Venezia</p>
<p>CSO MAREOGRAFICO Coordinate plane UTM - ETRF 2000 N: 5032617,418 E: 298646,861 Quota s.l.m.: m. 2,2439 Bullone in acciaio inox murato sulla banchina lato sinistro entrando della cabina mareografica</p>	<p>ORIGINE IGM CSV: 0170_D02_001 Punto GPS: 051801</p>	<p>Annotazioni: non essendo stazionabile la staffa mareografica con la stadia si è dovuto materializzare e misurare un eso ripettitore in allineamento con la staffa stessa</p>	
<p>CSV MAREOGRAFICO Quota s.l.m.: m. 4,4729 Plastra mensolata murata sulla parete sulla mezzera della porta di accesso alla cabina mareografica</p>			
<p>CSO RIFERIMENTO STAFFA MAREOGRAFICA Quota s.l.m. 1998: caso di riferimento inesistente Quota s.l.m. 2009: m. 2,2361 Bullone in acciaio inox murato sul pavimento della cabina in allineamento con la staffa mareografica</p>			
<p>STAFFA MAREOGRAFICA Quota s.l.m. 1998: m. 2,2905 Quota s.l.m. 2009: m. 2,1911 Staffa in ferro murata nel pavimento della cabina, aggettante sul pozzo di calina</p>			

The acquisition and processing software has a tool with the following automatic filters, which can be set during the survey, for the data quality control:

- Beam Quality*, detects and deletes beams with a bad quality level;
- Depth*, detects and deletes beams out of depth range settings;
- Statistic*, detects and deletes beams out of statistic settings;
- Beam reject*, deletes beams;
- Range*, detects and deletes beams out of range settings;

Nadir, detects and deletes beams out of angle range;
Slope, detects and deletes beams that generate an irregular slope on the seafloor;
Intersect, detects and deletes beams with a not tolerated intersection angle;
Flying object, detects and deletes beams referred to objects too high on the seafloor;
IHO error, detects and deletes beams with not tolerated IHO precision values;
Custom error, detects and deletes beams with vertical propagation errors.
 All these filters do not delete or modify the original data, so the operator can always choose and change the filter settings to reach the optimal result.
 During acquisition and post-processing only the *Beam quality* filter has been applied.
 Afterwards the data has been manually controlled so to avoid software detection errors.
 The manual data process is performed by a slowly data replay, with different points of view so to detect spikes and anomalies

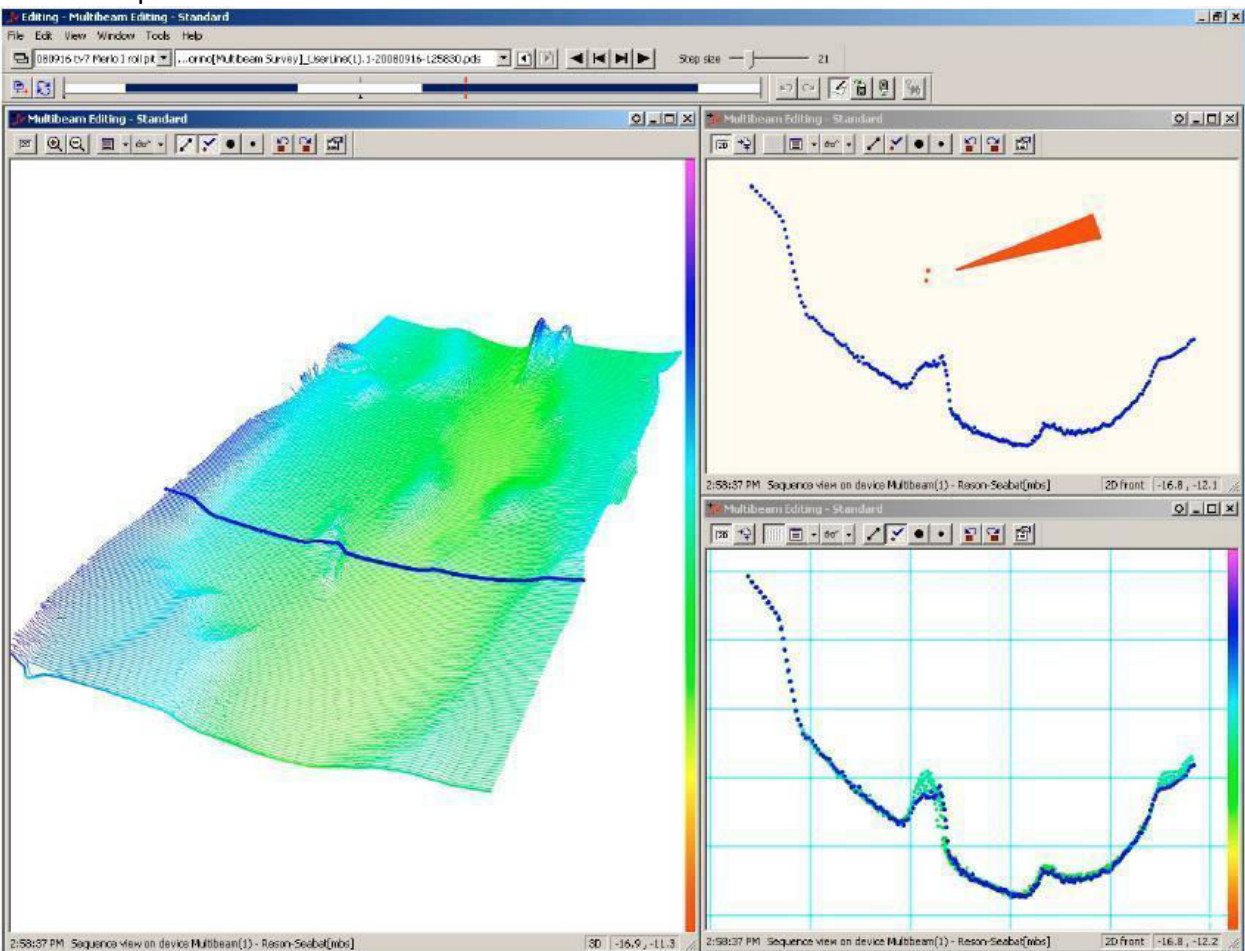


Figure 57. Data manual editing – Teledyne PDS.

Data Terrain Model

The last step of post processing is the 3D Data Terrain Model creation. To this purpose a square cell dimension is set and then all the points, inside the square cell, are averaged to obtain a DTM made by a point cloud with constant density.

DTM with square cell of 50 cm and 1 m have been created.

In the following table average depth and density are indicated.

Area (km ²)	Hit count (millions)	Average depth (m)	Average density (points/m ²)
1.05	54.2	14.4	51

Table 4. Average depth and density.

Final results.

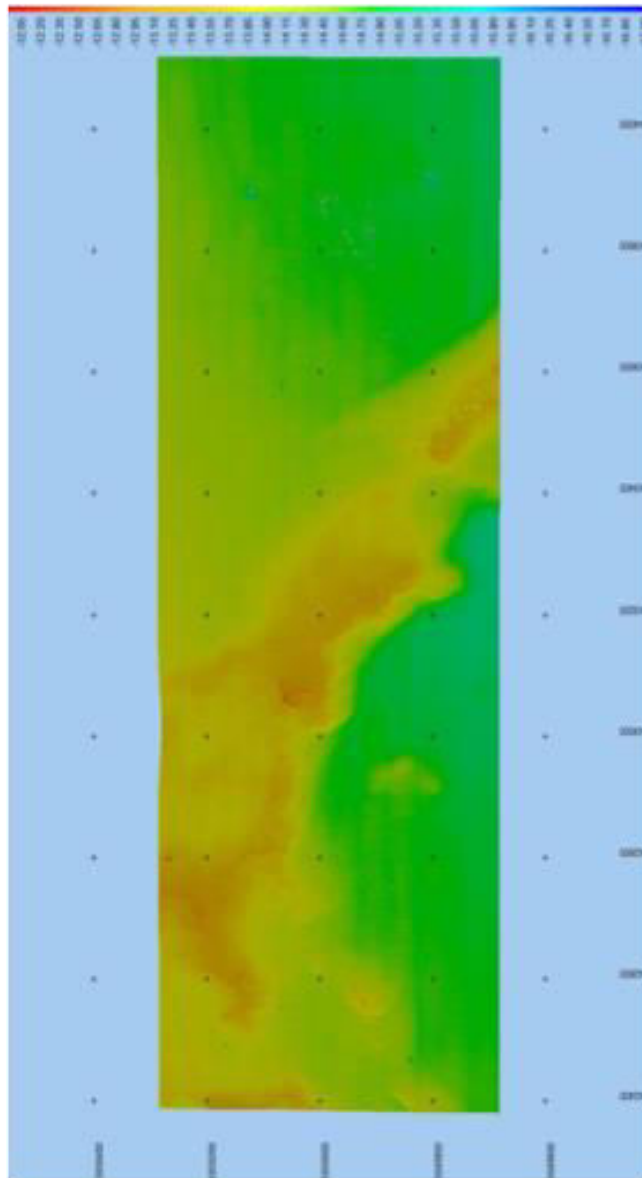
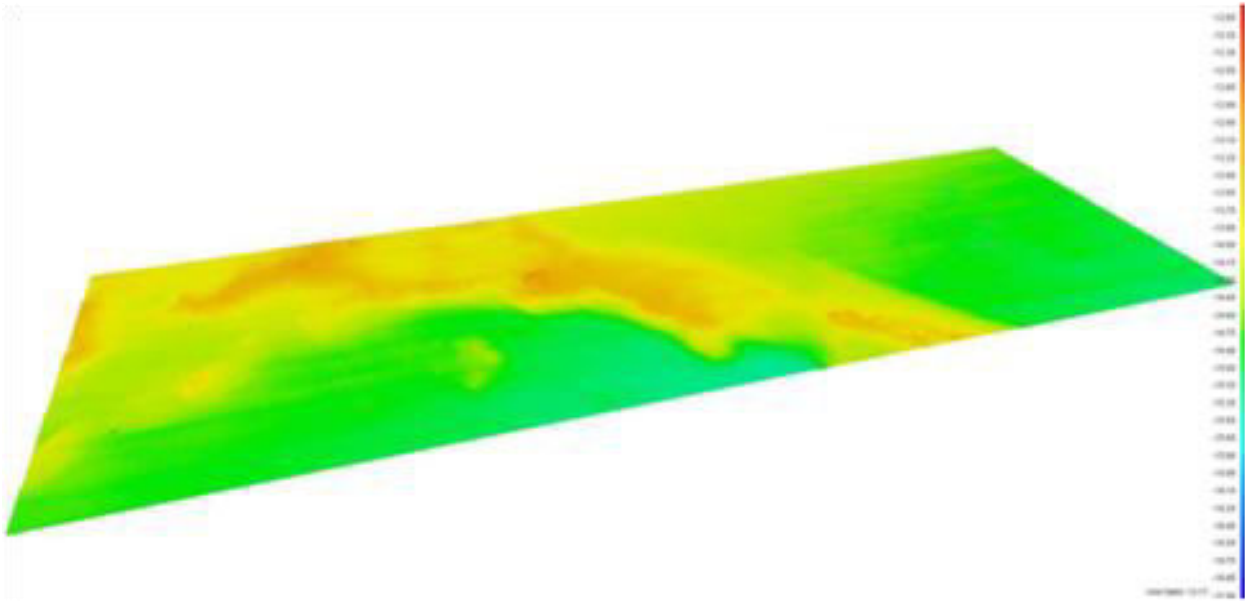


Figure 58. Final DTM cell 50 cm.



Final 59. Final DTM 3D

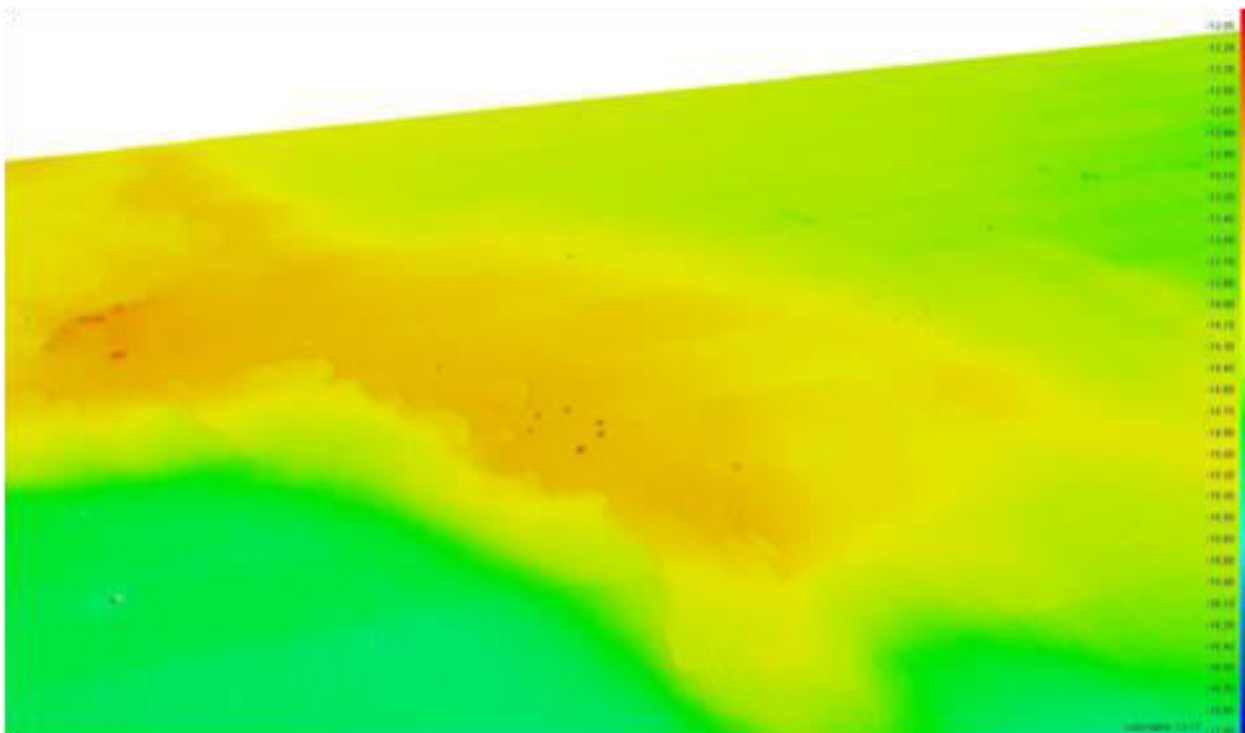


Figure 60. Artificial barrier 3D detail.

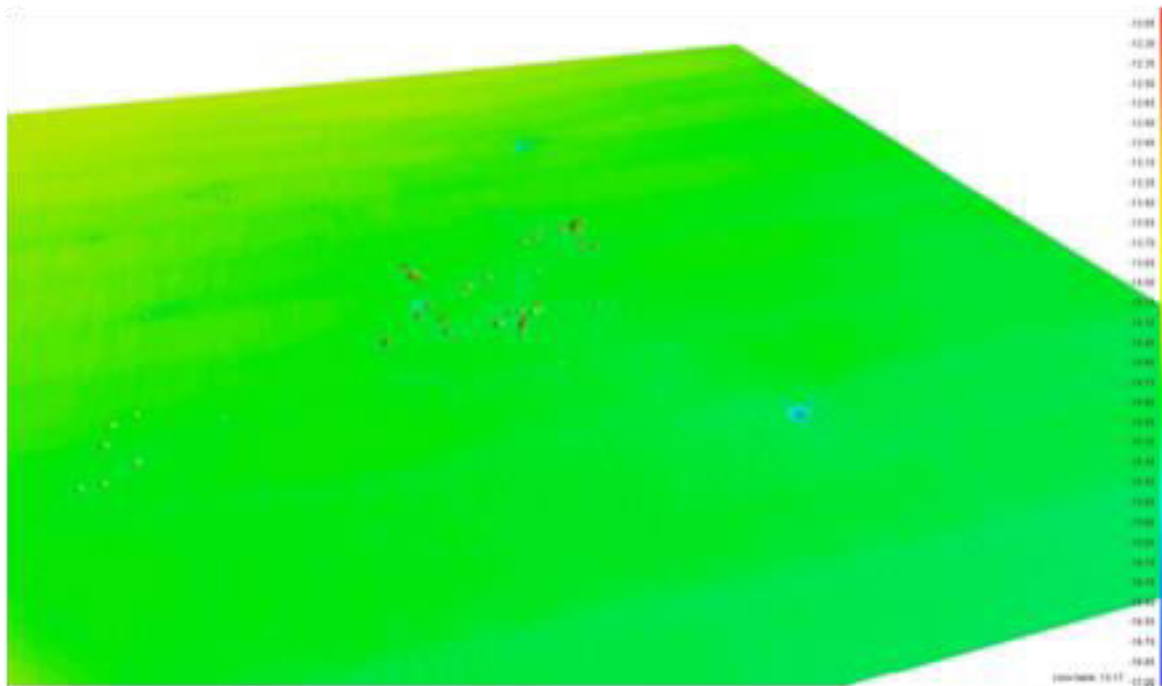


Figure 61. Artificial barrier 3D detail.

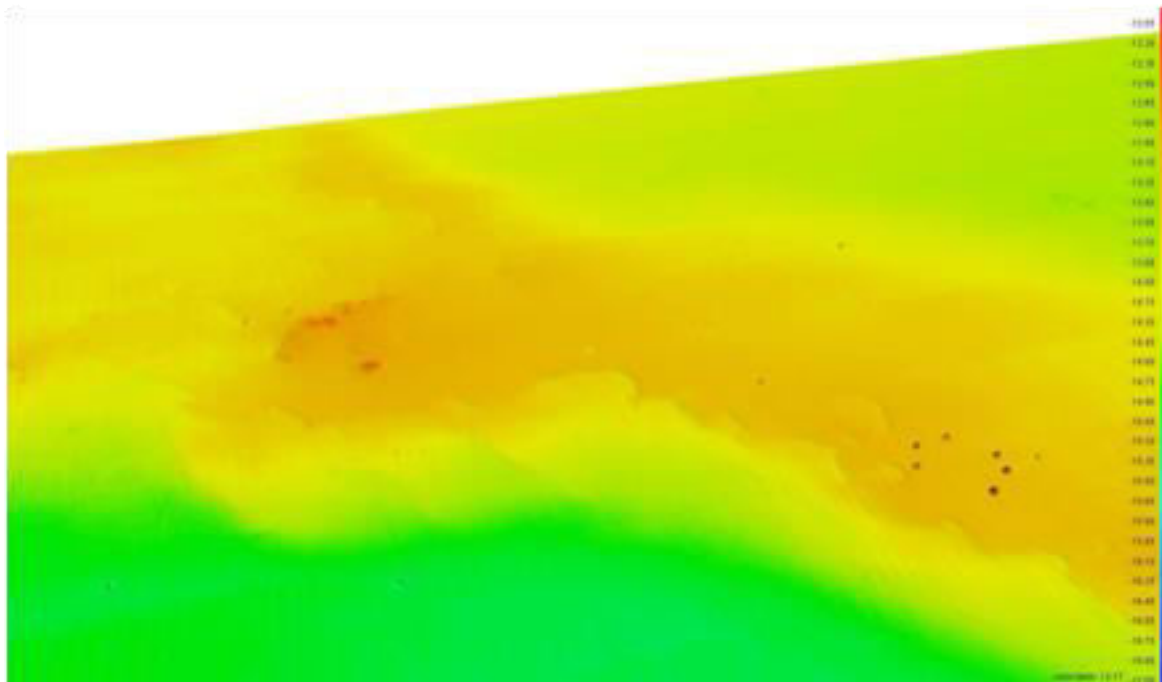


Figure 62. outcrops 3D detail.

4.1.4 Thermometric data

Thermography measurements were carried out on June 3 in the Canale Baseleghe and in front of the shore and June 24th in the area of Canale Baseleghe in front of the Marina.

It was necessary to operate in full darkness due to the sensibility of the camera that could detect even the smallest solar irradiation.

Measurements were carried out by the floating pontoon in the marine and from a boat.

All the images have been georeferenced with the instruments made available by Bibione Mare S.p.A. (*Table 1 – Georeferenced points*).

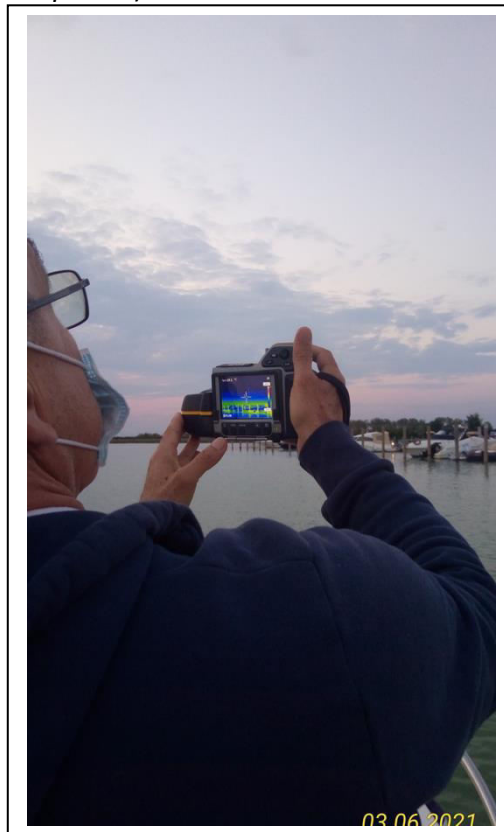


Figure 63. Data acquisition data in marina of Porto Baseleghe

Thermography is based on the measurement of the thermal energy released by object, a structure, the soil surface, water bodies or any other target.

The thermal energy is emitted in the range of infrared; higher is the temperature the higher is the irradiated energy. Thermocamera transforms the IR images into visual images, and after a proper calibration it is possible to measure the T° of the object of interest.

Measurements have been done by a thermocamera FLIR B335 (Figure 64). This camera has excellent performances and has high resistance to stress and humidity and works in accordance to the following conditions:

Operating temperature from -15°C to +50°C

Shell IP 54 IEC 529

Shock resistance: 25G, IEC 68-2-29

Vibrations resistance, 2G, IEC 68-2-6

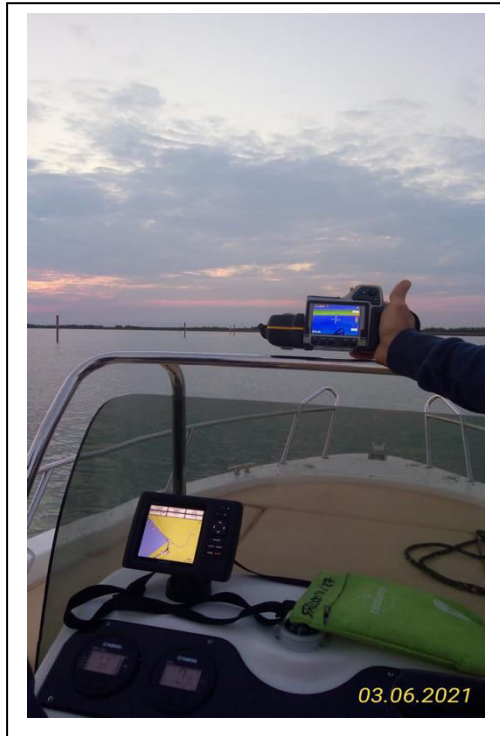


Figure 64. Data acquisition with Thermocamera FLIR B335.

The data have been recorded on June 3rd and June 24th 2021 (Figures 65,66).

The first one was recorded from a boat with the goal to map anomalies from the marina to the offshore in front of the Camping Capalonga and to the East; the second one was recorded in front of the marina from the floating pier and upstream of the channel from a boat.

Measurements started in full darkness to avoid interferences with the last ray of sunlight; in particular the second campaign start at after 10.15 P.M. (pictures show a different time because the stamp of time was not updated to summer light saving time). The movements of the boat decreased the quality of the pictures and, as it is well known, the low angle of measurement did not help the recording, but in general results can be considered satisfactory.



Figure 65. Survey carried out on June 3rd.



Figure 66. Survey carried out on June 24th.

Data have been processed by the FLIR package which has been developed by the camera's manufacturer for the handling, filtering and editing of thermographic data.

The typical sequence is the following:

Data acquisition:

- 1) Measurement of the reflected apparent T° by an aluminium foil and also with the lens toward the sky with calibration settings: $E=1$; distance =0.
- 2) Measurement of Emissivity by a material with known values ($\epsilon =0.98$)
- 3) Processing:
 - 1) Optimization of T° scale
 - 2) Identification of Sp (spots) and A (areas) with homogeneous characteristics.

The below pictures are representative of the situation near the marina North of the floating pier (Figures 67,68).

The original recorded picture (above) and the processed one are shown below.

It is important to note the timing is not updated to Daylight Saving, and for that one hour must be added.

As visible from the table at the right, the measured T° at Sp1 (spot measurement 1) located on the sandy swamp is 29.7 degree. The used scale is from 26 to 30.4. The thermal image was taken from the floating pier NE (point 1a) of the marina in North direction.

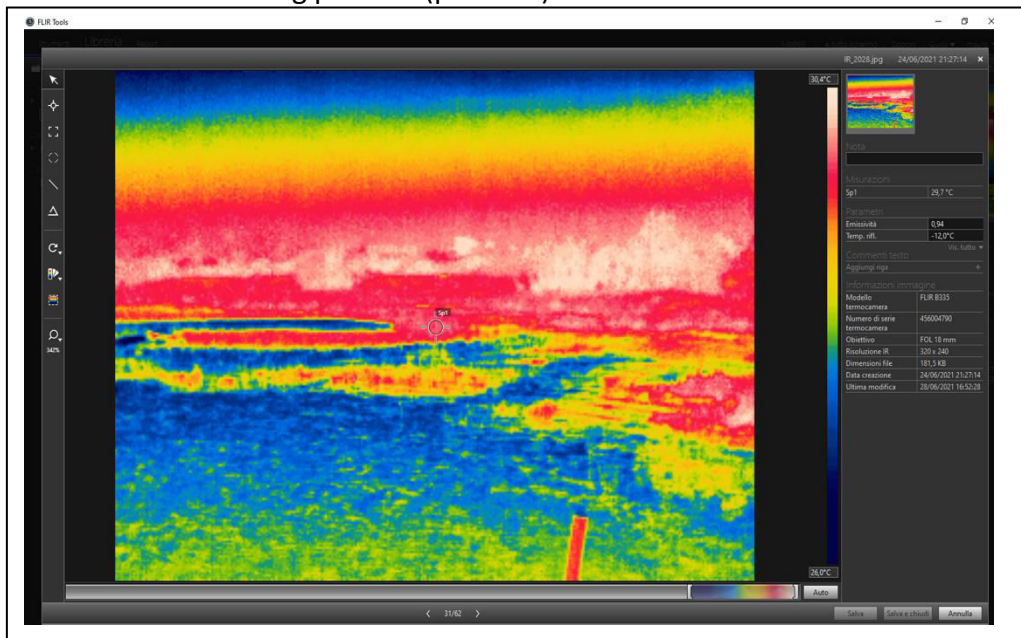


Figure 67. Thermal image 1a with evidence of the thermal contrast between land (red- white), colder water (blue) and the warmer water of port inside the pier

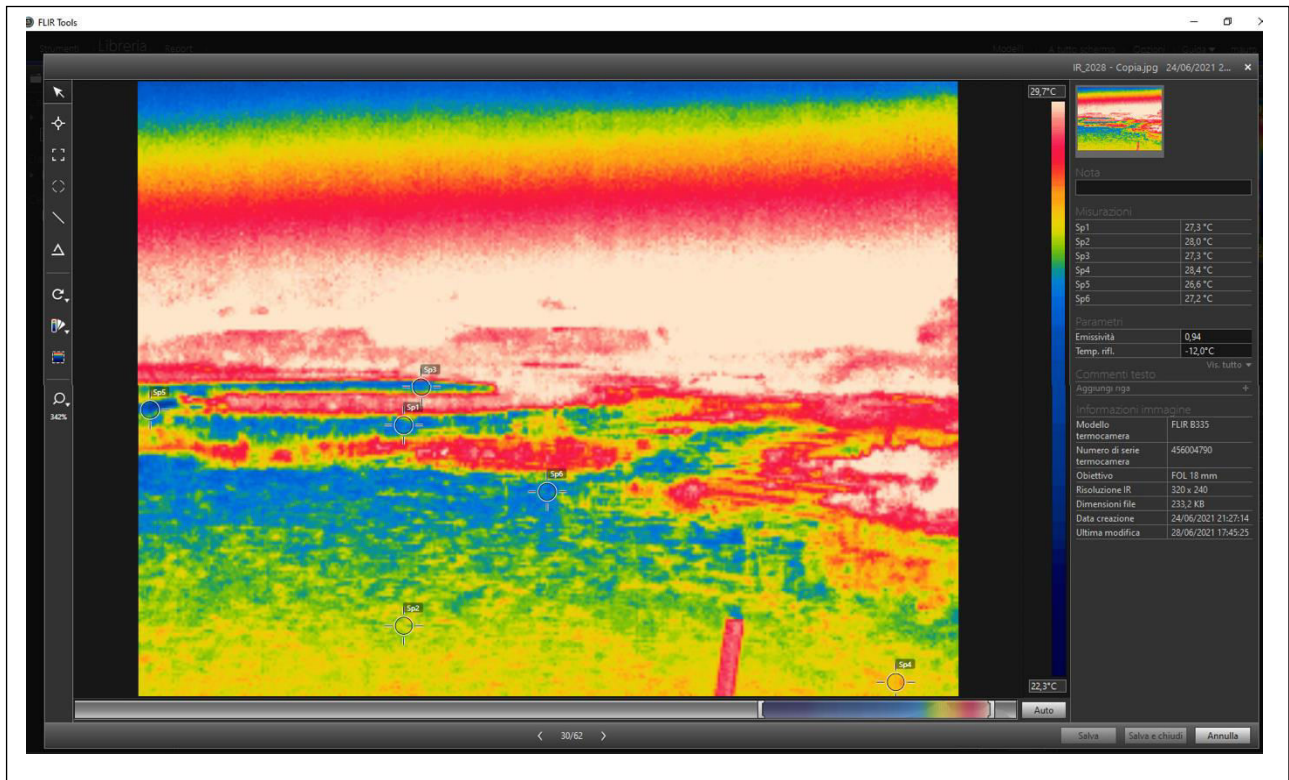


Figure 68. Processed image.

The processed image has more convenient scale from 22.3 to 29.7 and 6 Sp (Spot) measurements. The coldest areas have values from 26.6 to 27.3, whereas the sea water near the pier has 28 and 28.4 respectively.

The shore appears in white because of its higher temperature.

In conclusion, the thermographic survey recorded in front of the Marina Baseleghe and along the Canale has pointed out minimal differences of T° , in the order of less than 1.5° , inside the water body and near the shore.

The main variations are at the mouth of the Canale where the warmer waters coming from the lagoon, encounter the colder sea water.

Minor anomalies have been detected near the muddy shores to the North and NE of the marina pier.

5. Evolutionary scenarios

Introduction

In the test sites of ECOMAP project in the Adriatic areas, the coastal ecological system of the marine environment was investigated with interdisciplinary approaches in relation to the environmental pressures due to the mechanisms exerted by climate change and human activities (tourism, fishing, residential settlements, farms of animals, agriculture etc).

The goals of the WP 3.1 are the characterization of the marine environment in the project test sites through geophysical prospecting to support a suitable model of management to guarantee the quality of water and aquatic sediments and the biodiversity in order to define a resilience to climate change and anthropic impacts.

This action capitalizes on the results obtained in the geophysical surveys carried out by OGS (PP7) and by Eureka on behalf of Bibione MARE (PP6) to characterize the beaches and small ports selected for the activities of the ECOMAP project as representative contexts of the Adriatic coastal areas of the actions of the INTERREG Italy - Croatia program. The purpose of this action is to provide an analysis of the Evolutionary scenarios in the short, medium and long-term of the morphological features in order to program climate change adaptation interventions

The set of geophysical methods has provided rapid profile and 3D area survey reconstructions for the morphological and geological features in small ports and marines.

The results of the geophysical surveys in four areas characterized by small ports and marinas typical of the Adriatic context (Spinut, Podstrana, Bibione Mare and adjacent Laguna di Baseleghe, Port of Ancona) have been confirmed as representative for the understanding of the connections between ecosystem and services ecosystems were used to define the evolutionary scenarios at short, medium and long-term of the morphological features in order to program climate change adaptation interventions.

For marine habitats of the Adriatic one the focus of ECOMAP is the evaluation of freshwater contributions from the rivers but above from the freshwater sources in the seawater bottom as they have a high role to maintaining the mean marine values of pH above the useful value to allow the carbonate formation of sea taxa as calcareous algae, corals, plankton (approx. 8.0–8.3) in order to contrast the acidification of the sea and oceans related to the increase of CO₂.

Methods and results

Adriatic climate and anthropic pressure in relation to the results of the Geophysical survey. Coastal zones are under serious threat to extreme events, like sea storms for global warming and the propagation and amplification of meteo tsunamis for sea level rise, and these events are accelerated in the last years to the irreversible changes for coast erosion (Nicholls et al., 2007). In test sites of marinas and ports to Adriatic areas the ecological coastal system of sea environment was investigated with an interdisciplinary approach in relation to environmental pressures owing to the mechanisms exerted to climate change and to human activities (tourism, fishing, residential settlements, animal farming, agriculture etc). Understanding and managing ecological responses to the coastal areas require the characterization of the morphology of sea water, identification of geological geometries in relation to the exchange dynamics between fresh and saltwater that affect the diversity of marine biota and the ability to respond to climatic pressures and anthropogenic.

High-resolution bathymetric characteristics were provided through the geophysical survey and this action capitalizes on the exploitable results defining a short, medium and long-term evolutionary scenarios in relation to the pressures that will affect the coastal areas which are listed below:

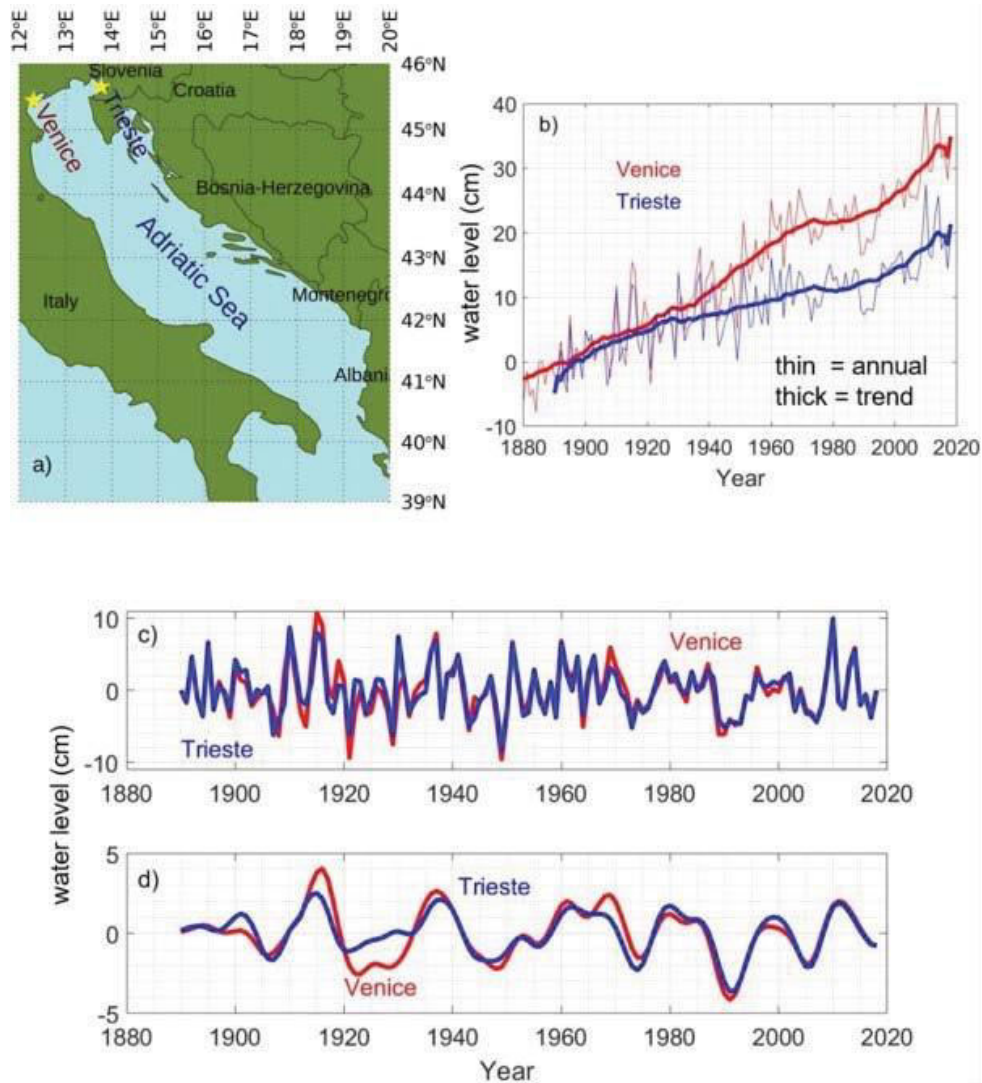


Fig 1: the sea-level variabilities a) global increasing trends over the period spanned by observations (~130 yr), b) a combined influence of lunar precessions and solar activity in the sea-level variabilities (Valle-Levinson et al., 2021). Valle-Levinson et al., 2021 evaluated the combined influence of lunar precessions and solar activity in the sea-level variabilities giving projections of interannual variability of mean sea level in the northern Adriatic for the 21st century whose peaks Expected to be centered around 2022 –23, 2049–50, 2066–67, and 2090–91. It was also found that mean sea levels have been anomalously high in the northern Adriatic during at least 75% of the last 12 highs in the solar cycles.

1. Increasing temperature changes in the Adriatic are very rapid (at the hourly scale, up to 2°C/h), especially in the summer when the temperature has a high-frequency variability

or in winter coinciding with the bora that is a north - easterly katabatic wind with high meteorological effects and impact on the Adriatic Sea circulation. The thermohaline circulation vulnerabilities are due to the sea environment characterized by shallow influenced by high variability of freshwater loads from contributions from karst aquifers. Global warming is amplifying this vulnerability which on a local scale has different impacts in relation to the morphology of the seabed and freshwater emergency areas. The analysis carried out made it possible to obtain the useful parameters for the impact balances To assess the temperature, increase Valle-Levinson et al., 2021 examined the annual mean sea- level data from the Italian “Maree Forecasting and Reporting Center” for Punta Salute Canal Grande, in Venice, and at the head of the Gulf of Trieste (Fig. 1). Valle-Levinson et al., 2021 collected data from 1890 (130 yr of annual values) at both stations. Invasion of alien species due to variation of rainy events that will worsen the quality of the water that from the rivers and springs distributed along the coast introduces fresh water into the sea basins. Species sensitive to changes in salinity will suffer and reduce their abundance, and these conditions will lead to the loss of endemic species and the filling of species from adjacent waters and transported from another sea basin via ballast water and the Suez Canal. These invasions have an impact not only on the biodiversity of marine habitats but also on strategic sectors for the Adriatic economy such as fishing, shellfish and tourism given that valuable species are replaced by non-commercial or inedible species

2. The strong footprint of Human presence related to planned exploitation of coastal resources as urbanization, sand extraction and overexploitation to coastal aquifers that promotes the degradation of fresh water and salinization of estuaries
3. Very high resolution seismic allowed us to define the thickness of the sediments and to map the freshwater outflows. The outflows of fresh water in the Spinut areas are characterized as outflows are greater in number than in the Podstrana area and in both areas, these outflows do not appear constant in time. In fact, at a cross point of two lines, in one line the outflow is present, while in the other one, acquired one hour later, it is not present and this is characteristic of the intermittent flows of karst systems

The activities of WP 3.1.3 assist in the analysis of the current structure of coastal areas in order to be able to provide a reference from the response at a local scale of coastal mereology induced by climate change and anthropogenic pressure.

Discussion and conclusion

In this action was investigated the results of a geophysical survey multidisciplinary approach in order to identify the descriptive indicators of sustainable management planning of the systems. High-resolution bathymetric characteristics have provided the morphology of the seabed that indicates the high vulnerability to the advancement of the sea level due to the urbanization of

the areas behind the beaches which with the expected sea rise in some areas will lead to the submersion of homes and infrastructures.

Most of the small ports have fixed piers that fail to adapt to the rising sea and also the embankments in the defences of the port areas will have to be remodelled to deal with the rise and both the storm waves that will damage themselves with greater intensity due to of global warming.

An important indication is derived from the role that freshwater sources have in the Upper Shoreface as they mitigate the acidification process with high pH water supplies. The water crisis affecting the Mediterranean and in particular the aquifers that feed the surface resources and the aquifers in the Adriatic area can reduce these inputs with very serious impacts on coastal habitats. This would have major consequences on fishing and shellfish farming.

Methodology used in the analysis of the exploitable results supported the management of ecological responses to these changes in coastal areas requires interdisciplinary approaches. The methodology developed with the ECOMAP project develop a new approach to coastal socio- ecological systems based on knowledge of the morphology and structure of the subsoil.

We have found that different indicators that characterize each scenario will put different pressures on WAC systems, in the forms of long-term printing and short-term pulsed events. Cross-cutting narratives of different future scenarios in the face of climate change using the mPPD framework offer valuable insight into the development of WAC strategies, policies and other management programs. It helps define the plausible implications of following a particular management path or not. The inconsistencies between the aspirations of the different users of resources and the lack of coordination of human activities that take place on land and in the coastal zone are highlighted, partly due to the fragmentation of institutions and weak coastal governance. In this context, the mPPD-CSES framework can be used to study how ecosystems can experience different pressure (intensities) as well as different pulse frequencies. Therefore, its adaptability to build future coastal vulnerability scenarios adds to its usefulness as a robust and reliable integrated coastal zone management tool. The increase in temperature that is affecting the Adriatic area can produce die-offs of organisms living in the intertidal area and foul- smelling emissions, this effect combined with a lower feeling of well-being can produce a thermic stress factor in the tourist. To avoid losses in terms of tourist presence due to a perception of the beach no longer as an area of well-being, it requires an information campaign that sensitizes tourists in managing the hours of greatest thermal stress.

The detection of the temperature by means of a thermal imaging camera highlights the best livability of the beach in the morning hours, a high thermal stress is observed in the intertidal environment linked to the partial emergence of the first bar and to the heating of the seawater trapped between the 1° bar and the area of backshore The temperature of the beach and the sea was recognized as a SMART indicator into beach management (Specific, Measurable,

Achievable, Realistic, Time-bounded) being the beach social-ecological systems whose management is endangered by global rescaling.

The observed dynamics make it has brought out the need to organize entertainment activities for tourists for the hottest days and daytime periods that allow them to face the variation of the daytime temperatures and to promote a beach sustainable use in relation to the stress on ecosystems of the beach. National policies can incentivize new plans for sustainable seasonal beach use in a standardized manner in order to improve management capacities (Fanini et al., 2020) and could be helpful to assess the cumulative impacts of multiple human activities, which is an increasingly important and complex management issue of the marine environment (Lonsdale et al., 2020).

References

Fanini L., Costa L.L., Zalmon I.R., Riechers M. (2021) Social and Ecological Elements for a Perspective Approach to Citizen Science on the Beach Frontiers in Ecology and Evolution 9.

Lonsdale J.A., Nicholson R., Judd A., Elliott M., Clarke C. (2020) A novel approach for cumulative impacts assessment for marine spatial planning, Environmental Science & Policy, 106, 125-135.

Nicholls, R. J., Wong, P. P., Burkett, V., Codignotto, J., Hay, J., McLean, R., ... & Saito, Y. (2007). Coastal systems and low-lying areas.

Valle-Levinson A., Marani M., Carniello L., D'Alpaos A., Lanzoni S. (2021) Astronomic link to anomalously high mean sea level in the northern Adriatic Sea Estuarine, Coastal and Shelf Science Volume 257, 31, 107418.